

ANGIOGENIC EFFECT OF SALT-LEACHED THAI SILK FIBROIN SCAFFOLDS WITH HUMAN  
ADIPOSE-DERIVED STEM CELLS



A Dissertation Submitted in Partial Fulfillment of the Requirements  
for the Degree of Doctor of Philosophy in Biomedical Chemistry  
Department of Biochemistry and Microbiology  
FACULTY OF PHARMACEUTICAL SCIENCES  
Chulalongkorn University  
Academic Year 2019  
Copyright of Chulalongkorn University

ผลการกระตุ้นการสร้างเส้นเลือดของโครงเลี้ยงเซลล์จากไฟโบรอินใหม่ไทยแบบชะเกลือที่มีเซลล์ต้น  
กำเนิดไขมันมนุษย์



วิทยานิพนธ์นี้เป็นส่วนหนึ่งของการศึกษาตามหลักสูตรปริญญาวิทยาศาสตรดุษฎีบัณฑิต  
สาขาวิชาชีวเวชเคมี ภาควิชาชีวเคมีและจุลชีววิทยา  
คณะเภสัชศาสตร์ จุฬาลงกรณ์มหาวิทยาลัย  
ปีการศึกษา 2562  
ลิขสิทธิ์ของจุฬาลงกรณ์มหาวิทยาลัย

Thesis Title	ANGIOGENIC EFFECT OF SALT-LEACHED THAI SILK FIBROIN SCAFFOLDS WITH HUMAN ADIPOSE-DERIVED STEM CELLS
By	Mr. Tanapong Watchararot
Field of Study	Biomedical Chemistry
Thesis Advisor	Peerapat Thongnuek, Ph.D.
Thesis Co Advisor	Krissanapong Manotham, M.D. WEERAPONG PRASONGCHEAN, Ph.D.

---

Accepted by the FACULTY OF PHARMACEUTICAL SCIENCES, Chulalongkorn University in Partial Fulfillment of the Requirement for the Doctor of Philosophy

..... Dean of the FACULTY OF  
PHARMACEUTICAL SCIENCES  
(Assistant Professor Rungpetch Sakulbumrungsil, Ph.D.)

DISSERTATION COMMITTEE

..... Chairman  
(Assistant Professor Chatchai Chaotham, Ph.D.)

..... Thesis Advisor  
(Peerapat Thongnuek, Ph.D.)

..... Thesis Co-Advisor  
(Krissanapong Manotham, M.D.)

..... Thesis Co-Advisor  
(WEERAPONG PRASONGCHEAN, Ph.D.)

..... Examiner  
(Wanatchaporn Arunmanee, Ph.D.)

..... Examiner  
(Eakachai Prompetchara, Ph.D.)

..... External Examiner  
(Ruttachuk Rungsiwiat, Ph.D.)

ธนพงษ์ วัชรโรจน์ : ผลการกระตุ้นการสร้างเส้นเลือดของโครงเลี้ยงเซลล์จากไฟโบรอินไหมไทยแบบ  
 ละเอียดที่มีเซลล์ต้นกำเนิดไขมันมนุษย์. ( ANGIOGENIC EFFECT OF SALT-LEACHED THAI SILK  
 FIBROIN SCAFFOLDS WITH HUMAN ADIPOSE-DERIVED STEM CELLS) อ.ที่ปรึกษาหลัก : อ.  
 ดร.พีรพัฒน์ ทองนิก, อ.ที่ปรึกษาร่วม : นพ.กฤษณพงศ์ มโนธรรม,อ. ภก. ดร.วิระพงษ์ ประสงค์จีน

กระบวนการสร้างเส้นเลือดมีบทบาทสำคัญในการซ่อมแซมเนื้อเยื่อและทำงานร่วมกับวัสดุชีวภาพและ  
 เซลล์ วัสดุชีวภาพที่อนุญาตและส่งเสริมการสร้างหลอดเลือดจึงมีประโยชน์ โครงเลี้ยงเซลล์จากไฟโบรอินไหม คือ  
 วัสดุที่ดีในการกระตุ้นการสร้างเส้นเลือดเพราะสามารถย่อยสลายทางชีวภาพ สามารถเข้ากันได้กับเนื้อเยื่อหรือ  
 เซลล์และการมีการทำงานร่วมกันกับเมทริกซ์นอกเซลล์ เซลล์ต้นกำเนิดไขมันมนุษย์สามารถซ่อมแซมความ  
 เสียหายของเนื้อเยื่อได้เช่นกัน งานวิจัยนี้มีวัตถุประสงค์เพื่อ ศึกษาศักยภาพของการสร้างเส้นเลือดของโครงเลี้ยง  
 เซลล์จากไฟโบรอินไหมบนเนื้อเยื่อ chorioallantoic ของเอ็มบริโอไก่ (CAM) ทั้งที่มีเซลล์ต้นกำเนิดไขมันมนุษย์  
 และไม่มีเซลล์ต้นกำเนิดไขมันมนุษย์ ประการแรก โครงเลี้ยงเซลล์จากไฟโบรอินไหมถูกขึ้นรูปขึ้นมาโดยมีความ  
 พอร์นร้อยละ  $77.34 \pm 16.96$  และเส้นผ่านศูนย์กลางรูพอร์น  $513.95$  ไมโครเมตร หลังจากนั้น นำเซลล์ต้นกำเนิด  
 ไขมันมนุษย์ใส่ลงไปโครงเลี้ยงเซลล์จากไฟโบรอินไหมและวางไว้บนเนื้อเยื่อ CAM ของเอ็มบริโอไก่ที่มีอายุ  $8$   
 วันเพื่อศึกษาคุณสมบัติในการสร้างเส้นเลือด ผลการทดลองพบว่า โครงเลี้ยงเซลล์จากไฟโบรอินไหมที่มีเซลล์ต้น  
 กำเนิดไขมันมนุษย์ มีการกระตุ้นการเกิดลักษณะวงล้อของเส้นเลือดที่เอ็มบริโอไก่อายุ  $11$  วัน และในกลุ่มที่ไม่มี  
 เซลล์ต้นกำเนิดไขมันมนุษย์ก็มีการเกิดวงล้อของเส้นเลือดเช่นกัน แต่เกิดช้ากว่า คือเกิดในเอ็มบริโอไก่อายุ  $14$  วัน  
 เมื่อนำโครงเลี้ยงเซลล์จากไฟโบรอินไหมไปทดสอบความเป็นพิษต่อเซลล์และการระคายเคืองต่อเส้นเลือด เพื่อ  
 ยืนยันว่า โครงเลี้ยงเซลล์จากไฟโบรอินไหมสามารถเข้ากับเนื้อเยื่อได้ สำหรับการตัดจากส่วนตรงกลางของโครง  
 เลี้ยงเซลล์จากไฟโบรอินไหมที่มีเซลล์ต้นกำเนิดไขมันมนุษย์ มีความบางขนาด  $30$  ไมโครเมตร พบการเข้าไปของ  
 เส้นเลือดในโครงเลี้ยงเซลล์ โดยสรุป สิ่งที่ค้นพบ ทำให้เห็นถึงการกระตุ้นการสร้างเส้นเลือดที่เร็วขึ้นในกลุ่มโครง  
 เลี้ยงเซลล์จากไฟโบรอินไหมที่มีเซลล์ต้นกำเนิดไขมันมนุษย์อยู่และสามารถเป็นประโยชน์ต่อการใช้ในการฟื้นฟู  
 เนื้อเยื่อต่อไป

สาขาวิชา ชีวเวชเคมี  
 ปีการศึกษา 2562

ลายมือชื่อนิสิต .....  
 ลายมือชื่อ อ.ที่ปรึกษาหลัก .....  
 ลายมือชื่อ อ.ที่ปรึกษาร่วม .....  
 ลายมือชื่อ อ.ที่ปรึกษาร่วม .....

# # 5576208733 : MAJOR BIOMEDICINAL CHEMISTRY

KEYWORD: silk fibroin scaffold, Adipose-derived stem cell, CAM assay, Chick embryo,  
tissue engineering, regeneration, Oxidative stress, anti-oxidant exzymes

Tanapong Watcharot : ANGIOGENIC EFFECT OF SALT-LEACHED THAI SILK FIBROIN  
SCAFFOLDS WITH HUMAN ADIPOSE-DERIVED STEM CELLS. Advisor: Peerapat  
Thongnuek, Ph.D. Co-advisor: Krissanapong Manotham, M.D., WEERAPONG  
PRASONGCHEAN, Ph.D.

Angiogenesis plays important role in tissue regeneration. Biomaterials that allow and promote angiogenesis are thus beneficial. Silk fibroin (SF) scaffolds are good candidates for angiogenesis activation because of the biodegradability, biocompatibility, and interaction of extracellular matrices. Human adipose-derived stem cells (ADSCs) are also promising for tissue regeneration. This study thus aims to investigate the angiogenic potential of SF scaffolds with/without ADSCs on chick chorioallantoic membrane (CAM). Firstly, the SF scaffolds were fabricated with a porosity of  $77.34 \pm 16.96\%$  and a pore diameter of  $513.95 \mu\text{m}$ . Then, ADSCs were seeded on SF scaffolds (SF-ADSC scaffolds) and placed on CAM on an embryonic day 8 (E8) to assess the angiogenic property. The result revealed that SF-ADSC scaffolds induced a spoked wheel-pattern of the capillary network on E11. The SF scaffolds without ADSCs induced the same pattern of angiogenesis later on E14. The cytotoxicity tests and angioirritative study reconfirmed the biocompatibility of the SF scaffolds. Cryosections ( $30 \mu\text{m}$ ) were obtained from the middle of the SF-ADSC scaffolds, and a histological study showed penetration of blood vessels into the scaffolds. In conclusion, this work highlighted the acceleration of angiogenesis from SF- ADSC scaffolds, and, therefore, they are beneficial for tissue regeneration.

Field of Study: Biomedical Chemistry

Academic Year: 2019

Student's Signature .....

Advisor's Signature .....

Co-advisor's Signature .....

Co-advisor's Signature .....

## ACKNOWLEDGEMENTS

This thesis is supported by the 100th Anniversary Chulalongkorn University Fund for Doctoral Scholarship.

The instruments are supported by the Department of Biochemistry and Microbiology and Pharmaceutical Research Instrument Center, Faculty of Pharmaceutical Sciences, Chulalongkorn University.

The biomaterials are supported by Biomaterial Engineering for Medical and Health Research Unit, Biomedical Engineering Research Center, and Biomedical Engineering Program, Faculty of Engineering, Chulalongkorn University.

Tanapong Watchararot



## TABLE OF CONTENTS

	Page
ABSTRACT (THAI).....	iii
ABSTRACT (ENGLISH).....	iv
ACKNOWLEDGEMENTS.....	v
TABLE OF CONTENTS.....	vi
LIST OF TABLES.....	xii
LIST OF FIGURES.....	xiv
CHAPTER I INTRODUCTION.....	17
Research questions and Objectives.....	18
Hypothesis.....	18
Objectives.....	18
Graphical conceptual framework.....	19
Benefits of this study.....	21
CHAPTER II LITERATURE REVIEW.....	22
Angiogenesis.....	22
Chick embryo development.....	25
Chorioallantoic membrane assay (CAM assay).....	27
Silk fibroin scaffolds (SF scaffolds).....	30
Structure of SF scaffolds.....	30
Physical and biological properties of SF scaffolds.....	32
SF scaffolds and tissue engineering.....	36
Stem cell biology.....	37

Adipose-derived stem cells (ADSCs) .....	40
Properties of ADSCs.....	40
Antioxidant enzyme properties in ADSCs .....	42
Regenerative medicine .....	45
The supportive data of extracellular vesicles and their potential.....	46
CHAPTER III MATERIALS AND METHODS .....	47
Equipment.....	47
Materials.....	47
Chemicals .....	47
Methods.....	50
ADSC cell culture.....	50
Trypsinization and freezing of cells .....	50
Characterization of ADSCs by immunocytochemistry.....	50
Adipogenic differentiation.....	51
Osteogenic differentiation.....	52
Determination of antioxidant enzymes activity .....	53
Cell lysis.....	53
Catalase activity .....	54
Glutathione peroxidase activity .....	55
Determination of glutathione level .....	56
Determination of SOD contents .....	57
RNA isolation.....	58
cDNA synthesis .....	59
Polymerase chain reaction (PCR) and agarose gel electrophoresis .....	59



Therapeutic potential of ADSCs.....	60
Ethic statements .....	60
Chick embryo incubation and windowing .....	60
Fabrication of salt-leached SF scaffolds .....	60
Scanning electron microscope (SEM) .....	63
Physical properties of SF scaffolds .....	63
Porosity liquid substitution .....	63
Gel fraction.....	64
Preparation of SF-ADSC scaffolds.....	64
MTT assay.....	64
Fluorescent staining of SF-ADSC scaffolds .....	65
CAM assay.....	65
Angiogenic scoring .....	66
Histological section.....	66
Statically analysis.....	67
CHAPTER IV RESULTS .....	68
The characterization ADSCs was determined by RT-PCR and immunocytochemistry .....	68
Differentiation capacity of ADSCs .....	72
ADSCs have antioxidant enzymes in non-induced condition.....	74
Filter paper with ADSC Passage 24 has not significantly different angiogenesis.....	79
SF scaffolds structure.....	82
The physical properties of salt-leached scaffolds; % dry weight of SF scaffolds, % porosity of SF scaffolds and % gel fraction .....	84

Angioirritative effect of SF scaffolds.....	87
Cell viability was detected by MTT assay and Live/Dead staining.....	89
Qualitative data of biodegradable of SF-ADSC scaffolds.....	91
Spoke-wheel pattern from CAM assay .....	92
Histological staining .....	95
CHAPTER V DISCUSSION .....	97
ADSCs express various protein markers.....	97
ADSCs have antioxidative properties. ....	103
Filter paper cannot be a good representative material for tissue engineering. ....	103
The 3D structure of salt-leached SF scaffolds versus SF scaffolds. ....	104
Solid scaffold can apply on angioirritation test on HET-CAM assay.....	106
The rigidity of SF scaffolds can activate angiogenesis.....	107
Effect of NaCl, Na <sup>+</sup> and Cl <sup>-</sup> from salt-leached SF scaffolds on angiogenesis on CAM assay. ....	110
ADSCs can be cocultured with SF scaffolds.....	111
SF-ADSC scaffolds induced angiogenesis.....	111
The possible mechanism to induce angiogenesis of SF-ADSC scaffolds.....	114
SF-ADSC scaffolds might have protein-protein interaction to induce biodegradable. ....	116
CHAPTER VI CONCLUSION .....	119
Appendix .....	120
Animal Ethic statements (No. 16-33-008).....	120
Supplement data from ADSC-EVs .....	123
ADSC-EVs characterization.....	124

Methods.....	124
Cell culture for EVs collection.....	124
EVs isolation and purification.....	124
Dynamic light scattering and Nano tracking analysis (NTA).....	125
Transmission electron microscope (TEM).....	125
Results.....	126
Determination of ADSC-EVs size.....	126
The structure of ADSC-EVs.....	128
Characterization of ADSC-EVs.....	130
Storage condition of ADSC-EVs.....	132
ADSC-EVs can store over 1 year and make an information for stabilization....	133
ADSCs gene expression after treated with serum-free condition.....	136
Discussion for ADSC-EVs.....	139
ADSCs secrete EVs into culture media.....	139
ADSC-EVs contains ADSC markers.....	140
Supplement data of SF-MCF-7 on angiogenesis.....	144
The result of cell viability was detected by MTT assay Live/Dead staining ....	144
SF-MCF-7 scaffolds activates angiogenesis on CAM assay that caused the spoked-wheel pattern.....	146
Secondary stock calculation for adipogenic differentiation.....	149
Secondary stock for Osteogenic differentiation.....	150
Calculation of 200nM L (+) ascorbic acid (Primary stock).....	150
Preparing incomplete media.....	150
Catalase activities law data.....	151

GPx activities law data .....	151
GSH levels Law data.....	154
Standard Curve of GSH ( $\mu\text{M}$ ).....	155
SOD contents law data.....	157
Standard curve of CU-Zn SOD .....	157
REFERENCES .....	2
VITA.....	18



## LIST OF TABLES

	Page
Table 1 The advantages and disadvantages of angiogenesis on different models.....	23
Table 2 The physical and biological properties of SF scaffolds.....	32
Table 3 The composition of SF scaffolds. ....	34
Table 4 The amino acid compositions of SF scaffolds. ....	35
Table 5 Antibody for immunocytochemistry.....	49
Table 6 Adipogenic differentiation reagents.....	52
Table 7 Osteogenic differentiation reagents.....	53
Table 8 CAT activity (U/g protein) compare between ADSCs and HaCaT cells.....	75
Table 9 GSH level ( $\mu\text{M}$ ) compare between ADSCs and HaCaT cells.....	76
Table 10 GPx activity (U/g protein) compare between ADSCs and HaCaT cells. ....	77
Table 11 SOD contents (ng/ ml) compare between ADSCs and HaCaT cells. ....	78
Table 12 The percentage of porosity of SF scaffolds. ....	84
Table 13 The percentage of porosity of filter paper.....	85
Table 14 Gel fraction via % weight loss of SF scaffolds. ....	86
Table 15 Angiogenesis scoring in different groups. ....	95
Table 16 The size distribution of ADSC-EVs from the old stock. ....	134
Table 17 The size distribution of ADSC-EVs from fresh preparation. ....	134
Table 18 The conclusion of size of ADSC-EVs from different bathes. ....	141
Table 19 Angiogenesis scoring of MCF-7 or no cell implanted with SF scaffolds. ....	147
Table 20 The conclusion of CAT activity (U/g prot.).....	151
Table 21 The absorbance and calculation data of GSH level ( $\mu\text{M}$ ). ....	156

Table 22 Standard curve of CU-Zn SOD.....	157
Table 23 The absorbance of SOD activities and the calculation of % inhibition and SOD contents.....	113



## LIST OF FIGURES

	<b>Page</b>
Figure 1 The graphical conceptual framework in this study. ....	20
Figure 2 The 21-day development of chick embryo. ....	26
Figure 3 Chorioallantoic membrane (CAM) origin. ....	28
Figure 4 SF scaffolds chemical structure. ....	30
Figure 5 $\beta$ -sheet structure of the peptide chains in SF scaffolds. ....	31
Figure 6 The capacity of stem cell. ....	39
Figure 7 The sources of ADSCs in body. ....	40
Figure 8 Key reactions and antioxidant enzymes. ....	43
Figure 9 The role of SOD activity in the chemical reaction. ....	58
Figure 10 Fabrication of salt-leached SF scaffolds from Thai Bombyx mori. ....	62
Figure 11 The morphology of ADSCs. ....	68
Figure 12 Gene expression of ADSC from RT-PCR. ....	70
Figure 13 Protein expression of ADSCs by Immunocytochemistry. ....	71
Figure 14 Differentiation capacity of ADSCs. ....	73
Figure 15 CAT activity in HaCaT and ADSCs lysates. ....	75
Figure 16 GSH level in HaCaT and ADSCs lysates. ....	76
Figure 17 GPx activity in HaCaT and ADSCs lysates. ....	77
Figure 18 SOD level in HaCaT and ADSCs lysates. ....	78
Figure 19 The angiogenesis of filter paper in different groups. ....	80
Figure 20 The flipped-filter paper of CAM assay on E11 chick embryo. ....	81
Figure 21 The structure of SF scaffolds. ....	83

Figure 22	Angioirritation testing of SF scaffolds on CAM assay.....	88
Figure 23	The effect of SF scaffolds on ADSCs viability by MTT assay and cellular live/dead fluorescence staining of SF-ADSC scaffolds by Hoechst and Acridine orange. ....	90
Figure 24	The biodegradable properties of SF-ADSC scaffolds.....	91
Figure 25	Angiogenic properties of SF scaffolds on CAM assay.....	93
Figure 26	Angiogenic properties of SF-ADSC scaffolds.....	94
Figure 27	Histological analysis of the SF-ADSC scaffolds compared with SF scaffolds in different embryonic days. ....	96
Figure 28	The mRNA and Protein expression of ADSCs.....	98
Figure 29	The adipogenic differentiation media on transcription factor regulation..	100
Figure 30	The osteogenic differentiation media on transcription factor regulation..	102
Figure 31	Biological Unit of Fibroin Heavy Chain (pink color) for 3UA0: tetrameric; determined by author and by software (PISA) [140].....	105
Figure 32	The reaction of SF scaffolds structure after dissolved in water/liquid solution.....	109
Figure 33	The overview of CAM assay on tissue repair and regeneration.....	113
Figure 34	The possible mechanism of angiogenic potential of SF-ADSC scaffolds...	115
Figure 35	Purpose of protein-protein interactions between albumin and fibroin.....	118
Figure 36	Biogenesis of EVs and their types. ....	123
Figure 37	Dynamic light scattering (DLS) of ADSC-EVs. ....	127
Figure 38	Transmission electron microscope (TEM) of EVs. ....	129
Figure 39	The expression of ADSC-EVs performed by RT-PCR. ....	131
Figure 40	The graph of Nanoparticle tracking analysis (NTA) in different storage conditions.....	135



Figure 41 The effect of serum-free condition on ADSCs gene expression after 48 h treatment. ....	137
Figure 42 The gene expression of serum-free condition after treated with serum-free media. ....	138
Figure 43 The concept of ADSC-EVs from cell cultured in serum-free media. ....	143
Figure 44 The effect of SF scaffolds on MCF-7 viability by MTT assay and cellular live/dead fluorescence staining of SF-MCF-7 scaffolds by Hoechst and Acridine orange. ....	145
Figure 45 The vascular network formation of blood vessels on SF-MCF-7 scaffolds. ....	148



## CHAPTER I INTRODUCTION

Biomedical scaffolds vary in composition, and hence their properties. Polymeric scaffolds can be fabricated from synthetic or/and natural polymers. Synthetic materials are generally reproducible, cheap to fabricate, and readily available while natural polymers are more biocompatible [1]. Examples of materials used for scaffold fabrication are chitosan, gelatin, elastin, collagen, silk fibroin, ceramic and metal scaffolds [2]. The scaffolds from natural materials work well together with extracellular matrices, leading to decent cell-cell communication, and release of pro-angiogenic factors to induce the inflammatory response [2, 3]. One of the interesting scaffolds are salt-leached silk fibroin scaffolds (SF scaffolds), which are made from SF protein extracted from cocoons of Thai *Bombyx mori*. They were shown to have low cost, decent biocompatibility, tunable biodegradability [4], and, most importantly, they enhance osteogenesis [5, 6]. SF consists of repetitive amino acid sequences. The SF forms  $\beta$ -sheet structures due to the dominance of hydrophobic domains consisting repeats of Gly-Ala-Gly-Ala-Gly-Ser in the primary structure. These structures bind tightly with hydrogen-bonded anti-parallel chains of the protein [7]. Apart from osteogenesis, the SF scaffolds were shown to facilitate regeneration of diverse tissues/organs such as nerves, cartilage, cornea, skin, etc.

Tissue regeneration is a complex process that relies on stimulation of angiogenesis [8]. In the angiogenic process, inflammation and the lack of oxygen in the wounded tissues result in the release of pro-angiogenic factors [9]. These factors promote degradation of basement membrane, proliferation and migration of endothelial cells (ECs) from an existent vessel [10]. Tissue regeneration is slowed down when angiogenesis is interrupted. For example, many lines of evidence showed that inhibition of angiogenesis decelerated osteogenesis [4,5]. Indeed, the lack of vascular endothelial growth factor (VEGF), which results in impaired angiogenesis, led to halted bone regeneration [6,7]. Therefore, angiogenesis is needed for tissue regeneration, and it is one of the key processes for tissue regeneration [11, 12].

Tissue engineering materials composed of cells and silk fibroin may be able to activate angiogenesis. Adipose-derived stem cells (ADSCs) were shown to secrete angiogenic growth factors [13, 14]. These factors can stimulate regeneration process in wound repair [15, 16]. Indeed, the lack of ADSCs leads to loss of angiogenesis [17]. For example, the co-culture of ECs and ADSCs triggered a higher rate of

angiogenesis than that with ECs alone because VEGF is released by ADSCs [17]. This suggests that ADSCs may be able to enhance angiogenic potential when seeded into a scaffolds [18].

One of the critical challenges in tissue engineering is selecting a good model and to show clearly the activation of angiogenesis [19]. The animal models including mice, rats, salamanders, rabbits, and chick embryos have been considered. The advantageous chick embryos have low cost, short observation time, fast growth rate, and clearly visible blood vessels. An angiogenesis assay has been established in chick embryos called chorioallantoic membrane (CAM) assay [20].

This study aims to investigate the angiogenic effect of the combination between ADSCs and SF scaffolds using CAM assay. The ability of SF scaffolds containing ADSCs (SF-ADSC scaffolds) and those without ADSCs (SF scaffolds) was compared in term of the activation of angiogenesis.

## **Research questions and Objectives**

### **Hypothesis**

ADSCs improves the angiogenic potential of the SF scaffolds.

### **Objectives**

- 1 . To characterize and investigate the properties of adipose-derived stem cells.
2. To investigate the salt-leached SF scaffolds as an effective carrier for adipose-derived stem cells.
3. To examine the angiogenic properties of the combination between SF scaffolds and ADSCs.



Figure 1 The graphical conceptual framework in this study.

ADSCs were cultured in appropriated condition and characterized ADSCs by using gene expression, protein expression, differentiated properties and antioxidant properties. Moreover, the physical properties of SF scaffolds need to be considered. These evidences can support the value of SF scaffolds and support *in vivo* testing (CAM assay) of SF scaffolds with/without ADSCs. However, the potential of SF-ADSC scaffolds might apply on wound healing process as well because there might have angiogenic effect to support that process.



**Benefits of this study**

1. The salt-leached SF scaffolds would benefit to activate angiogenesis itself.
2. The combination of ADSCs and SF scaffolds can co-activate angiogenesis.
3. The salt-leached SF scaffolds were reported the irritation, first time, for discovered solid scaffold on CAM.
4. The SF-ADSC scaffolds will be developed into tissue engineer product.



## CHAPTER II LITERATURE REVIEW

### Angiogenesis

Angiogenesis is a process to activate the formation of blood vessels for supplying the oxygen, nutrients and mass to our body [21]. It is used as a fundamental step in the regeneration of tissue damage. It begins when oxygen becomes insufficient called 'a hypoxic state' and hence releases angiogenic growth factors [22]. A vascular network to repair damaged tissues also becomes more complex. This principle plays an important role in tissue repairing and tissue engineering, cell transplantation, and drug development system [23].

There are many experiments on assaying angiogenesis *in vitro* and *in vivo*. *In vitro* assay of angiogenesis, it focuses on proliferation, migration, and tube formation. *In vivo* assay, it only focuses on an animal model for drug development [24].

Interestingly, angiogenesis, an essential event in the repair of tissues, is the process of forming new blood vessels arising from pre-existing ones. According to Ruenn Chai Lai et al., MSC mediated cardioprotective paracrine effect by secreting exosomes. The purified exosomes reduced infarct size in a mouse model of myocardial ischemia and reperfusion injury in a rat model [25].

In addition to oxidative stress, angiogenesis can activate and boost a regeneration system. For example, angiogenesis and neurogenesis are the outstanding contexts in neurological disease, either as pathophysiological factors or as responses to injury. One common growth factor that induces angiogenesis and neurogenesis is vascular endothelial growth factor (VEGF, or VEGF-A), which was identified not only based on its vascular effects but also recognized as an important signaling molecule in the nervous system. [23].

Moreover, the angiogenesis is a supporting process for wound healing. While healing, there is an integration of the complex biological and molecular events of cell migration and proliferation, extracellular matrix (ECM) deposition, angiogenesis, and remodeling. During this stage, the angiogenic factors are activated from cells or biomaterials and are released into the damage site. This is how it boosts the wound healing process [8].

The angiogenesis on various models for testing the drug or biomaterial scaffold have been reported. There are advantages and disadvantages as follows.

Table 1 The advantages and disadvantages of angiogenesis on different models.

Angiogenesis on different models	Advantages	Disadvantages	Reference
Chick embryo (CAM assay)	<ul style="list-style-type: none"> <li>- convenience</li> <li>- flexibility for multi-testing per individual CAM</li> <li>- fast vascular development</li> <li>- no immune response</li> <li>- real-time observation</li> <li>- no requirement for the animal ethics (depend on country)</li> <li>- ease of monitoring</li> <li>- low cost</li> <li>- very fast screening</li> </ul>	<ul style="list-style-type: none"> <li>- repaid change in organs and blood vessels</li> <li>- extreme sensitivity to environmental factors</li> <li>- drug mechanism which is different from that of human</li> </ul>	[26]
Mice/Mouse Mesentery	<ul style="list-style-type: none"> <li>- suitability for intravital microscopy</li> <li>- suitability for molecular activity</li> <li>- enhancement of angiogenesis by sprouting process in the vascular system</li> </ul>	<ul style="list-style-type: none"> <li>- requirement for animal ethics</li> <li>- time-consuming observation</li> <li>- involvement with a lot of technical equipment</li> <li>- ten times quality when using rats as test agents comparing to that when using mice</li> </ul>	[27, 28]
Rabbit's eye test (The Corneal Micro Pocket)	<ul style="list-style-type: none"> <li>- More convenience to observe the rabbit's eye which is bigger</li> </ul>	<ul style="list-style-type: none"> <li>- difficult control in terms of different factors</li> </ul>	[29]



Assay)	than that of a mouse during the experiment	involved in the experiment. - long feeding time - Unavailability to make use of the rest of the rabbit's organs after the eye removal surgery	
--------	--	---	--

However, there are many animal models used for screening the angiogenic drug. From the report, the CAM assay is better than other animal models because there is no immune response. Moreover, in this developmental model, it can discover several teratogenicity agents, screen mechanism for pharmaceuticals, and identify the tumor-related substances caused by angiogenesis. Some of the substances have potential risks to cause tumors while some of them have opposite outcomes which can prevent tumors instead [30].

### Chick embryo development

The development of the chick begins with forming the two parental cells, an egg and a sperm, known as fertilization. After the process, the cell comes to morula stage that divides one cell into 2, 4, 8, 16 and 32 cells. Then, the hundreds of cells are grouped in a small, whitish spot (the blastoderm or germinal disc) that is easily seen on the surface of the yolk.

Embryonic membranes forms within the egg. There are many organs including the yolk sac, amnion, and allantois. These structures can protect the embryo and provide it with nutrients, gas and excretion. For example, yolk sac supplies food to the embryo body. The amnion encloses the embryo to provide the protection. The allantois can be a functional main part that allows the gas to flow through respiratory organs, receives minerals from the shell and handles the waste.

The embryo grows and develops rapidly. Starting at embryonic (E) day 1 to E4.5, it rapidly changes. The heart and blood vessel islands are formed. The wings and feet appear on E17. At this stage, the embryo looks like a bird. After ten days of incubation, the feathers become visible and it is close to be a chick. On E14, the claws are forming, and nearly E21; the embryo moves into the position for hatching. [31].

The stage of chick embryo development before hatching contains many details. A brief information on essential periods is as follows [32].

E1: This stage includes the rapid development of organs, such as alimentary tract, vertebral column, nervous system, head and eyes.

E2: After 24 hours, the embryo starts to form the heart, and in the following 35 hours, its heart begins to beat.

E3: At 60 hours, a nose and wings begin to form

E9 - yolk sac appears and gradually enters the chick's body cavity

E20 - yolk sac completely moves inside the chick's body cavity.

E21 - hatching of chick

After 21 days of incubation, the chick finally begins to escape from the eggshell by using its beak [31].

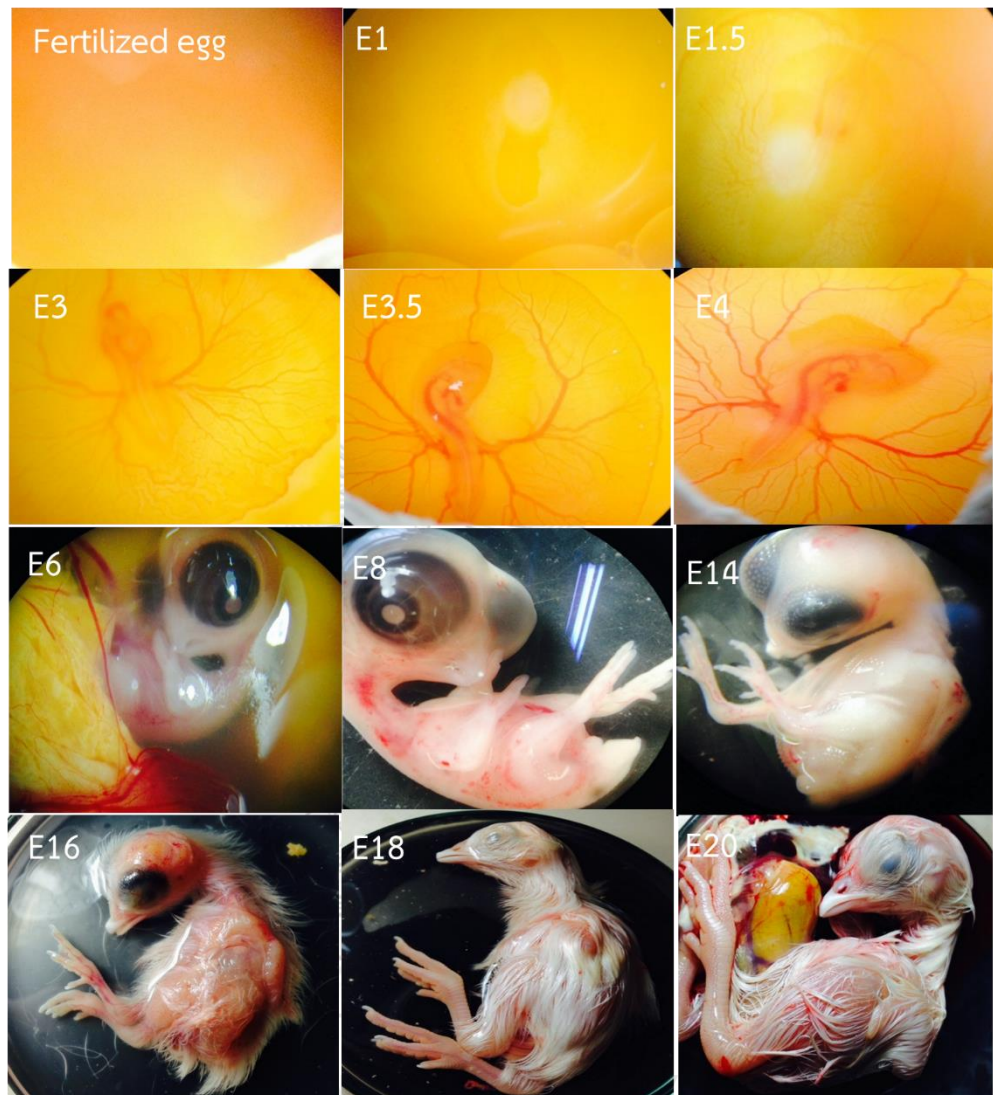


Figure 2 The 21-day development of chick embryo.

The observation of the visible chicken embryo starts from the stage E1, the existence of a fertilized egg. Vascularization is initiated at E3. Chick's organs have developed and become distinguishable since E6 until it hatches at Day 21.

For these applications, animal models are critical components of drug discovery and development. Importantly, chick embryo has been extensively using for cell transplantation, drug screening, tissue engineering, tissue transplantation, angiogenesis, and other cells or cell-free therapeutic applications [33]. There are many models (in vitro, in vivo and ex ovo), such as elbow joint regeneration, limb regeneration [34], cardiac conduction system (CCS) [35], spinal cord injury [36, 37], and angiogenesis [38-40].

The advantage of using the chick embryo is the biological model in terms of rapid growth in its physical development which takes a reasonable time for the observation. In other words, while the chick embryo is naturally developing, manipulation with continued investigation can be conducted in a short period of time. Within the egg, the in ovo chick can be highly controlled and easily set for the experiment. Also, the process includes the low cost and requires no immune response [41].

#### **Chorioallantoic membrane assay (CAM assay)**

CAM is the thin outer layer of chick embryos. It is formed by the fusion of the allantois and the adjacent mesodermal layer of the chorion. The development of vessels starts from embryonic day 4 (E4), expands gradually to a capillary plexus from E8 to E11 [42, 43]. This evidence suggests that the study should focus on drug screening, chick development, biomaterial's properties, angiogenesis molecules, cell metastasis, and microsurgical interventions. [44]. It is also useful to study in a short-term transplantation and drug delivery system [45, 46]. Although the chick embryo is not widely used to discover a new drug, the US-FDA has approved the preclinical aspect by using the chick embryo since 2006 as an alternative method [46], and It is hoped to be a part of testing method for fulfilling the intermediate step between in vitro and preclinical trial [46].

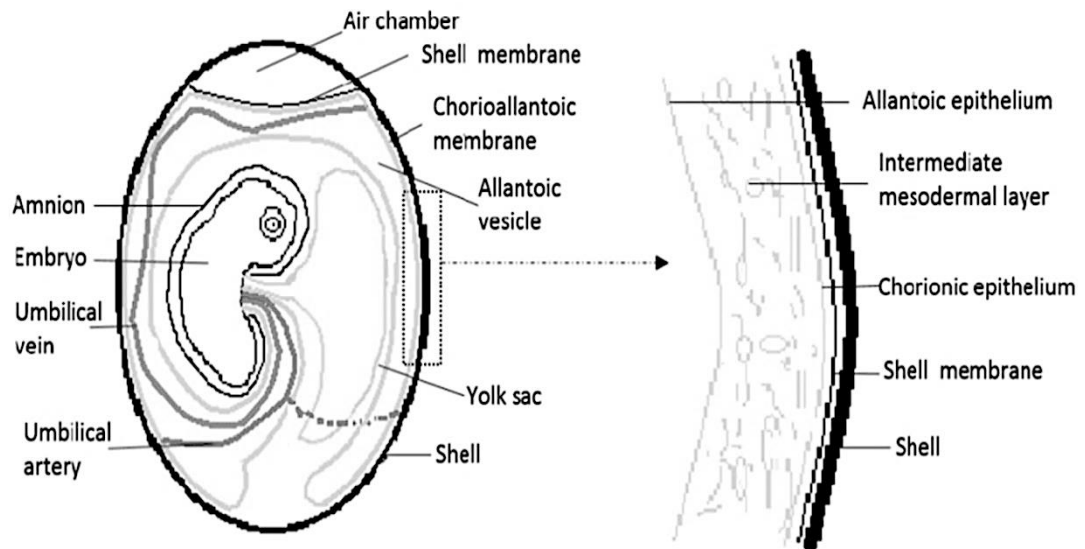


Figure 3 Chorioallantoic membrane (CAM) origin.

The CAM are developed by mesodermal layers of allantoic epithelium and chorionic epithelium. This membrane is created on embryonic (E) day 4 to supply the gas, nutrients, and mass transfer. The composition of CAM covers the chick embryo during the development [15].

CAM assay has many advantages. It is cost-effective, allows extensive scale screening, short experimental assay (days), closed system, multiple tests per individual CAM, and immature immune system. However, there are some limitations, such as rapid morphological changes and short observation periods [38]. Interestingly, the lack of immune response is the advantage of another animal model. We can add anything on CAM, and it can show the angiogenic potential of chemical or drug testing.

CAM has been studied in short-term transplantation and drug delivery system [45, 46]. According to Belen Martinez-Madrid et al., the CAM model provides a useful new approach to study human ovarian tissue transplantation in its first ischemic stages before the establishment of neovascularization.

The regeneration process for injured tissues/organs depends on the renew of blood vessel formation and relates to metabolic support. For example, acellular

brain scaffold can induce a robust angiogenic response, comparable to that of fibroblast growth factor-2 (FGF-2). This result may be considered the angiogenic growth factors [47].

The angiirritation used the HET-CAM (Hen's Egg Test-Chorioallantoic Membrane) assay, which has the same principle as CAM assay. This model is an in vitro alternative to the in vivo Draize Rabbit Eye test that determined the vascular changes in short-term and long-term observation in the CAM [48]. It was referred to an angiirritative effect [49]. This situation replied to the action of hemorrhage, vessel bleeding, and vessel lysis [49, 50]. The qualitative method showed the irritative potential of chemicals. This test was analyzed by irritative score (IS) to show the possible application for innovative chemicals [48] or SF scaffolds (in this case).

Certainly, the angiirritation was first tested in solid SF scaffolds on CAM assay. That is why there must be some evidence or guidelines to support in this study. The OECD TG 405 about alternatives to in vivo Draize rabbit eye and skin irritation tests was selected this paper. The test was conducted with various types of materials, such as liquid, solid and aerosols. The dose level of tested solid form mentioned, "the amount used should have a volume of 0.1 mL or weight of not more than 100 mg" [51].

## Silk fibroin scaffolds (SF scaffolds)

### Structure of SF scaffolds

SF scaffolds are made from Thai *Bombyx mori*. SF Scaffolds contain fibroin, an insoluble-water protein, and sericin, a soluble-water protein. Most composition of SF scaffolds is fibroin consisting of glycine, alanine, and serine leading to antiparallel  $\beta$ -pleated sheet, alpha-helix, amorphous structure, and random coil formation in the fibers [52, 53].

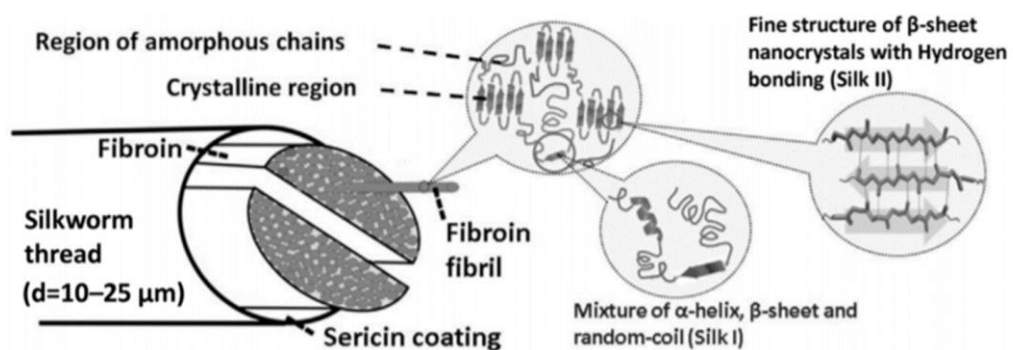


Figure 4 SF scaffolds chemical structure.

There are mainly two components in SF scaffolds, sericin and fibroin. The hydrophilic coat is sericin. The hydrophobic core is fibroin which comprises region of amorphous chain, crystalline region, mixture of alpha-helix,  $\beta$ -sheet and random-coil [52, 53].

SF scaffolds are made from Thai *Bombyx mori*. The main composition of SF scaffolds includes sericin and fibroin. Sericin is a soluble-water protein and acts as the hydrophilic coat. In contrast, fibroin is an insoluble-water protein and is embedded as the hydrophobic core. Most composition of fibroin is glycine, alanine and serine leading to antiparallel  $\beta$ -pleated sheet, alpha-helix, amorphous structure, and random coil formation in the fibers [52, 53].

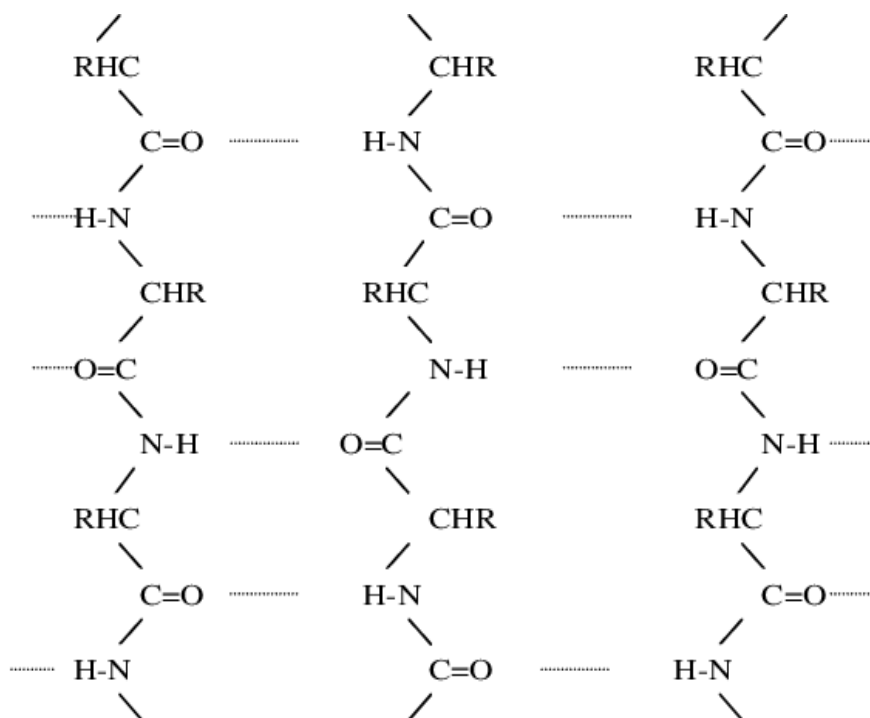
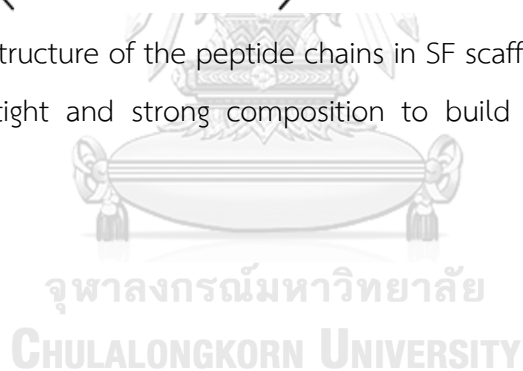


Figure 5  $\beta$ -sheet structure of the peptide chains in SF scaffolds.

This structure is tight and strong composition to build the solid structure of SF scaffolds [52, 53].





### Physical and biological properties of SF scaffolds

There are many kinds of physical and biological properties of biomaterial such as amino acid contents, mechanical properties, water absorption, biodegradable properties, and biocompatibility [54] as follows.

Table 2 The physical and biological properties of SF scaffolds.

Physical properties of SF scaffolds	Description	The reported data
Amino acid contents	The main structure of SF scaffolds from fibroin and sericin	Glycine, alanine and serine [52].
Mechanical properties from scaffolds	SF scaffolds is popular for using the sponge form.	There are highly mechanical properties. For salt-leached scaffolds, they are $355 \pm 38$ kPa [55].
Water absorption of SF scaffolds	The water absorption capabilities of SF scaffold depend on porosity.	No leakage of the cell suspension and good support the cell proliferation and increase DNA content [56, 57]
Biocompatibility of SF scaffold	The biomaterial has no toxicity for normal cells and the degradation product cannot cause of adverse problems for organisms.	The silk fibroin scaffold exhibits a good biocompatibility, it has been made as porous biomaterial in tissue engineering for a long time [6, 58].
Biodegradation of SF scaffold	Theses scaffolds should exit in the body only for a particular time during the healing period.	The degradation product should not affect on cell growth [6, 58].

SF scaffolds were investigated physical properties in terms of the mechanical properties. Shao [59] reported that the mechanical properties of B. mori silk can be produced by strongly artificial reeling and be more extensible than that spun naturally. Moreover, the mechanical property of SF scaffold fulfills the requirement of tissue engineering, as it is better mechanical property than other biomaterials. Because of  $\beta$ -sheet structure given the elasticity, good intensity, and toughness [6, 58].

The water absorption, which is caused by different pore size, is an important role for cell proliferation and cell expansion [57]. These data are for evaluation of cell proliferation and distribution in the silk scaffold. For example, no leakage of the cell suspension, which is a highly desirable feature for cell seeding and growth in the SF scaffolds is a water absorption criterion [57].

The biocompatibility of SF scaffold should be concerned because these properties can distinguish between synthesis polymer and natural polymer. The SF scaffold has been reported that there is no toxicity and no adverse effect to organism. Moreover, the biodegradable is also important issue in term of cell viability and cell growth. The degradation product should not affect on cell growth [6, 58].

Table 3 The composition of SF scaffolds.

Compositions	The percentage composition	Reference
Fibroin	70-80	[53]
Sericin	20-30	
Carbohydrate	1.2-1.6	
Wax matter	0.4-0.8	
Inorganic matter	0.7	
Pigment	0.2	
Totally	100	



Table 4 The amino acid compositions of SF scaffolds.

Amino acid compositions	Percentage of amino acids in fibroin	Percentage of amino acids in sericin	Reference
Glycine	42.8	8.8	[59]
Alanine	32.4	4.0	
Serine	14.7	30.1	
Leucine	0.7	0.9	
Isoleucine	0.9	0.6	
Valine	3.0	3.1	
Arginine	0.9	4.2	
Histidine	0.3	1.4	
Lysine	0.5	5.5	
Aspartic acid	1.9	16.8	
Glutamic acid	1.7	10.1	
Threonine	1.2	8.5	
Phenylalanine	1.2	0.6	
Tyrosine	11.8	4.9	
Proline	0.6	0.5	
Methionine	0.2	0.1	
Tryptophan	0.5	0.5	
Cystine	0.1	0.3	

## SF scaffolds and tissue engineering

Silk fibroin has been widely used as a biomaterial for tissue engineering applications [60, 61]. For example, the advantages of using the SF scaffold for bone regeneration regularly are that it can activate the bone calcification process and enhance bone mineralization [62].

The scaffolds provide surface area for cell adhesion. Their porosity allows enough mass to flow through cells to maintain their lives. Moreover, the degradation product of SF scaffolds may be beneficial to angiogenesis. The previous research reported that cell adhesion was caused by the deposition and remodeling of the extracellular matrix, which could modulate biochemical signaling [63]. Besides, cell adhesion affects cellular function, such as proliferation and differentiation. Thus, it is necessary to study the adhesion characteristic [64]. Another report of SF scaffold for cell adhesion indicated that SF scaffold alone could allow cell attachment even though the amino acid residue needed to be modified for increasing cell adhesion [65].

Secondly, the porosity of the scaffold can support cell proliferation, cell differentiation, cell aggregation, and vascularization of blood vessel formation [66]. It was established that there were some recommendations from articles of porosity range that can be accepted. The porosity was also critical to provide enough prospects and maintain transport, with higher than 100-micron diameter, which is considered a minimum requirement [67].

Interestingly, the experiment of various sizes could be considered. Cells are loaded into various pore sizes of scaffold such as 30  $\mu\text{m}$ , 315-500  $\mu\text{m}$ , and 500-1000  $\mu\text{m}$ . They found that the smallest size was the best cell adhesion although 500-1000  $\mu\text{m}$  scaffolds still showed the cell adhesion from the Live/Dead assay [68].

Thirdly, the degradation products of SF scaffolds activate angiogenesis. The silk fibroin contains a large percentage of glycine, alanine and serine [69-71]. SF scaffold degradation can be due to enzymatically assisted proteolysis, such as by chymotrypsin and carboxylase, which are in CAM [72-74]. Once degraded, these amino acids are resorbed by the surrounding cells. The previous data from immunohistochemistry staining indicated that SF scaffold-degradation products could promote endothelial cell proliferation, as evidenced by the CD34 marker [75].

All SF scaffold properties play a role in tissue engineering because the physical properties of the SF scaffolds above can allow cell attachment. Moreover, when humans and animals get the tissue and organs damaged, human body has much lower regenerative potential than that of amphibians and salamanders [76, 77]. Typically, cells can be transplanted into a new tissue/organ for regeneration. The other technique that is more beneficial than transplanting directly onto the damage site is combining cells and scaffold, which are carriers or homing of the cells to be able to functionalize regeneration by angiogenesis activation. This technique is called tissue engineering [76].

To carry out tissue engineering research, there are three main focuses: cells, scaffolds as biomaterial and compounds. A number of significant data has been discovered shown in a lot of tissue engineering research. This information has been applied for further studies in the fields of tissue engineering and regenerative medicine. This trend has an impact on three-dimensional bioprinting of tissues and organs [77]. 3D bioprinting holds great promise for revolutionizing the field of regenerative medicine. Moreover, 3D bioprinting has been approved for use as tissue replacement by the Food and Drug Administration (FDA) and the European Medicines Agency (EMA) for ten years [76, 77].

Moreover, in terms of tissue engineering and stem cell-based therapy, the idea of utilizing stem cells and tissue engineering to benefit each other has emerged. There can be the system to apply all SF scaffolds with stem cells or cells on CAM assay soon.

### **Stem cell biology**

Stem cell biology has recently been one of the most popular models in terms of biomedical research such as cell therapy, anti-aging, cell transplantation, tissue engineering and regenerative medicine. There is a capacity to self-renew and differentiate into various cell types. [78].

Playing the important roles in regenerative medicine, cell/tissue dysfunction has linked to anti-aging and severe diseases. These properties give rise to the stem cells' capacity for cell-replacement therapies. [79-81].

Stem cells can be classified into two major types which are embryonic stem cells (ESCs) and adult stem cells or somatic stem cells. Embryonic stem cells are

isolated from inner cell mass of blastocysts stage. This stage can develop to all three germ layers: ectoderm, mesoderm, and endoderm [81]. Human's ESCs have the potential to provide tissue transplantation [82] whereas somatic stem cells can generate many organs in the body because they can grow rapidly to be precursor cells or progenitor cells.

In terms of therapeutic application and regenerative medicine, adult stem cells can generate only the same lineage of cell origin. This property is called multipotency. Adult stem cells can develop into more than one cell type but be more limited than pluripotent cells.

Moreover, there is another type of stem cell like ESCs called induced pluripotent stem cells (iPS cells), which are cell reprogramming. The process was reprocessed into pluripotent cells again via adding "reprogramming factors" [81]. We can use this cell to differentiate into any tissues like ESCs. However, there was direct reprogramming from mature cells to target cells by using reprogramming factors as well.

Application to using stem cells is for studying development, regeneration, and tissue engineering. That is pluripotency and self-renewal properties. This potential can be developed in clinical trials and stem-based therapeutics. These tissues have been damaged by diseases or injuries [78]. For Example, bone marrow stem cells are the primary source for using transplantation [83]. Interestingly, stem/progenitor cells are alternative cells to therapeutic angiogenesis because it can be hypothesized that there could be the release of many angiogenic molecules, such as VEGF, FGFs, angiopoietin, and interleukin-6 (IL-6).

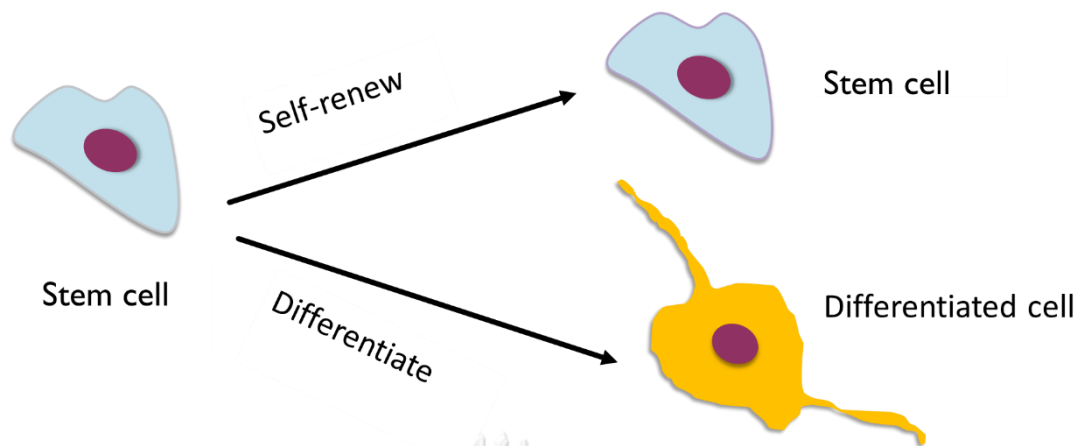


Figure 6 The capacity of stem cell.

The stem cell can self-renew to give the new stem cell and differentiate into the differentiated cell.



## Adipose-derived stem cells (ADSCs)

### Properties of ADSCs

ADSCs are a subtype of somatic stem cells, which can be isolated from the adipose tissue and found in abundance. It can be cultured easily because it can find in many sources of the body. However, there are two sources of ADSCs. One is Visceral fat, which is intra-abdominal fat and located inside the cavity of tissue. The other is subcutaneous fat, which is found under the skin.

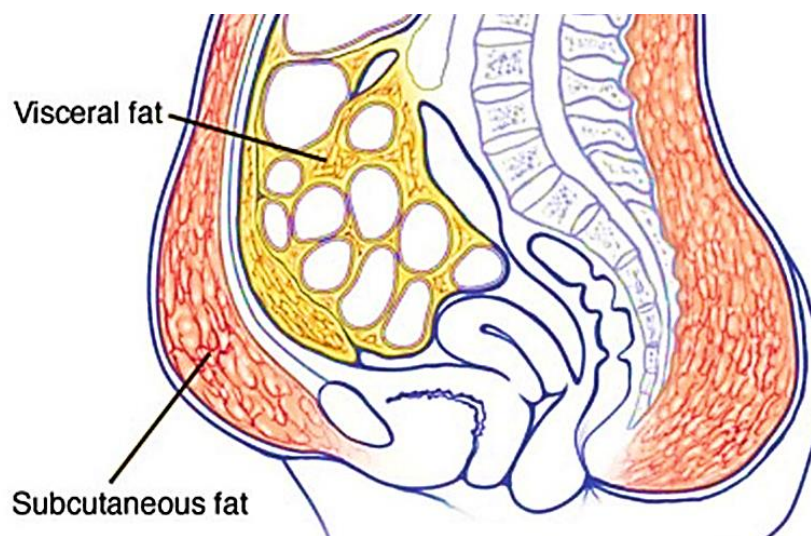


Figure 7 The sources of ADSCs in body.

The visceral fat is inside the organ cavity, dense in between the internal organs. The subcutaneous fat is under skin [84].

There were reports suggesting that ADSCs can be maintained for more extended growing periods by returning to senescence rate. The higher proliferation rate increased differentiation potential [85].

Currently, collagenase enzyme digestion is very popular for isolation method of the ADSCs [86]. After that, they are centrifuged and separated into three layers. The stroma-vascular fraction (SVF) is a part to collect ADSCs [87].

The morphology of ADSCs is fibroblastic under a microscope [88]. ADSCs express the conventional makers that are CD105, CD90, CD73, and CD11 [89].

Additionally, the expression of other markers is found, including SOX2, nestin, and  $\beta$ -III tubulin [90].

The differentiation process is controlled by transcription factors [91]. For example, adipocytes can be regulated by transcriptional and non-transcriptional events that occur in human life [91]. The adipogenesis begins with activation of a couple of key transcription factors, peroxisome proliferator-activated receptor gamma (PPAR- $\gamma$ ) and CCAAT/enhancer-binding protein (C/EBP $\alpha$ ) [92].

The osteogenesis begins with osteoblasts, which are responsible for rebuilding the extracellular matrix and remodeling of osteocytes [93]. The first stage consists of day one to day four, where a peak in the number of cells occurs. Alkaline phosphatase (ALP) is involved in the second stage at E5 to E14. After an ALP level decreases, Collagen type I matrix, which leads to mineralization, will increase. The final stage occurs on day fourteen today to twenty-eight day [93].

### Antioxidant enzyme properties in ADSCs

In recent years, a defense mechanism evidence has developed to protect the free radicals [94]. Many diseases are caused by the accident or physical environment and by cellular internalization effect, oxidant molecules (called radicals or reactive oxygen species (ROS)), and aging [95, 96].

ROS is generated from numerous factors such as pollution, UV light, stress and poor diet. These are main sources of the primary free radical as superoxide ( $O_2^{\cdot-}$ ). Superoxide may occur in one minute to anytime. This free radicals result in the damage in the normal tissue [97].

The cells can overcome oxidant agents if they produce antioxidant enzymes in the cellular reactions such as superoxide dismutase, catalase, peroxidase, glutathione peroxidase, and glutathione reductase [98].

Superoxide dismutase (SOD) is a converting enzyme that changes superoxide radicals to hydrogen peroxide (Equation 1). Three forms of SOD are present in humans. SOD1 was found in the cytoplasm, SOD2 was found in the mitochondria and SOD3 was found in the extracellular part of cells.

Catalase (CAT) is a main enzyme to expose  $H_2O_2$  to  $H_2O$  and  $O_2$ . Therefore, the cellular function is to protect cells from oxidative stress (Equation 2). Moreover, other antioxidant enzymes, such as glutathione peroxidase (GPx), glutathione (GSH), and glutathione reductase (GR) are involved in catalase enzyme reaction.

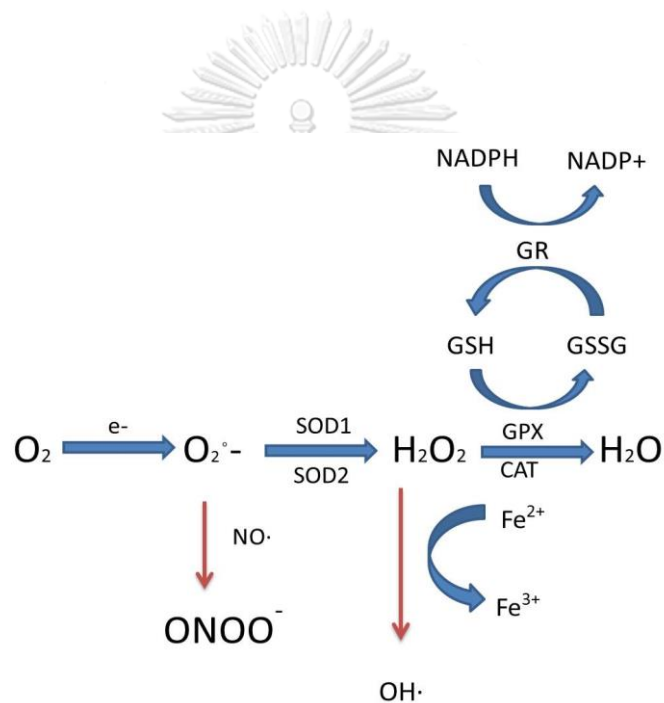


Figure 8 Key reactions and antioxidant enzymes.

This picture presents the relationship for removing radicals from superoxide dismutase (SOD), Catalase (CAT), glutathione peroxidase (GPx), and the molecules called glutathione (GSH) and glutathione reductase (GR), which support the final reaction to change into water and oxygen. The GPXs requires GSH as a cofactor. GR reduces the oxidized form of GSH (GSSG) [99].

The essential cell properties involved in regenerative medicine are antioxidant properties, which counteract the free radicals with cell therapy, stem cell therapy and cell-based scaffold engineering [100, 101]. According to Shiekh, PA, the study of how antioxidant polymers access oxidative stress is a current field of biomaterial research with a massive impact in the field of tissue engineering and regenerative medicine [101].

In this case, antioxidant enzymes of ADSCs need to be considered. Generally, the defense mechanism of action on free radicals normally happens in every cell. However, the comparison of ADSCs and keratinocytes have not been reported [102]. There are many reports on the relationship between ADSCs and other cells such as human epidermal keratinocytes (HEKa cells) and melanocytes [103, 104]. They are essential features for the maintenance of homeostasis of the system in the body and for the cell protection from radicals in the standard system. Therefore, ADSCs should have the same capacity, and ADSCs are expected to be able to decrease radicals or protect themselves from oxidative stress.

## Regenerative medicine

Regenerative medicine should be considered in active biomolecules or compounds that create healing on the damage site. This process is caused by angiogenesis. Cell culture has been what is investigated first for a long time. They secreted growth factors, activated substrate, and other molecules in conditioned media (CM). The CM contains essential substance to activate itself or to protect other cells. The last composition to fulfill the regenerative medicine is biomaterial called SF scaffolds. These data show that stem cells, SF scaffolds and released molecules are key factors to activate angiogenesis.

Nowadays, there are many countries that synthesized the stem cells and their released biological products for regenerative medicine. Since 2008, there have been many organizations related to food and drug administration to approve the Advance Therapy Medicinal Product (ATMP), namely European Medicine Agency (EMA) and United stated food and drug administration (US-FDA). ATMP is classified into four main types which are stem cell products, genetic medicinal products, tissue engineered products and combine therapy medicinal products. [105]. Moreover, in Thailand, there is the regulation following ATMP that allows stem cells to be officially used as a drug. Therefore, the value of tissue engineering products from biomaterial is the capability of enhancing the angiogenesis process. The biomaterial is likely to be approved by Thai-FDA and applied to use in various aspects in the future.

### **The supportive data of extracellular vesicles and their potential**

The trend of research on extracellular vesicles (EVs) is rapidly increasing in the PubMed database. There has been the potential to investigate in many kinds of research and development. [100]. The size and structure of EVs can be identified into two major types, namely microvesicles (MVs) and exosomes [106].

Microvesicles and exosomes, which are secreted from body plasma, bronchoalveolar lavage fluid, breast milk, and urine, have a size of 30 -100 nm diameters and more than 100 nm diameter, respectively. EVs play a role in biological functions [107]. They have ability to transfer transcription factors, surface receptors, and marker proteins. The marker proteins include tetraspanin (CD63, CD81), integrins, Tsg 101, Alix, and heat shock protein (HSP70, 90) [108]. Besides, they contain a range of nucleic acids such as mRNA, microRNA (miRNA), and non-coding RNA (ncRNA), which can affect the translational process in acceptor cells. For example, the recent study of therapeutic in mesenchymal stem cells (MSCs) showed that the paracrine hypothesis introduced a different way to the therapeutic applications of MSCs. Exosomes may also uptake the therapeutic proteins or RNAs into damaged cells [109].

Therefore, this potential might relate to this study because the EVs can be found from ADSCs. This principle of EVs might support one part of the thesis work. However, the investigation into the mechanism of how EVs from ADSCs induce angiogenesis in terms of localization and molecular mechanism will be omitted in this thesis.

## CHAPTER III MATERIALS AND METHODS

### Equipment

- Agilent Carry 60 UV-Vis Spectrophotometer (Agilent, USA)
- Bottle-Top Vacuum Filters (Corning Inc., USA)
- Centrifuge (Allegra X-12R, Germany)
- CO<sub>2</sub> Incubator (Thermo Fisher Scientific, USA)
- Electrophoresis (Bio-Rad Laboratories, Inc, USA)
- Eppendorf Mastercycler PCR (Eppendorf, USA)
- Gel Doc (Bio-Rad Laboratories, Inc, USA)
- Microplate reader CALIOstar (BMG LABTECH, Germany)
- Olympus Ix51 Invert Microscope (Olympus, Japan)

### Materials

- Cell culture 24-well plate (SPL, South Korea)
- Cell culture 96-well plate (SPL, South Korea)
- Cell culture flask 25 cm<sup>2</sup> (SPL, South Korea)
- Cell culture flask 75 cm<sup>2</sup> (SPL, South Korea)
- Cell culture conical tubes (SPL, South Korea)
- Chamber slide (SPL, South Korea)

### Chemicals

- 0.25% trypsin-EDTA (Gibco, New Zealand)
- 2.5 mM dNTP (TaKaRa, USA)
- 3-Isobutyl-1-methylxanthine (IBMX) (Sigma-Aldrich, USA)
- 40 μM oligo-dT (Biobasic Canada, Canada)
- Acridine Orange (Thermo Fisher Scientific, USA)
- Alizarin Red-S (Sigma-Aldrich, USA)
- Ascorbic acid (Sigma-Aldrich, USA)
- β-glycerophosphate (Sigma-Aldrich, USA)
- Dexamethasone (Sigma-Aldrich, USA)
- Dulbecco's Modified Eagle Medium (DMEM; Cat No. 12800-58, Gibco, New Zealand)
- Fetal bovine serum (FBS; IVG10270-106, Gibco, New Zealand)



- Glutathione reductase (Sigma-Aldrich, USA)
- Hoechst33342 (bisBenzimide H 33342 trihydrochloride, Sigma-Aldrich, USA)
- Insulin transferrin selenium (ITS) (Sigma-Aldrich, USA)
- KAPA2G Fast HotStart ReadyMix with loading dye (KAPA biosystem, USA)
- M-MuLV reverse transcriptase (New England BioLab, USA)
- Nitrobluetetrazolium (NBT) (Sigma-Aldrich, USA)
- Oil red O (Sigma-Aldrich, USA)
- Paraformaldehyde (Cat No. P6148, Sigma-Aldrich, USA)
- Penicillin/streptomycin (IVG 15140-122, Gibco, New Zealand)
- TRIzol reagent (Thermo Fisher Scientific, USA)
- Xanthine oxidase (Sigma-Aldrich, USA)



Table 5 Antibody for immunocytochemistry.

Cat No.	Name	Company
AB97959	Rabbit polyclonal antibody to SOX2 100 µg	Abcam
AB6994	Rabbit polyclonal to Von Willorbrand factor 100 µl	Abcam
AB18723	Rabbit polyclonal Double cortin Neuronal marker 50 µg	Abcam
AB27952	Rabbit polyclonal to Nestin Azide free 50 µl	Abcam
MAB1637	Anti-tubulin β III 100 µl	Merck and Millipore
AB9566	Anti-otx2 100 µl	Abcam
A11001	Alexa 488 goat mouse IgG	Thermo Fisher Scientific
A11012	Alexa 594 anti-rabbit IgG	Thermo Fisher Scientific

## Methods

### ADSC cell culture

Normally, ADSCs from lipoaspirates were digested by enzymatic digestion. In this study, Krissanapong Manotham, M.D. isolated liposuction from patients and subculture to send to our research group. [110]. The ethical statement of this protocol was approved by the Ethic Committee of Lerdsin General Hospital, Bangkok, Thailand. ADSCs were cultured in Dulbecco's Modified Eagle Medium (DMEM) (Invitrogen Corporation Company), with 10% (V/V) fetal bovine serum (FBS) and 100 U/ml penicillin and 10 µg/ml streptomycin incubate at 37 °C, 5% CO<sub>2</sub>.

### Trypsinization and freezing of cells

Trypsinization is enzymatic digestion to separate attached cells into a single cell. The cells were trypsinized when the cell reached at 80% density. These media were removed into the waste tube. Then, the cells were added PBS to wash the flask and added 0.25% trypsin-EDTA for 1 ml; incubated at 37°C 5% CO<sub>2</sub> for 3 mins. Next, this flask was stopped the reaction with adding new media 2-3 ml. Then, cells were removed and centrifuged at 1,200 rpm at 4° C for 5 mins. Finally, the cells were cultured in T75 flask and were waited to expand into many flasks.

For the freezing cells, we were added new media with 10% DMSO in complete media 1 ml after centrifugation step, suspended cells, and moved into the new cryovial. They were moved in the cryobox at -80 °C overnight and were kept the cryovial into the liquid nitrogen.

### Characterization of ADSCs by immunocytochemistry

This method is modified from Huaxian Chen and Peng Luan [111]. Briefly, ADSCs P. 12 were seeded to the chamber slide in a small drop and were fixed with 4% paraformaldehyde (PFA); incubated at 20 mins in room temperature, this chamber slide with ADSCs were wash with PBS in 3 times 5 mins each and were added blocking solution containing 3% BSA, 10% FBS and 0.2% Triton X-100 in PBS for 30 mins. The cell was added primary antibody in blocking solution (the ratio was 1:200), as anti-nestin azide free, anti-βIII tubulin.

The cells were incubated at 1 hour in room temperature. The glass slide was washed in PBS in 3 times for 5 mins each. The cell was incubated with a secondary antibody as Alexa 594 goat anti-rabbit and Alexa 488 goat anti-mouse in blocking solution (the ratio was 1:500). Then, the cells were added Hoechst stain solution; incubated for 45 mins. The chamber slide was closed with a coverslip and sealed with nail polish. Finally, a glass slide was detected on an inverted fluorescent microscope. The picture was analyzed by image j software.

#### Adipogenic differentiation

ADSCs passage 12 (5,000 cells/ml) were seed in 24 well plates in DMEM, 10% (V/V) fetal bovine serum (FBS) and 100 U/ml penicillin and 100 µg/ml streptomycin (5 well: 4 well for differentiation and others for control) and were incubated at 37 °C for three days before adding the differentiation media.

For adipogenic differentiation can be induced by culture medium supplemented with adipogenic differentiation media (Table 6). The media were changed every three days. The mature adipocytes were obtained after 18 days of differentiation process. Oil Red-O will be selected to stain the accumulation of lipids.

The mature differentiated cells and undifferentiated cells were fixed with 4% paraformaldehyde (PFA) for 30 mins at room temperature. The fixed cells were washed with PBS.

The mature adipocytes were stained by Oil Red-O dye. The mature adipocytes were incubated at 30 mins in room temperature. The mature adipocytes were stained by Oil Red-O Then, we washed the differentiated staining cells with water until clearly staining the cell. The specimens were observed under an electron microscope and compared with the undifferentiated cells.

### Osteogenic differentiation

ADSCs Passage 12 (5,000 cells/ml) were seed in 24 well plates (5 well: 4 well for differentiation and others for control) and were incubated at 37 °C for three days before adding the differentiation media (Table 7). The media were changed every three days. The mature osteocytes for approximately 15 days. Mineralization of osteocytes was staining with 1% Alizarin Red-S. The control was an undifferentiated cell that used DMEM containing 10% (V/V) fetal bovine serum (FBS) and 100 U/ml penicillin and 100 µg/ml streptomycin.

The mature differentiated cells and undifferentiated cells were fixed with 4% PFA for 30 mins at room temperature and were washed with PBS.

The mature osteocytes were stained by 1% Alizarin Red-S. We selected the mature osteocytes incubated at 45 mins in the darkroom. After incubation, the differentiated cell staining was washed with water until clearly staining the cell. The specimens were observed under an electron microscope and compared with the undifferentiated cells.

Table 6 Adipogenic differentiation reagents.

Adipogenic differentiation	Final conc.
Dexamethasone	1 µM
IBMX	0.5 µM
Indomethacin	100 µM
ITS (Insulin Transferrin selenium)	1%

Table 7 Osteogenic differentiation reagents.

Osteogenic differentiation	Final conc.
Dexamethasone	10 nM
$\beta$ -glycerophosphate	10 mM
Ascorbic acid	200 $\mu$ M

#### Determination of antioxidant enzymes activity

This assay determined the ADSCs properties for removal the ROS in cellular level. All this experiment was use ADSCs passage 14. They were seeded into T75 flask and were incubated at 37°C and 5% CO<sub>2</sub> until confluent.

The controls of antioxidant action were HaCaT. They are representing the major cell type of the top layer of skin, found in epidermis layer. The uppermost layer consists of 90% HaCaT and protects pathogen, antigen, strange chemicals, and infectious agents [112]. HaCaT, which has highly antioxidant enzymes plays a role for protect radicals in the body. The experiment was started form lysis of ADSCs following;

#### Cell lysis

In each antioxidant enzyme activities had different cell lysis conditions. For catalase and glutathione peroxidase activity, cell suspension in 0.5 ml in PBS was added 0.1 mM sodium cholate 0.2 ml and was lysed six times for 10 sec. They were centrifuged at 5,000 g for 10 mins on ice. Then, the cell lysates were removed supernatant in a new tube.

For SOD contents, the cells were added in 50 mM NaHCO<sub>3</sub> buffer pH 10.2. Then, they were sonicated at 2 s 5 times each. They were centrifuged at 10,000 g for 10 mins at 4°C. The supernatant was kept for the activity analysis.

For GSH level, ADSCs were added in 0.1 ml lysis buffer that contain 0.05 %v/v triton X-100 in 0.05 ml, 0.5 mM EDTA in PBS 10 ml. They were Incubated on ice for 10 mins. The solution was sonicated on ice 2 s; followed by added 5% trichloroacetic (TCA) to precipitate protein for 2 s.

Finally, the cells were centrifuged at 10,000 g for 5 mins. The supernatant was analyzed the enzyme activities.

#### Catalase activity

This method modified from Cristofol Vives-Ba uza and Garcia-Arumi [113] briefly; Catalase can change H<sub>2</sub>O<sub>2</sub> to oxygen and H<sub>2</sub>O and detect the decay of H<sub>2</sub>O<sub>2</sub> at absorbance 240 nm. The reaction should have a substrate (H<sub>2</sub>O<sub>2</sub>), 50 mM phosphate buffer pH 7.0, and sample. To use kinetic mode on a spectrophotometer, then determined activity by following equation 3

$$U/g \text{ protein} = \left( \frac{\Delta A}{\text{mins}} - \frac{\Delta A}{\text{minb}} \right) \times \left( \frac{V_t}{V_s} \right) \times \left( \frac{1}{\epsilon} \right) \times \frac{1}{\text{prot} [\mu\text{mol}/(\text{min g prot})]}$$

$$\text{CAT activity} = \left( \frac{\Delta A}{\text{mins}} - \frac{\Delta A}{\text{minb}} \right) \times \frac{725}{\text{prot} [\mu\text{mol}/(\text{min g prot})]} \quad \text{Equation 3}$$

V<sub>t</sub> = total volume (ml) for catalase 2.9 ml

V<sub>s</sub> = sample volume (ml) for catalase 0.1 ml

ε = extinction coefficient

ΔA = different absorbance

Mins = time for sample (min)

Minb = time for blank (min)

Prot = protein concentration

ADSCs in density 1×10<sup>5</sup> cell/ml were seeded in 75 cm<sup>2</sup> culture flask and were incubated at 37°C, 5% CO<sub>2</sub> overnight. The cells were trypsinized by 0.25% trypsin-EDTA solution, centrifuged at 1200 g 4°C 5 mins. Then, they were resuspended in 0.5 ml PBS. The cells can keep in -80°C for making the stock. Then, the cell lysates were added 0.2 ml of cold 0.013% sodium cholate and were sonicated for 10 s, stopped the reaction for 10 s in 6 times, and centrifuged at 12000 g 4°C 10 mins. The supernatant was collected and determined the amount of protein by Bradford assay compared with BSA standard curve.

Before starting the reaction, the blank cuvette containing 2.9 ml of 50 mM phosphate buffer without H<sub>2</sub>O<sub>2</sub>. This blank was reminded to set blank before reaction

starts. Then, the reaction was started by adding 0.1 ml of the cell supernatant (approx. 2–4 mg/ml of protein) to 2.9 ml of the reaction buffer with H<sub>2</sub>O<sub>2</sub>. The range of time was 5 mins in total, 30-s intervals. Finally, the A240 has calculated the activity by using equation 3. (extinction coefficient = 0.04 mM<sup>-1</sup> cm<sup>-1</sup>)

#### Glutathione peroxidase activity

This method was modified from Cristofol Vives-Ba uza and Garcia-Arumi [113] briefly. In this method, oxidized glutathione (GSSG), which produced on the reduction of organic peroxide by GPx, was recycled to its reduced state by glutathione reductase (GR). The reaction mixture was composed following.

The reaction mixture	Volume (ml)
50-mM phosphate buffer pH 7.0	0.1 ml
1-mM EDTA	0.1 ml
5-mM NaN <sub>3</sub>	0.2 ml
1-mM NADPH	0.2 ml
GR (from a stock of 0.312 U/ml)	6.4 ml
5-mM GSH	0.2 ml
sample-containing GPx (1–3 mg/ml of protein).	0.1 ml
phosphate buffer	0.1 ml of blank

The substrate of this enzyme activity assay was 0.2 ml of 0.25-mM H<sub>2</sub>O<sub>2</sub>.

ADSCs were seeded and incubated at 37°C, 5% CO<sub>2</sub> until 80% confluent cells. The cells were trypsinized by 0.25% trypsin-EDTA solution, centrifuged at 1,200 g 5 mins. The cells were counted approximately 10<sup>5</sup> cell/ml. They were resuspended by 1 ml PBS and added 0.013% sodium cholate in cold condition, sonicated cell 10s. Then the solution has stopped the reaction for 10 s in 2 mins and centrifuged at 12000×g 4°C 10 mins. The supernatant is collected and determined the amount of protein compared with a BSA standard curve.

The reaction of this experiment was started with added the reaction mixture above. Then, the reaction mixture was added 0.1 ml of sample (1-3 mg/ml protein) and was set blank by using 0.1 ml of 50 mM phosphate buffer.



The reaction mixture was resuspended gently and incubated at 37° C for 5 mins in the spectrophotometer, added 0.2 ml of 0.25 mM H<sub>2</sub>O<sub>2</sub> for starting the reaction. Last, the decay of NADPH in absorbance 340 nm 5 mins. Calculate absorbance in this equation 4: (extinction coefficient = 6.22 mM<sup>-1</sup> cm<sup>-1</sup>) see derived equation as catalase activity. (Vt = total volume (ml) for GPx in 1 ml.

Vs = sample volume (ml) for GPx 0.1 ml)

$$U/g \text{ prot} = \left( \frac{\Delta A}{\text{mins}} - \frac{\Delta A}{\text{minb}} \right) \times \frac{1.608}{\text{prot} [\mu\text{mol}/(\text{min g prot})]} \quad \text{Equation 4}$$

$\Delta A$  = different absorbance

Mins = time for sample (mins)

Minb = time for blank (mins)

Prot = protein concentration

#### Determination of glutathione level

The cell from -80°C was thawed at the room temperature. Remove the PBS with centrifugation at 10,000 ×g 3 mins 4°C. Then, cells were added lysis buffer 100 µl and were sonicated 2 s time. Then, the 10 µl solution was removed to determine the amount of protein by BSA assay, followed by adding 5% TCA (w/v) 90 µl to precipitate the cells and centrifuged at 10,000 g 5 mins. Finally, the supernatant was determined GSH activity.

In addition. cell lysates were added 10 µl of 0.1 M sodium phosphate buffer containing 1 mM EDTA pH 7.5 90 µl was incubated with 10 U of GR 10 µl, 0.25 mM NADPH 80 µl and 1.5 mM DTNB 10 µl, respectively.

In this process, the enzyme GR catalyzes oxidized glutathione form to reduced form. Then, the reaction mixtures were measured at 405 nm every 30 s 10 mins. Every reaction has occurred in 96- well plate, and the blank were used 0.1 M phosphate buffer contain EDTA pH 7.5. Finally, a standard curve with GSH reduced form was made and calculated the total glutathione from the equation 5 below.

$$\text{Total glutathione} = \left( \frac{A_{\text{blank}} - A_{\text{sample}}}{A_{\text{sample}}} \right) \times 100 \quad \text{Equation 5}$$

#### Determination of SOD contents

This method is modified from VI Sun, et al. [114]. The cell lysate was mixed 100 ml containing 0.3 mM xanthine oxidase 40 ml, 0.6mM EDTA 20 ml, 150  $\mu$ M NBT 20 ml, 400  $\mu$ M  $\text{Na}_2\text{CO}_3$  12 ml and 1 g/l BSA 6 ml, used for the reaction.

The reaction was occurred in quartz cuvette and was determined by spectrophotometer. First, 2.45 ml of the reaction mixture was mixed with 0.5 ml of cell lysate or distilled water or Cu-Zn SOD as a standard enzyme.

The reactions were started with adding xanthine oxidase enzyme to generate superoxide anion, incubated at 25°C for 20 mins. This reaction was in a 15 ml tube. Second, the reaction was stopped by adding 0.8 mM  $\text{CuCl}_2$  1 ml.

Finally, this solution was measured by the absorbance of 560 nm to determine the increase of SOD contents. We observed the reaction by changing the color solution from dark blue to light blue. If cell lysate had SOD contents, the color was turned to dark blue. The activity was calculated by % inhibition followed by equation 6

$$\% \text{ inhibition} = \left( \frac{A_{\text{blank}} - A_{\text{cell lysate}}}{A_{\text{blank}}} \right) \times 100 \quad \text{Equation 6}$$

The reaction occurred when superoxide anion generated by xanthine oxidase (XOD) and form with NBT then form NBT-diformazan complex in blue color. When the system has a SOD, the color was changed into light blue or colorless. If colorless occurs, it may have a high SOD activity or SOD contents. [115]

The SOD contents were calculated from the standard curve of CU-Zn SOD. The SOD contents were showed in the table. Data are presented as mean  $\pm$  SEM (n=3).

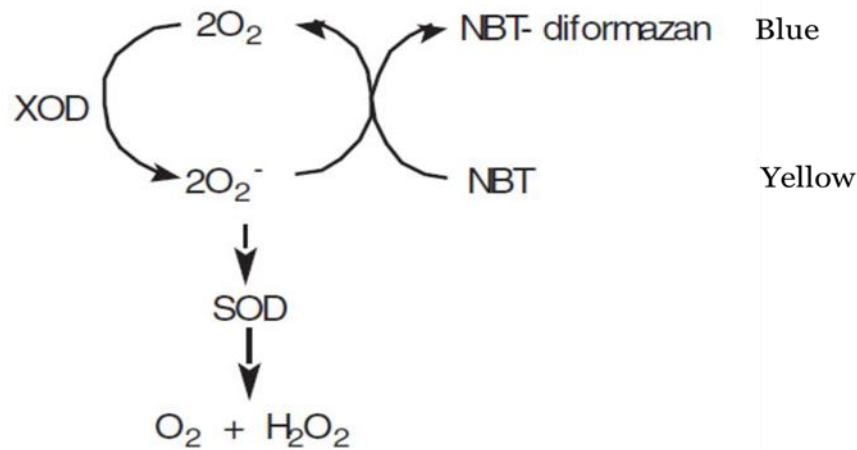


Figure 9 The role of SOD activity in the chemical reaction.

NBT-diformazan complex is dark blue and is in the system without SOD contents. When the system has SOD contents, SOD reduces superoxide anion to hydrogen peroxide and oxygen: see the light blue or colorless. The amount of SOD contents indirectly concentrate color in the system [116].

#### RNA isolation

This method used to determine by gene expression for the characterization of ADSCs and ADSC-EVs. Total RNA from ADSCs and ADSC-EVs were extracted by Trizol reagent 1 ml (Invitrogen, USA) [117]. The solution was mixed with chloroform 0.2 ml/ 1 ml Trizol reagent and followed by centrifugation at 12,000 g for 15 mins at 4°C. The three phases were separately clear; RNA, which in the top phase was collected. Isopropanol was added to RNA precipitation at -20°C for 30 mins, followed by centrifugation at 12,000 g for 10 mins at 4°C. The RNA pellets were washed by 75% ethanol solution 1 ml/ 1 ml Trizol reagent, followed by centrifugation at 7,500 g for 5 mins at four °C. The final pellets were kept dry 10 mins. Total RNA was determined by a spectrophotometer to check the purity of RNA in 260/280 ratio. (The ratio is more than 1.8).

### cDNA synthesis

RNA used for complementary synthesis DNA (cDNA) with 10X reaction buffer, 40  $\mu\text{M}$  oligo-dT (Biobasic Canada, Canada), 2.5 mM dNTP (TaKaRa), RNase inhibitor and M-MuLV reverse transcriptase (New England BioLab, USA). The protocol starts with mixed the reaction mixture containing RNA, 2.5 mM dNTP, 40  $\mu\text{M}$  oligo-dT, and nuclease-free water. The total volume is 16  $\mu\text{l}$ . Then, the mixture was heated at 70°C for 4 mins and was placed on ice immediately. Next, the reaction was added 10X reaction buffer 2  $\mu\text{l}$ , RNase inhibitor 1  $\mu\text{l}$ , and M-MuLV reverse transcriptase 1  $\mu\text{l}$  into the previous reaction mixture. The mixture was incubated for 42°C for 1 hour and inactivated enzyme at 90°C for 10 mins. Finally, the tube was placed on ice or was cooled down the mixture until 4°C.

### Polymerase chain reaction (PCR) and agarose gel electrophoresis

PCR is a technique used in molecular biology to amplify a few copies of a piece of DNA, generating thousands of millions of copies of a DNA sequence. This method has been needed to check the gene expression of new markers.

The reaction mixture was prepared in a PCR tube. cDNA was used as a template for PCR amplification using KAPA2G Fast HotStart ReadyMix with loading dye (KAPA biosystem). 10  $\mu\text{M}$  forward and reverse primer were added into the reaction mixture. The reaction was amplification in Thermocycler for 35 cycles of 3 mins at 95°C for initial denaturation, 15 s at 95°C for denaturation, 15 s at 54.4°C for annealing, 2 mins at 72°C for extension and 72°C for the final extension after 35 cycles. Then, agarose gel was prepared by weight 0.75 g of agarose powder and added 1X TAE or 1X TBE buffer 50 ml. Then, a gel solution was heated by a microwave oven until a clear agarose solution.

For sample loading, 3-5  $\mu\text{l}$  of sample and Ladder 2-3  $\mu\text{l}$  were dropped in a gel. Run the PCR product on 1.5% agarose gel electrophoresis 90 volts for 50 mins. Finally, the gel was stained with ethidium bromide for 5 mins and de-stained gel with water for 5-10 mins.

Primers used in this study (PubMed)

Markers	Forward primer (5' →3')	Reverse primer (5' →3')
Nestin	AACAGCGACGGAGGTCTCTA	CCTTTCCCAGGTTCTCTTCC
β-III tubulins	AGCTGGTGGAAAACACGGAT	ACGTTGTTGGGGATCCACTC
CD 105	AGAGGTGCTTCTGGTCCTCA	AGTTCCACCTTCACCGTCAC
CD 90	GACCCAGTGAAGATGCAGGT	GGTGGACACGAGGACAGATT
Stro-1	AGAGCCAACGTCAAGCATCT	CAGGGGGACCATTACACATC
GAPDH	CCACATCGCTGAGACACCAT	AAATGAGCCCCAGCCTTCTC

### Therapeutic potential of ADSCs

#### Ethic statements

All experimental animal procedures were approved by Chulalongkorn University Animal Care and Use Protocol (CU-ACUP), Faculty of Pharmaceutical sciences, Chulalongkorn University (no. 1633008).

All experimental human procedures were approved by the Ethic Committee of Lersin General Hospital (Permit number IRB 019/2560).

#### Chick embryo incubation and windowing

Fertilized eggs (White leghorn) were obtained from Kasetsart University. They were incubated in an incubator at 39 °C. Then, the eggs were incubated on 3 days. They were windowed their eggshell and were removed the albumin (2-3 ml). Then, we closed the space with Scott tape.

For the chick windowing process, this chick embryos were increased the space to start the experiment and to check the chick life. This stage (E3) can calculate the survival rate of chick embryo. The process started incubated until the described Hamburger and Hamilton (HH) development stage in incubator at 39 °C and 70% humidity. Chick eggs windowing were performed when reach the HH stage 18 (3-day incubation).

#### Fabrication of salt-leached SF scaffolds

Silk fibroin solution was prepared from cocoons of Thai silkworms *Bombyx mori* (kindly provided by Queen Sirikit Sericulture Center, Nakhonratchasima province,

Thailand). Briefly, the cocoons were degummed by boiling for 20 mins in aqueous solution of 0.02 M  $\text{Na}_2\text{CO}_3$  to remove the sericin. Silk fibers were retrieved from the solution and washed three times with deionized water. The degum process and washing were repeated once more. The resulting fibers were then dissolved in aqueous 9.3 M LiBr for 4 h at 60 °C. Next, the solution was dialyzed for 3 days against deionized water using dialysis tubing (MWCO 12,000-16,000, Viskase Company Inc, Japan) [118]. The dialysate was centrifuged, and the supernatant was used to make the non-porous SF scaffolds. The porous scaffolds were prepared using NaCl as a porogen [118, 119]. Briefly, 7 g of NaCl was added to the dialysate solution in container. The salt was removed by stirring for 3 days in deionized water. The dry weight after fabrication was 8.22 g on average. For all the experiments, the porous SF scaffolds, in our study, used in terms “SF scaffolds” were cut in 5 x 5 x 2 mm, and were sterilized under the UV light overnight in laminar flow cabinet.



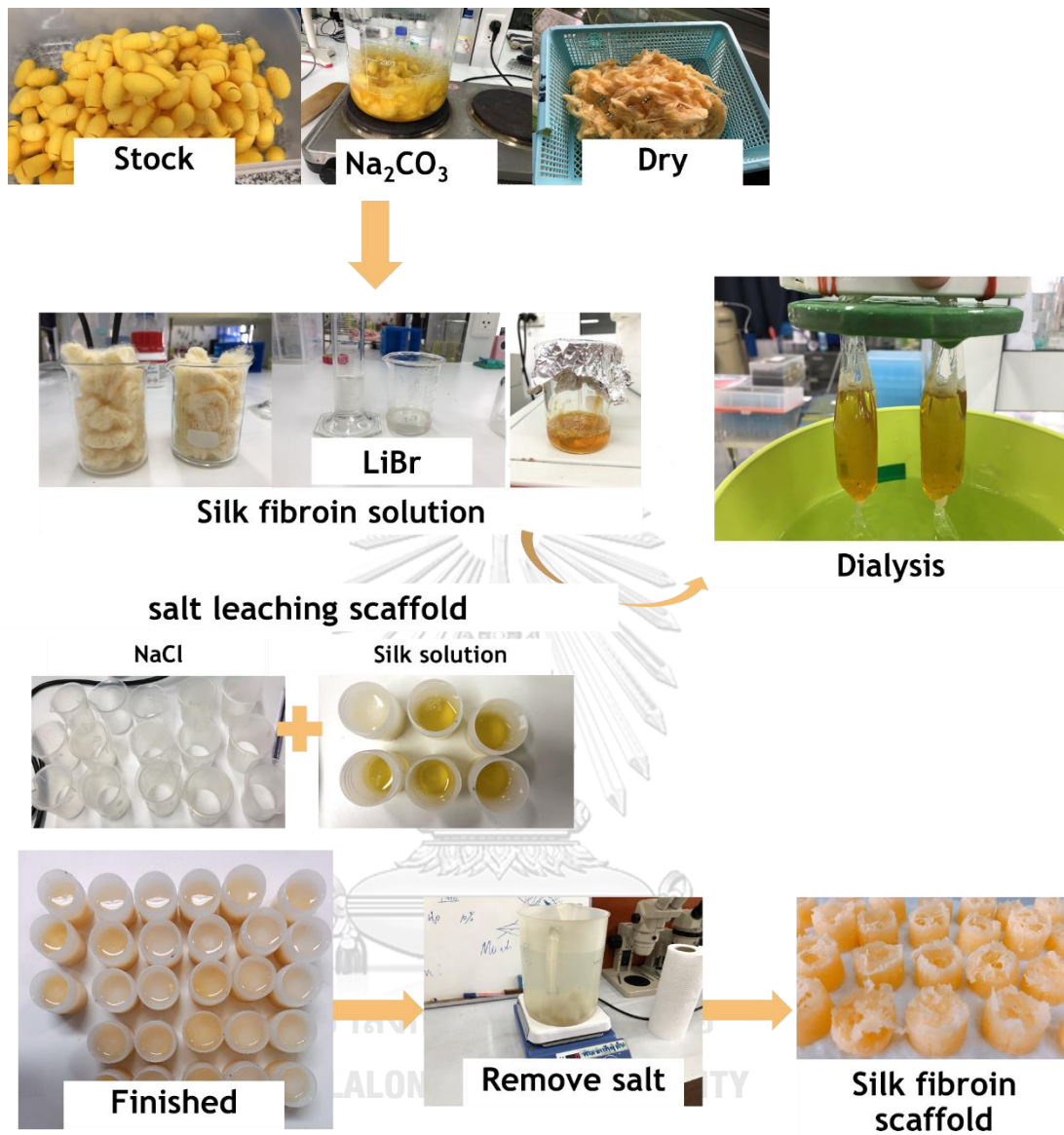


Figure 10 Fabrication of salt-leached SF scaffolds from Thai Bombyx mori.

Silk stock was mixed with  $\text{Na}_2\text{CO}_3$  and dried to obtain silk fiber. Silk fiber was then dissolved with LiBr to make silk fibroin solution. To remove LiBr, silk fibroin solution was subjected to dialysis. NaCl, which was used as a salt for making salt-leached porous SF scaffolds, was incubated with dialyzed silk fibroin solution at 60 °C. Finally, the SF scaffolds were washed with water for several days in order to remove NaCl.

### Scanning electron microscope (SEM)

The SF scaffolds (size 5 x 5 x 2 mm) was visualized by scanning electron microscope (JSM-IT500HR, JEOL, USA). SF scaffolds were glued on a copper plate and sputtered with gold before SEM imaging. The pore diameters of scaffolds were measured by Image J software [120].

### Physical properties of SF scaffolds

These physical properties can support the porosity and solubility of SF scaffolds. This SF scaffolds might support the angiogenic properties so far.

#### Porosity liquid substitution

The porosity of the SF scaffolds (5x5x2 mm) was measured by liquid displacement. Hexane was used as the displacement liquid as it permeates through the SF scaffold without swelling or shrinking the matrix [121]. This test also selected filter paper to test the porosity. The SF scaffolds and filter papers (N=5) (dry weight, W) were immersed in hexane 1 ml for 5 mins (W1). Then, SF scaffolds with hexane were weighed (W2). Finally, the SF scaffold was removed and weighted remaining hexane (W3). The porosity of SF scaffolds can calculate followed.

$$\% \text{ porosity of SF scaffolds} = \frac{W1-W2}{W2-W3} \times 100 \text{ Equation 7}$$

W1 = Weight of hexane 1 ml

W2 = Total weight of SF scaffolds with hexane

W3 = The remaining weight of hexane



### Gel fraction

This method is needed to determine the weight loss after dissolving with deionized water. Firstly, SF scaffolds (5x5x2 mm) (N=5) were weighted and recorded (W0). Then, SF scaffolds were brought into 1 ml of deionized water and incubated at 37°C 24 hours. Secondly, the remaining SF scaffolds after incubation were dried and weighted dry SF scaffolds (W1). Finally, The SF scaffolds were calculated followed. [122];

$$\% \text{ weight loss of SF scaffolds} = \frac{W_0 - W_1}{W_0} \times 100 \text{ Equation 8}$$

W0 = The starting weight of SF scaffolds

W1 = The dry weight after incubated with deionized water 24 hours

### Preparation of SF-ADSC scaffolds

The effect of ADSC (Passage 20-22) on SF scaffolds is observed. The method is followed by Nai-ChenCheng et al. [123]. SF scaffold was put on 24 well plate with culture media (DMEM, 10% FBS and 1% antibiotic); called prewet SF scaffolds.  $10^5$  cells of ADSCs were seeded on SF scaffolds. Then, SF-Ad scaffolds were incubated for 3 days before they were removed on CAM.

### MTT assay

The effect of SF scaffolds on ADSCs viability was performed by MTT assay. The SF scaffolds were pretreated with culture media for 24 hours. Subsequently, the scaffolds were incubated in 24-well tissue culture plates with ADSCs (PASSAGE14) at a density of  $5 \times 10^4$  cells/scaffold. The SF-ADSC scaffolds were incubated at 1, 2 and 3 days at 37°C, 5% CO<sub>2</sub> in an incubator. The solution of MTT was added to each well and was incubated for 3.5 hours at 37°C in a culture hood. At each time point, the media was removed carefully and added DMSO followed by agitation in a shaker for 15 mins. The absorbance was measured at 570 nm using a microplate reader [124].

### Fluorescent staining of SF-ADSC scaffolds

This technique modified from Aneesia Varkey et al, 2015 [125]. SF scaffolds (2 mm thick, n = 3) was pretreated with culture media on 24 well plate for 24 h. Later, cell-seeded scaffolds ( $1 \times 10^5$  cell/scaffold) were incubated at 3 days. The SF-ADSC scaffolds were stained with  $1 \mu\text{g}/\mu\text{l}$  Hoechst and 0.67 mM Acridine orange. The cell-seeded scaffolds were observed under an inverted phase contrast fluorescence microscope.

### CAM assay

The SF-ADSC scaffolds (From P. 22,  $1 \times 10^5$  cells/scaffold, N= 5), which pretreated followed protocol above were placed on the CAM at E8. All groups were monitored every 24 hours by photograph under a stereomicroscope (Micro instruments LTD., Long Hanborough, Oxford, UK).

For angi irritation test, this assay modified from P. Wutzler et al. This testing has been selected for the potential of substances on irritation. The samples were divided into three groups (n = 5 each) containing SF scaffolds, 0.1 M NaOH as a positive control, and 0.9% NaCl as a negative control.

The experiment was starting on E10 of incubation. The liquid tested was used 100  $\mu\text{l}$  to apply on CAM (this test called HET-CAM assay). The irritation time, after dropped or put liquid/solid tested was started observation within 5 mins. The data of vessel hemorrhage, vessel lysis, and coagulation were photographed under a stereomicroscope [126].

The appearance data of vascular hemorrhages, vascular lysis or vascular coagulation as morphological criteria to the test scaffolds were then used in the following equation: [50]

$$\text{Irritation score (IS)} = \left( \frac{301-t(h)}{300} \right) \times 5 + \left( \frac{301-t(l)}{300} \right) \times 7 + \left( \frac{301-t(c)}{300} \right) \times 9 \quad \text{Equation 9}$$

T indicates the time of stopping each process (recorded in sec.)

h indicates vascular hemorrhage,

l indicates vascular lysis,

c indicates vascular coagulation.

After calculation, the value of IS was showed between 0 and 21.

Moreover, the researcher was grouped the IS scored to categorized 0 to 3 depended on the level of irritation, there were categorized four ranges followed.

0 = no irritation (IS = 0.00 – 0.90)

1 = slightly irritation (IS = 1.0 – 4.9)

2 = moderate irritation (IS = 5.0 – 8.9)

3 = strong irritation (IS = 9.0 – 21.0)

#### Angiogenic scoring

The photograph was taken with digital camera and analyzed by giving the score from blind method [127]. This score represents the intensity of blood vessels under a stereomicroscope after put SF scaffolds with/without ADSCs from day 8 to day 18 (10-day observation) by given the score with blind people.

This score can be divided into 0 to 5 depended on the blood vessel density, spoked-wheel pattern and blood vessel branching. The given score, in this study, is modified by [128].

0 describes no changed from day 8 to day 18

1 indicates a slightly increase of blood vessels density

2, 3, 4 and 5 indicate a gradual increase in a vessel density and vessel branching. [128].

#### Histological section

After ten days of incubation, at E18, the CAM was fixed with 4% paraformaldehyde for three hours at room temperature. Then, the fixed SF scaffolds with CAM was cut and photographed under a microscope by a digital camera. Finally, The sections were kept at 4 °C for cryostat machine (Leica CM 1800 Cryostat, Singapore) [115]. The fixed scaffolds were added 30 % sucrose and were placed at 4 °C for 48 h. Samples were then processed for cryostat sectioning. 40 µm of sections were prepared by cryostat machine. The photographed was taken by digital camera.

### Statically analysis

All statistical analyses were performed using IBM SPSS statistics 22. Parametric One-Way ANOVA with post-hoc; Duncan were used to compare two set of samples. For angiogenic scoring, data were expressed as mean  $\pm$  standard error of the mean. P value < 0.05.



## CHAPTER IV RESULTS

### The characterization ADSCs was determined by RT-PCR and immunocytochemistry

Utilizing stem cells and their bioactive cargos for clinical application requires evidence of phenotypic properties, differentiation capability, and potential for therapeutic use.

The characterization of ADSCs displays a fibroblastic morphology at early passages and change to apoptosis or old age morphology in passage no. 30. Protein expression of ADSCs is studied by immunocytochemistry technique and visualized under a fluorescent microscope. ADSCs expressed some neural protein markers,  $\beta$ III tubulin and Nestin.

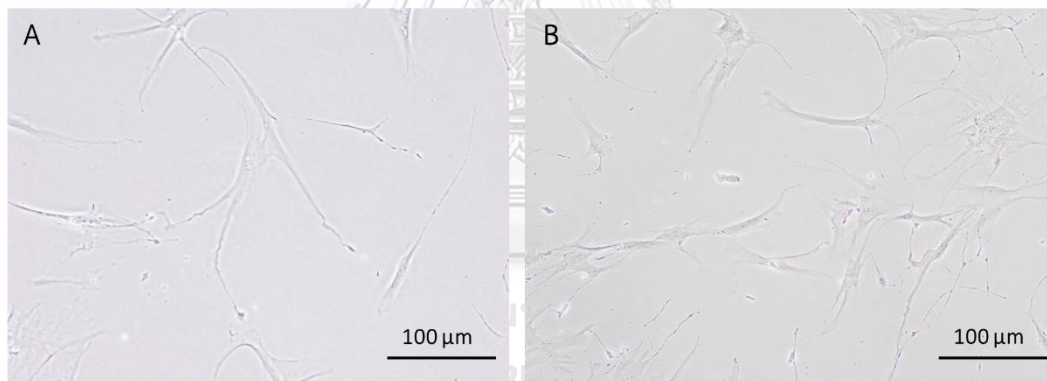


Figure 11 The morphology of ADSCs.

A) indicates the early passage of ADSCs passage 3 showed fibroblastic shape. and B) indicates the aging cells or apoptosis cells are different shape in magnification = 20X at passage 30.

The characterization of ADSCs needs to be considered before we started the experiment. The selected technique for characterization was RT-PCR and immunocytochemistry.

Firstly, RT-PCR was identified as the gene level of ADSC markers such as CD105, CD90, and stro-1. They also expressed the neuron-specific markers such as  $\beta$ -III tubulin and nestin. However, the band of each gene expression was different in intensity.

Secondly, in the protein expression of ADSCs were showed  $\beta$ -III tubulin and nestin expression by immunocytochemistry.



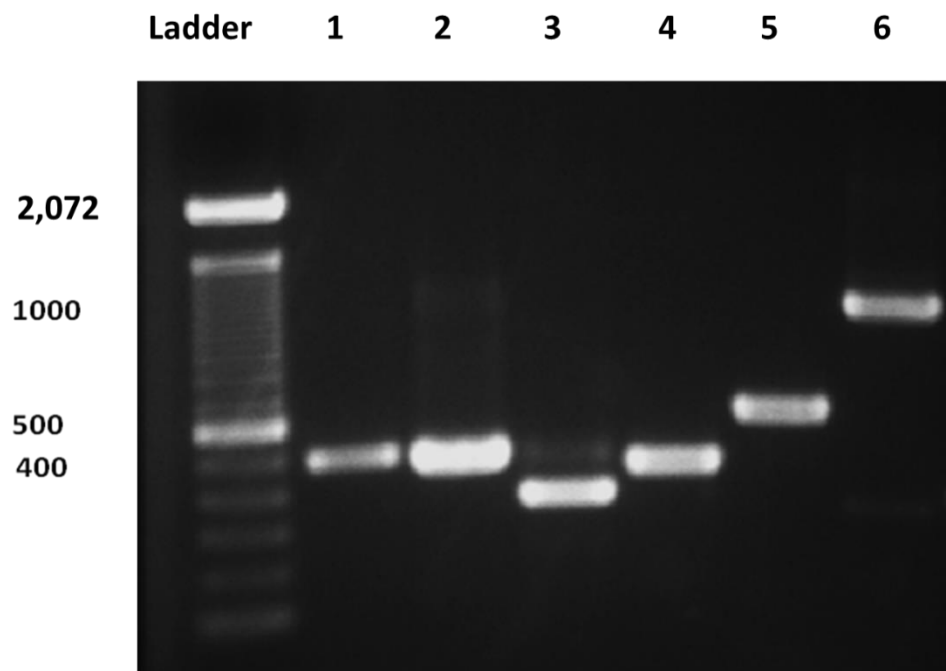


Figure 12 Gene expression of ADSC from RT-PCR.

1) indicates nestin, 2) indicates  $\beta$ III tubulin, 3) indicates GAPDH, 4) indicates CD 105, 5) indicates CD 90 and 6) indicates Stro-1.

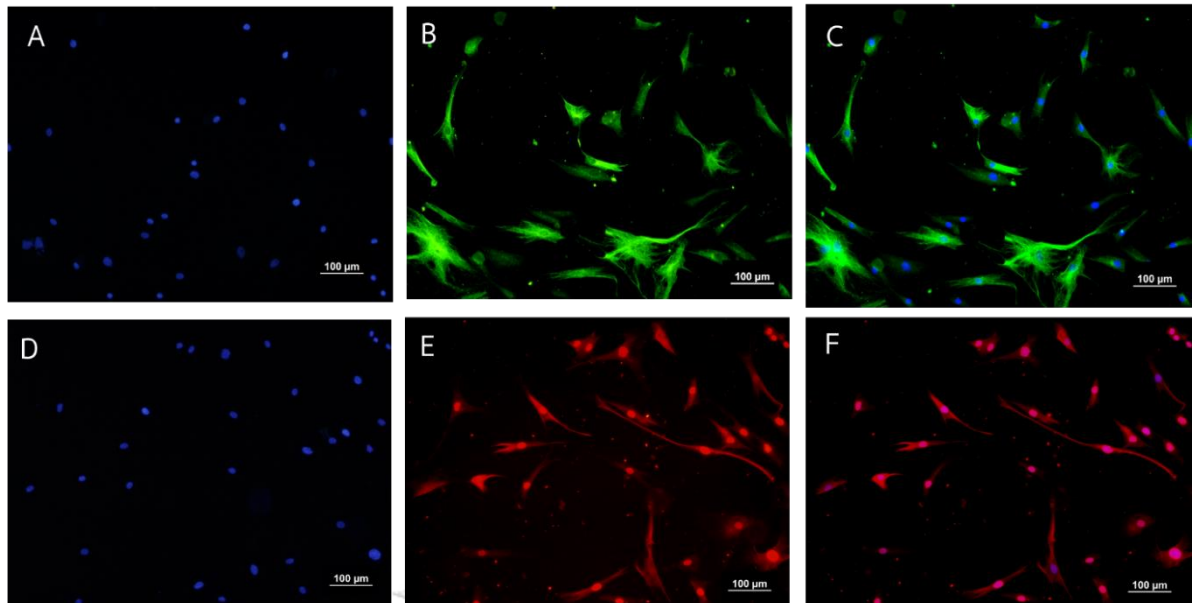


Figure 13 Protein expression of ADSCs by Immunocytochemistry.

It reveals protein marker expression of ADSCs. A) indicates Hoechst staining B) indicates the  $\beta$ III-tubulin expression C) indicates the merge picture of Hoechst nuclear staining and  $\beta$ III-tubulin, D) indicates Hoechst staining E) indicates the nestin expression and F) indicates the merge picture of Hoechst nuclear staining and nestin. Blue spots indicate Hoechst, Red spots indicate nestin, Green spots indicate  $\beta$ III tubulin. Scale bar indicates 100  $\mu$ m.



### Differentiation capacity of ADSCs

Cell differentiation is the process by which cell changes from one cell type to more specific cell types. ADSCs can differentiate into three main kinds of cells, such as adipocytes, osteocytes, and chondrocytes, by adding the growth factors [91]. We can see the accumulated off lipid droplet on day 10. At the end of the experiment, the result showed that adipocytes were enriched with the lipid droplets, which can see the white spot within the cells on day 18. Then, Oil Red-O staining was detected lipid or triglyceride in ADSCs after day 18 compared with undifferentiated cells. The lipid droplet displayed in vacuoles.

The result from osteocytes was starting the packed cells on day seven, and then, they enriched with calcification on day 15. Staining Alizarin Red S was detecting the mineralization process of osteoblasts, which can see the red group of cells. They proliferated rapidly and formed tightly packed colonies.

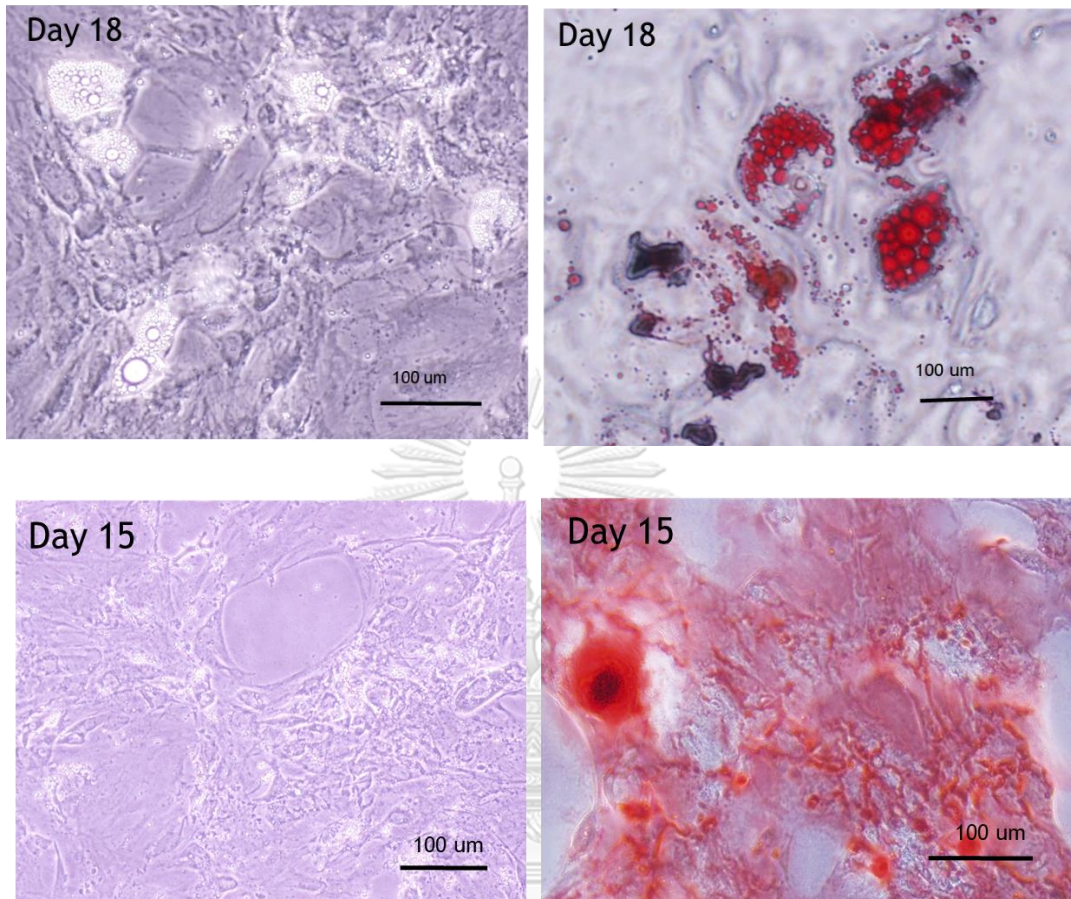


Figure 14 Differentiation capacity of ADSCs.

The top row represents adipogenic differentiation of ADSCs on day 18 and stained oil Red O on day 18 as well. The bottom row represents osteogenic differentiation of ADSCs and stained Alizarin Red-S on day 15. The scale bar indicates 100  $\mu$ m.

### **ADSCs have antioxidant enzymes in non-induced condition**

Antioxidant enzymes were determined by kinetic spectrophotometry assay as the previously described method. We were interested in many antioxidant enzymes such as CAT activity, SOD contents, GPx activity, and GSH level.

In this experiment, we want to use the positive control cells that were HaCaT cells. The most researcher usually used as a positive control because this is the first layer of protection against the toxic environment. HaCaT plays a role in defending itself from radicals higher than other cell types. [129].

Firstly, the decomposition of  $H_2O_2$  determined by catalase activity. The decay monitors the change in  $H_2O_2$  concentration in absorbance at 240 nm. This assay is modified from C. Vives-Bauza, et al [113]. CAT activities of ADSC was significantly lower than the activity of HaCaT lysates.

The total intracellular GSH levels were measured by enzymatic recycling assay. This assay was modified from H. Chirdchupunseree et al. [130] GSH, which is a substrate in GPx activity have been measured, and the GSH levels in ADSC lysate was lower than in HaCaT.

GPx converts  $H_2O_2$  to water and oxygen, the same as CAT. In our result, the trend of GPx activity was directly the same as catalase. It was confirmed that CAT and GPx are co-ordinated enzymes. They are an essential protective role in cellular damage.

SOD contents were represented as SOD enzyme to assert to the SOD level in cellular tissue. The result showed that ADSC lysates were not significantly lower than the SOD contents of HaCaT lysates. Therefore, ADSCs have antioxidant enzyme properties to protect their cell life.

Table 8 CAT activity (U/g protein) compare between ADSCs and HaCaT cells.

Cell types	CAT (U/g protein)			
	N1	N2	N3	Mean $\pm$ SEM
HaCaT	48.744 $\pm$ 0.04	63.924 $\pm$ 1.30	63.874 $\pm$ 8.72	58.847 $\pm$ 5.05
ADSCs	13.704 $\pm$ 0.02	4.195 $\pm$ 0.41	6.125 $\pm$ 0.16	6.980 $\pm$ 1.90

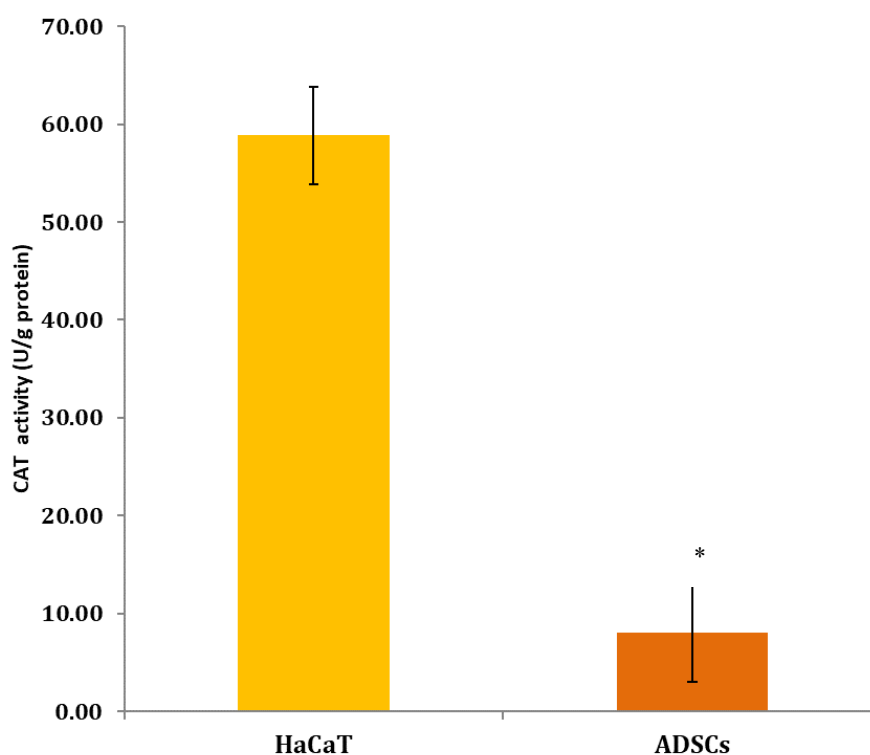


Figure 15 CAT activity in HaCaT and ADSCs lysates.

Non-treated HaCaT and ADSCs were lysed in PBS added 0.1 mM sodium cholate buffer. CAT activity in cell lysates were measured by spectrophotometry method. Data are presented as mean  $\pm$  SEM (n=3). P-Value < 0.05 compared with HaCaT.

Table 9 GSH level ( $\mu\text{M}$ ) compare between ADSCs and HaCaT cells.

Cell types	GSH level ( $\mu\text{M}$ )			
	N1	N2	N3	Mean $\pm$ SEM
HaCaT	$2.93 \pm 0.42$	$2.57 \pm 0.34$	$1.45 \pm 0.19$	$2.32 \pm 0.32$
ADSCs	$1.45 \pm 0.01$	$2.40 \pm 0.00$	$1.93 \pm 0.01$	$1.93 \pm 0.01$

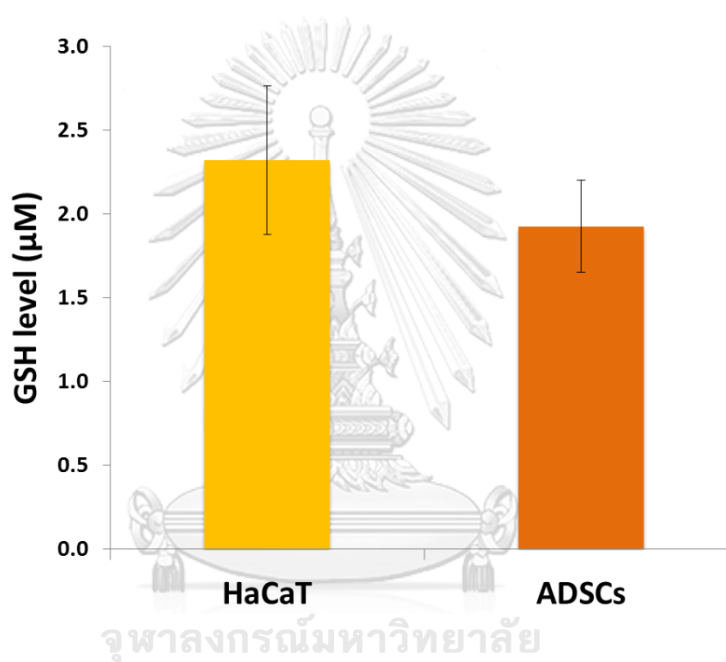


Figure 16 GSH level in HaCaT and ADSCs lysates.

Non-treated HaCaT and ADSCs were lysed in 0.05 %v/v triton X-100 in 0.05 ml, 0.5 mM EDTA in PBS buffer. Levels of GSH in cell lysates were measured by spectrophotometry method. Data are presented as mean  $\pm$  SEM (n=3).

Table 10 GPx activity (U/g protein) compare between ADSCs and HaCaT cells.

Cell types	GPx activity (U/g protein)			
	N1	N2	N3	Mean $\pm$ SEM
HaCaT	3.97 $\pm$ 0.57	3.69 $\pm$ 0.55	3.20 $\pm$ 0.27	3.97 $\pm$ 0.46
ADSCs	3.68 $\pm$ 0.51	2.75 $\pm$ 0.74	3.68 $\pm$ 0.57	3.68 $\pm$ 0.58

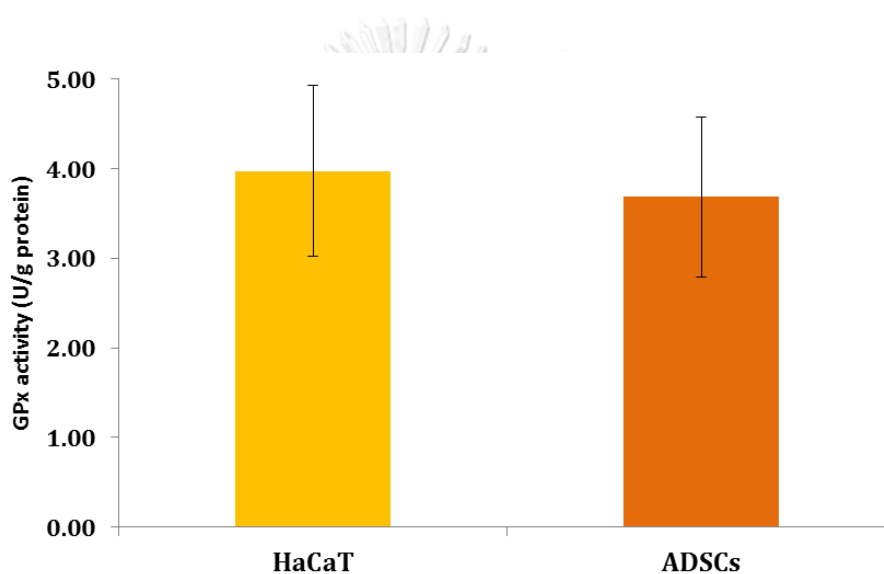


Figure 17 GPx activity in HaCaT and ADSCs lysates.

Non-treated HaCaT and ADSCs were lysed in PBS added 0.1 mM sodium cholate buffer. The activity of GPx in cell lysates were measured by spectrophotometry method. Data are presented as mean  $\pm$  SEM (n=3).

Table 11 SOD contents (ng/ ml) compare between ADSCs and HaCaT cells.

Cell types	SOD contents (ng/ml)			
	N1	N2	N3	Mean $\pm$ SEM
HaCaT	2.77 $\pm$ 0.08	3.03 $\pm$ 0.01	1.45 $\pm$ 0.16	2.42 $\pm$ 0.07
ADSCs	2.97 $\pm$ 0.27	0.77 $\pm$ 0.27	2.63 $\pm$ 0.27	2.12 $\pm$ 0.27

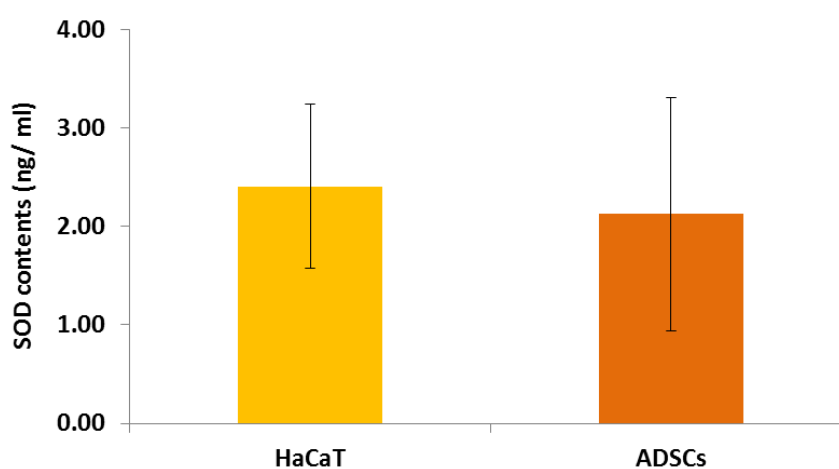


Figure 18 SOD level in HaCaT and ADSCs lysates.

Non-treated HaCaT and ADSCs were lysed in 50 mM NaHCO<sub>3</sub> buffer pH 10.2. Levels of SOD in cell lysates were measured by spectrophotometry method. Data are presented as mean  $\pm$  SEM (n=3).

### **Filter paper with ADSC Passage 24 has not significantly different angiogenesis**

Even though the filter paper was trendy to study angiogenesis, we cannot find the absorptivity of filter paper after seeded ADSCs. We also found the ADSCs moved out from filter paper (white sheet around filter paper). When we flip the filter paper on E11 to see the blood vessel penetrate inside and determine the branching of blood vessels, there was not showing any change of blood vessels. Moreover, conditioned media from ADSC in serum-free media cannot induce angiogenesis as well.

Moreover, the flipped-filter paper of CAM assay was showed on E11. There were not penetrated inside the material and not appeared the branching and intensity of blood vessels. Therefore, this material cannot use as a material for tissue engineering.





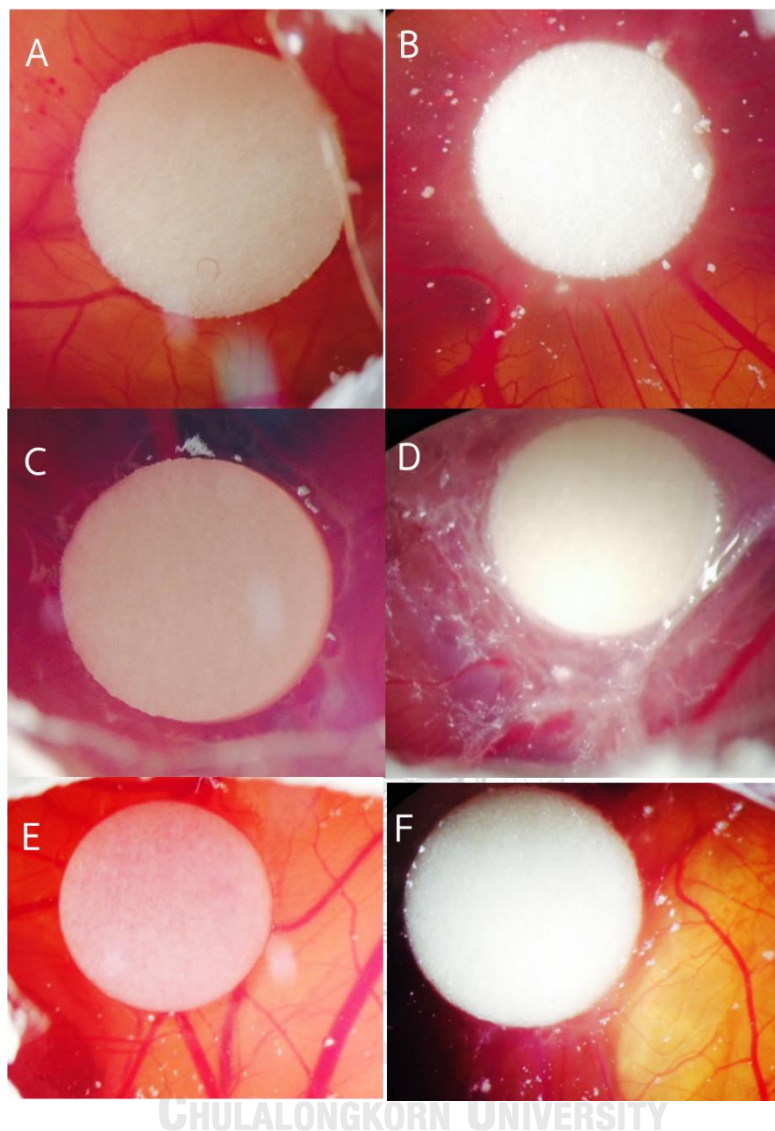


Figure 19 The angiogenesis of filter paper in different groups.

A), C) and E) indicate PBS. D) indicates ADSCs Passage 24 (3,400 cells/paper) and F) indicates conditioned media (serum free media) from ADSC P.24 at 48h. The photo was taken by digital camera under microscope. The magnification of image indicates 10X. (n=5).

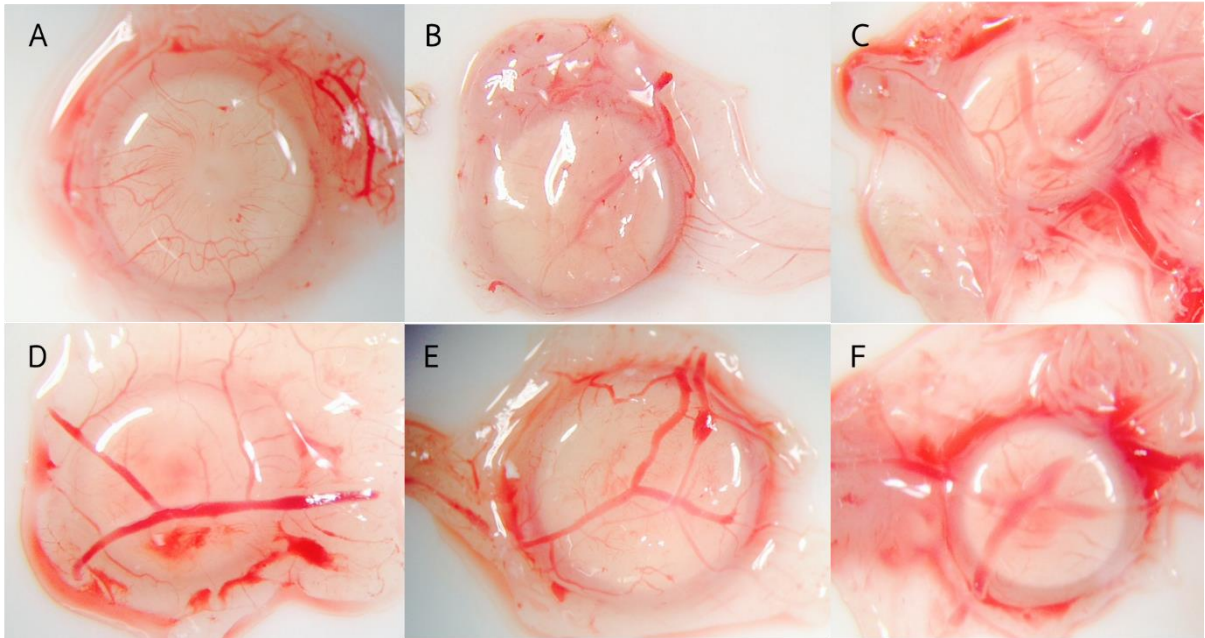


Figure 20 The flipped-filter paper of CAM assay on E11 chick embryo.

A) and D) indicate PBS (pH 7.4) solution was used as a control. B) And E) indicate conditioned media from 48 h serum free condition of ADSCs Passage 24 and C) and F) indicate ADSCs passage 24. The photo was taken by digital camera under microscope. The magnification of image indicates 10X (n=5).

### SF scaffolds structure

A common challenge for the fabrication the SF scaffolds from salt-leaching is to construct the 3D structure randomly. It depended on NaCl crystal during the synthesis process. In theory, the SF scaffolds has been designed the appropriate porosity to allow mass transfer. The morphology of the SF scaffolds using a JSM-IT500HR, JEOL microscope under 20 kV [131]. All the samples were coated with a thin gold layer. As a result, the structure of the SF scaffolds made from NaCl salt leaching, which was a variation in pore size (see white arrow). We determined the average size by image J software. The size in diameter was averagely  $513.95 \pm 4.99 \mu\text{m}$  ( $p < 0.05$ ).

Figure 21 shows scanning electron micrographs of the cross section of the porous scaffolds after salt-leached scaffold fabrication. The morphology is uniform, and the pore size distribution is heterogenous (randomly) in all the scaffolds. The pore size appears largest. The pore size from SEM image was  $513.95 \pm 4.99 \mu\text{m}$ . This might be benefited to allow oxygen, nutrients and mass transfer into the cells ( $p < 0.05$ ). We weighted the SF scaffolds on analytical balance (METTLER TOLEDO – AX205 Dolta Range, USA). The SF scaffolds were weighed 7.70 mg on average ( $n=5$ ).

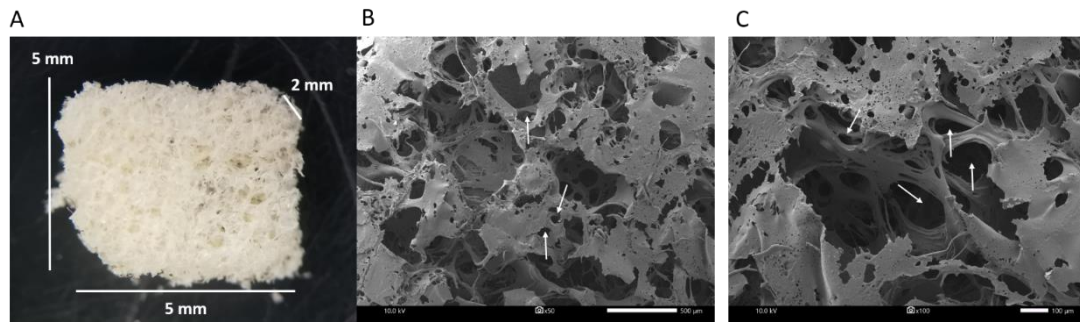


Figure 21 The structure of SF scaffolds.

A) indicate the cutting SF scaffolds in size 5 x 5 x 2 mm. The magnification of image in 50X (B) and 100X (C) indicate high magnification morphology of the porous walls of the scaffolds. The white arrows indicate the different size of porous scaffolds. This finding was determined by Image J software.

### The physical properties of salt-leached scaffolds; % dry weight of SF scaffolds, % porosity of SF scaffolds and % gel fraction

After fabrication by salt-leached scaffolds, % dry weight should be calculated by determination of the quality of SF scaffolds. The result of % dry weight was 8.22 on average.

This physical property of SF scaffolds needs to be considered. The porosity of liquid substitution was the solvent absorption via porosity by using hexane. Data are presented as mean  $\pm$  SD (n=5). The result of % porosity was  $77.34 \pm 6.96$  on average. This average size was significant. There is some suggestion that the higher porosity of SF scaffolds leads to having the connection between pore and surface. This evidence was allowed nutrients and oxygen to make the cell growing. [132].

However, we compared the % porosity of filter paper, which was mock control on CMA assay. The result found that the % porosity of filter paper was  $47.44 \pm 13.80$ , which was lower than SF scaffolds. These pieces of evidence suggested that the SF scaffolds were appropriated material of this study.

Table 12 The percentage of porosity of SF scaffolds.

porosity liquid substitution	Weight (mg)				
	N1	N2	N3	N4	N5
Weight of 1 ml hexane (W1)	605.00	592.77	777.14	583.15	754.93
Weight of 1 ml hexane + SF scaffold (W2)	755.02	632.56	841.61	720.14	908.93
Weight of 1 ml remaining hexane (W3)	268.73	301.36	593.79	217.23	12.85
%porosity = $((W1-W3)/(W2-W3)) \times 100$	69.15	87.99	73.99	72.76	82.81
Mean $\pm$ SD	77.34 $\pm$ 6.96				

Table 13 The percentage of porosity of filter paper.

porosity liquid substitution	Weight (mg)				
	N1	N2	N3	N4	N5
Weight of 1 ml hexane (W1)	605.00	592.77	777.14	583.15	754.93
Weight of 1 ml hexane + filter paper (W2)	855.02	832.56	1041.61	820.14	1908.93
Weight of 1 ml remaining hexane (W3)	268.73	301.36	593.79	217.23	403.81
% porosity = $((W1-W3)/(W2-W3)) \times 100$	57.36	54.86	40.94	60.69	23.33
Mean $\pm$ SD	47.44 $\pm$ 13.80				

Moreover, another physical property of the SF scaffold was gel fraction, which was investigated the capacity of the solubility of SF scaffolds. This property was reported % weight loss or % weight remaining, which are inverted properties. This study was selected % weight loss of SF scaffolds, which was  $18.13 \pm 4.65$ . Therefore, the SF scaffolds were not good solubility in water.

Table 14 Gel fraction via % weight loss of SF scaffolds.

Gel fraction	Weight (mg)				
	N1	N2	N3	N4	N5
Weight of SF scaffolds before added DI water (W0)	10.70	10.20	10.30	10.50	10.25
Weight of dried SF scaffolds (W1)	8.50	8.70	8.50	7.90	8.90
% weight loss of SF scaffolds = $((W0 - W1)/W0) * 100$	20.56	14.70	17.48	24.76	13.17
Mean $\pm$ SD	18.13 $\pm$ 4.65				

### Angioirritative effect of SF scaffolds

Angioirritative effect of SF scaffolds has not been reported by using solid scaffolds although they have been shown many times to activate angiogenic processes [19, 133]. Angioirritative reactions of the CAM were glaring as coagulation, vascular congestion and hemorrhages [49]. This might cause the toxic on CAM assay and chick embryo life. Therefore, we studied the possibility of angioirritation from the SF scaffolds by CAM assay.

The IS score showed 0 means no changes in the blood vessels. Finally, the long-term observation of angioirritation has not been found.

This assay is in comparison to the in vivo scaffolds test by CAM assay because these were a long-term observation of angioirritation [20, 134]. This CAM assay can determine the long observation of angioirritation. (60 mins above) [126]. This test showed that silk fibroin was no irritative effect on chick embryo because there is no blood vessel bleeding, vessel lysis and hemorrhage during 10 days of observation.





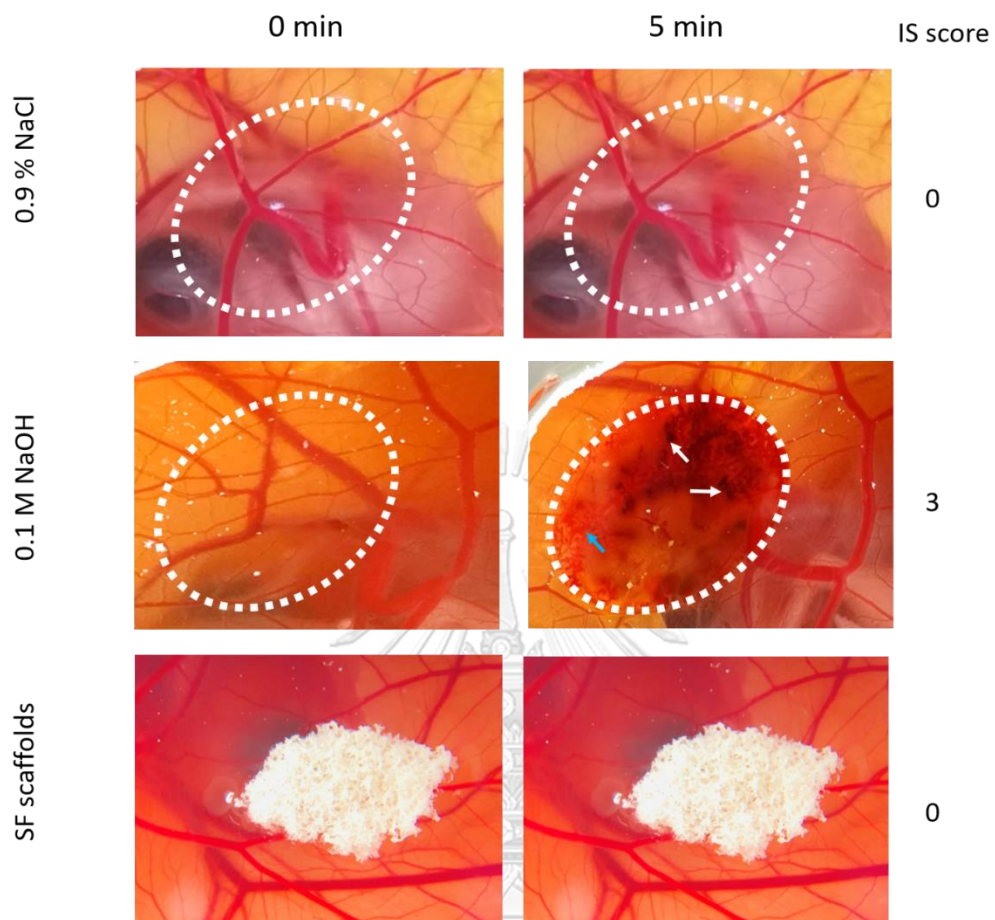


Figure 22 Angioirritation testing of SF scaffolds on CAM assay.

SF scaffolds (5 X 5 X 2 mm) were incubated with E10 egg for 5 min. IS score was used to evaluate the angiogenic property. White dash circles indicate area of interested of 0.9% NaCl and 0.1 M NaOH. White arrows indicate coagulation of blood vessel. Blue arrow indicates hemorrhage and vessel lysis. The magnification of image indicates 10X.

### Cell viability was detected by MTT assay and Live/Dead staining

ADSCs can apply on surface area and make it promptly compatible material in tissue engineering. We can prove that ADSCs can attach to the SF scaffold surface by monitored with a fluorescence microscopy [63].

The viability of cells, after combined with scaffolds, was also studied. First, the MTT assay was performed to determine the effect of SF scaffolds on cell viability. We found that ADSCs were lived after combine with SF scaffolds. However, the relative absorbance of SF-ADSC scaffolds was slightly decreased. Therefore, ADSCs on SF scaffolds was not proliferated. They were live on SF scaffold surface.

This data calculated from the absorbance of SF-ADSC scaffolds minus the absorbance of SF scaffolds. It showed no significant difference and no proliferation of ADSCs. Then, cell staining by acridine orange and Hoechst 33342 to validate cell live/viability for all kinds of SF scaffolds, indicating a non-toxic effect of SF scaffolds. This data showed the brighten blue/green spot inside SF scaffolds. The data supported the cell viability of ADCSs on SF scaffolds after three days of incubation and showed the localization of ADSCs on silk scaffolds. These results indicated that ADSC still lives and can refer to the activation of angiogenesis on CAM assay.

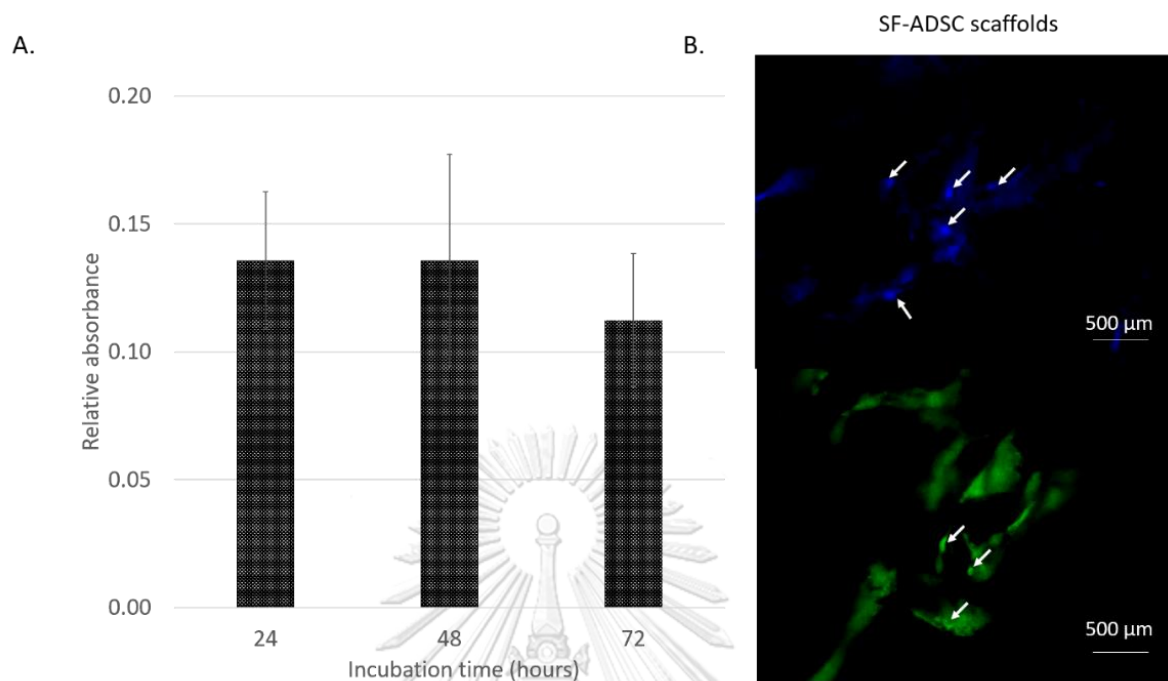


Figure 23 The effect of SF scaffolds on ADSCs viability by MTT assay and cellular live/dead fluorescence staining of SF-ADSC scaffolds by Hoechst and Acridine orange. A) The relative absorbance of SF-ADSC scaffolds for 72 hours. B) Live/dead fluorescence staining after 3 days of incubation. The bright green spots are live cells, and the bright blue spots are the nucleus.

### Qualitative data of biodegradable of SF-ADSC scaffolds

In this study. We determined the biodegradable properties of SF-ADSC scaffolds. During 10 day of observation, the diameter of SF-ADSC scaffolds were decrease with in E18. However, the diameter size was decreased from CAM covered some part of SF scaffolds. We hypothesized that the SF scaffolds were biodegradable capacity. This data was interestingly qualitative result because the diameter size was decreased since E14 (after 6 day of incubation).

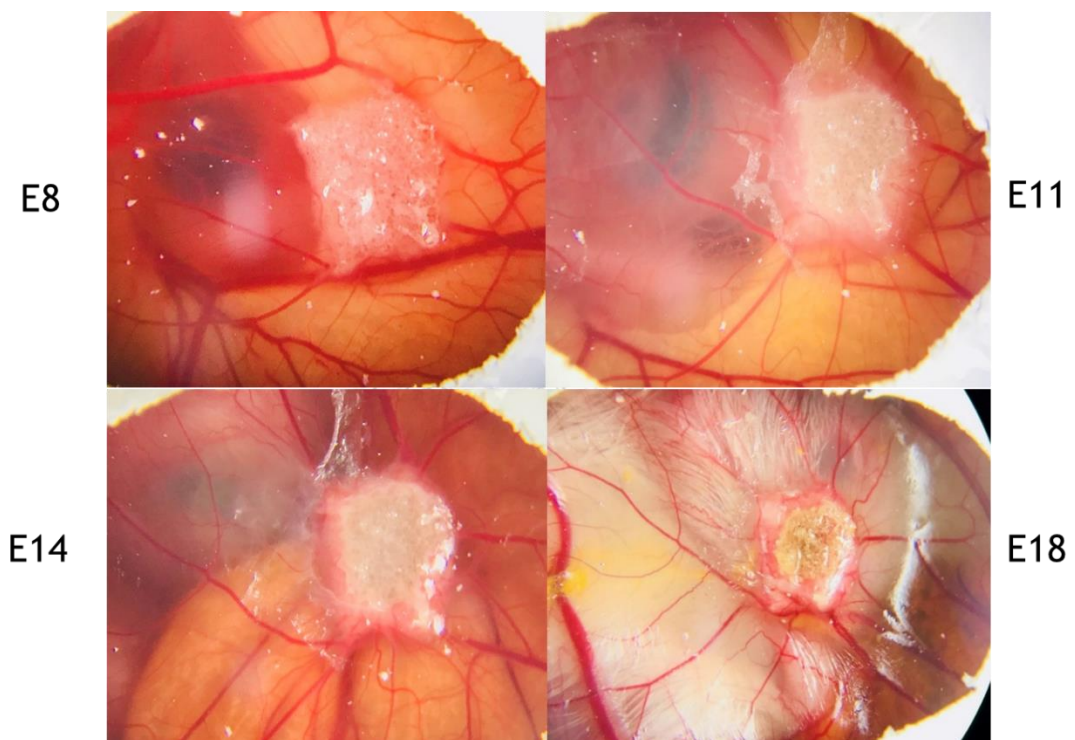


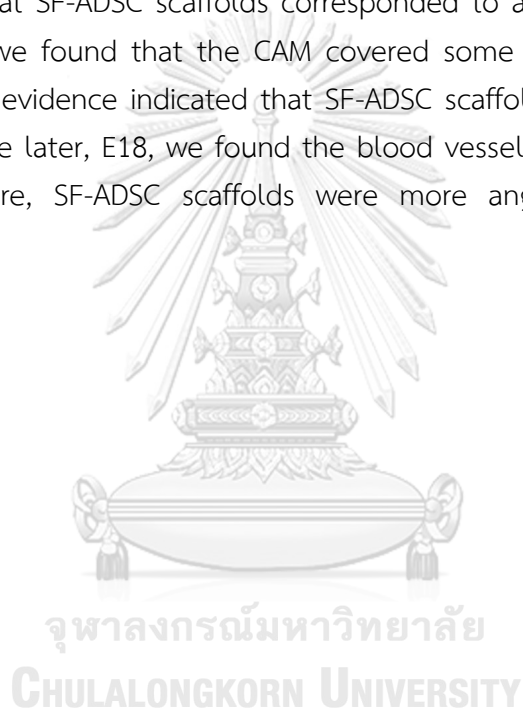
Figure 24 The biodegradable properties of SF-ADSC scaffolds.

The diameter size was decreased within 10 day of observation. The CAM was covered some part of SF-ADSC scaffolds that led to decrease smaller size. The magnification of image indicates 10X.

### Spoke-wheel pattern from CAM assay

This result can show the angiogenesis properties of SF scaffolds when compare among SF-ADSC scaffolds and SF scaffolds. The result showed the spoke-wheel pattern on E11 compare with E8 and the untreated group, which no blood vessel direction showed spoked-wheel pattern on E14. These findings indicated the SF scaffolds could activate vascularization themselves.

The angiogenesis occurred; the semi-quantitative score system had been analyzed. The score on E11 was indicated  $2.40 \pm 0.24$  as for SF scaffolds and  $3.20 \pm 0.20$  for SF-ADSC scaffolds averagely using the vessel density evaluation system. This score indicated that SF-ADSC scaffolds corresponded to a gradual increase in vessel density. Besides, we found that the CAM covered some part of SF-ADSC scaffolds' area on E14. This evidence indicated that SF-ADSC scaffolds had strongly angiogenic potential. The time later, E18, we found the blood vessels penetrate inside SF-ADSC scaffolds. Therefore, SF-ADSC scaffolds were more angiogenic capacity than SF scaffolds itself.



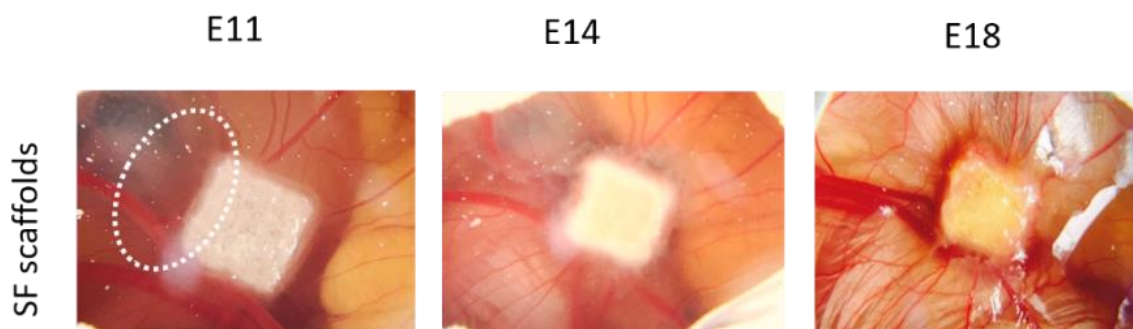
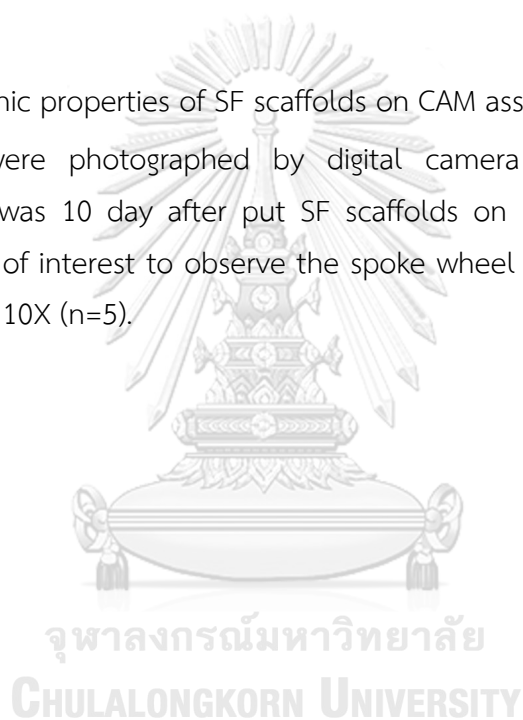


Figure 25 Angiogenic properties of SF scaffolds on CAM assay.

These pictures were photographed by digital camera under microscope. The observation time was 10 day after put SF scaffolds on E8. The white dash circle indicates the area of interest to observe the spoke wheel pattern. The magnification of image indicates 10X (n=5).



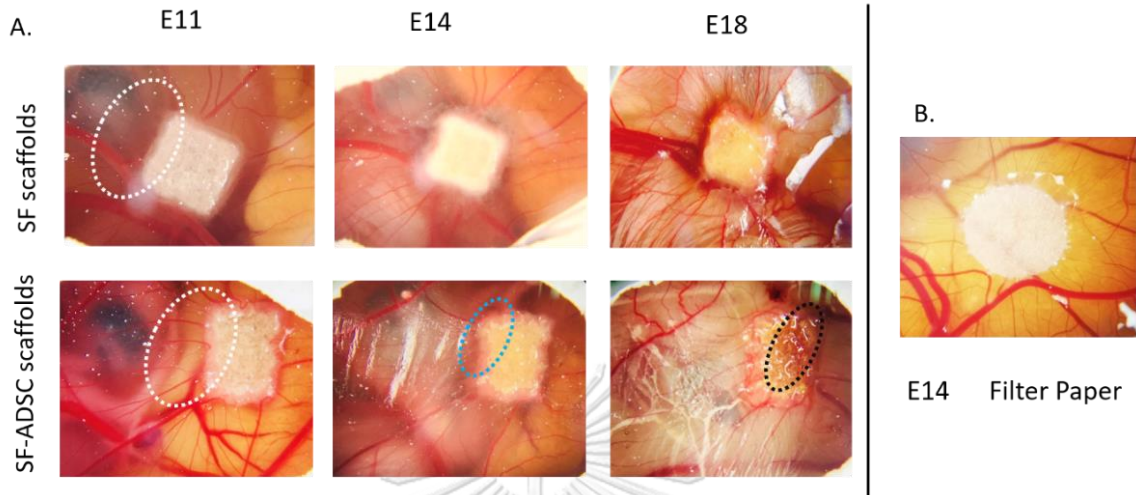


Figure 26 Angiogenic properties of SF-ADSC scaffolds.

A) indicates the vascularization appeared on E11 of SF-ADSC scaffolds and E14 of SF scaffolds, respectively. B) indicates the control group; filter paper on E14. The white circle dashes indicate the area of interested in new blood vessel formation. The blue circle dash indicates CAM covered on the edge of SF-ADSC scaffolds and the black circle dash indicates the blood vessels penetrated at the center of SF-ADSC scaffolds (n=5).



Table 15 Angiogenesis scoring in different groups.

Scaffolds	Angiogenesis score* (0-5)		
	E11	E14	E18
SF scaffolds	2.40 ± 0.24	3.60 ± 0.24	3.75 ± 0.25
SF-ADSC scaffolds	3.20 ± 0.20	3.80 ± 0.20	4.00 ± 0.00
Filter papers	0.00 ± 0.00	2.33 ± 0.57	2.50 ± 0.34

\* The score showed mean ± SEM.

### Histological staining

The implanted SF scaffolds were retrieved and dissected to visualize whether blood vessels from chick embryo penetrated the porous structure in the SF scaffolds. We detected blood vessels in both groups on E11, E14, and E18 without any dye staining. Histological analysis revealed that the blood vessels penetrated throughout the SF scaffolds. The section of SF-ADSC scaffolds showed blood vessel penetration incidence in a randomized. This evidence also supported that the significant porosity of SF scaffolds can allow blood vessel penetration, although this process is slower than the SF-ADSC scaffolds. Moreover, the density of blood vessels inside SF-ADSC scaffolds and SF scaffolds increased depending on the time of incubation.



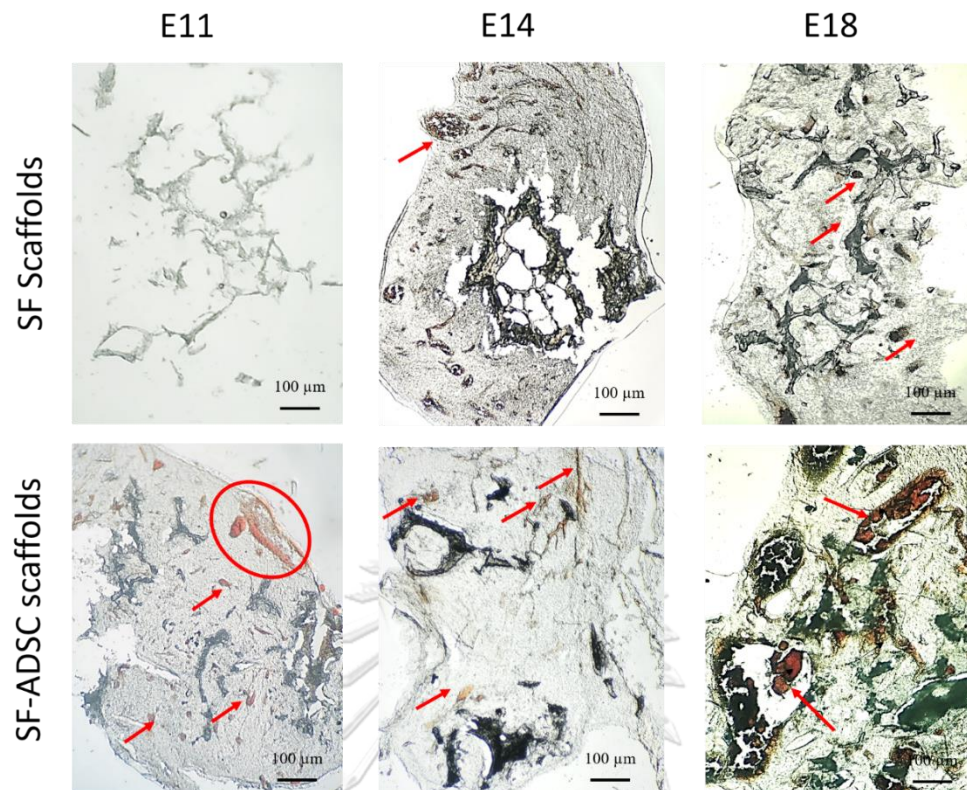


Figure 27 Histological analysis of the SF-ADSC scaffolds compared with SF scaffolds in different embryonic days.

The sections were 40  $\mu\text{m}$  thickness. The red arrows indicate the blood vessels, the red circle indicates a group of the blood vessels. The scale bar indicates 100  $\mu\text{m}$ .

## CHAPTER V DISCUSSION

### **ADSCs express various protein markers.**

From the result, we can discuss the reason why ADSC expressed the various makers. Even though, there were already known the expression of ADSCs or mesenchymal stem cells. Most researcher need to characterize because this cell is primary cell from the patient. We should characterize before starting experiment.

In our study, we use a CD marker, which is the cluster of differentiation (CD). This marker refers to cell surface protein. This CD marker usually uses to identify cell phenotype. However, the CD marker refers to a cell surface marker. There are not unique specific for just one cell or only one cell lineage. [135].

First,  $\beta$ III-tubulin, which is a microtubule element of the tubulin family found almost exclusively in neurons. It was possible to express because most cell types should have cytoskeleton for supporting and transportation.

For nestin is intermediate filament (IF) protein, which expressed mostly in nerve cells where they implicated in the radial growth of the axon. This marker usually identifies the neural cells. However, in the real expression, no markers were specific for one cell type. For example, ADSCs expresses the only CD105, but CD105 can find in endothelial cells as well. [136].

In our case, several candidates of MSC cell surface marker were possibly related to their stemness, including CD90, Stro-1, SSEA-4, CD271, and CD146 [137]. In our study, we found Stro-1 and CD90 expression. Therefore, ADSCs were stem cell and mesenchymal stem cells.

Moreover, the previous researcher found the expression of neuron specific marker on ADSCs [90] (Figure 28). That's confirm that there are ADSCs.

		mRNA	Protein
Neural	Pax6	—	ND
	<b>Nestin</b>	+++	Yes
	GFAP	++++	Yes
	A2B5	All	ND
	S100	+	ND
	HNK-1	+++	ND
	<b>β3-Tubulin</b>	++++	Yes
	Doublecortin	—	ND
	NF200	++++	Yes
	NSE	ND	Yes
	P75NTR	++++	ND
	EAG1	ND	—
	Kv 4.3	ND	—
	Growth factors/receptors	<b>VEGF</b>	All
TGFβ1		All	ND
TGFβ3		All	ND
FLK-1		All	ND
Pluripotency		c-Myc	ND
	KLF4	ND	Yes
	Nanog	ND	Yes
	<b>OCT4</b>	—	Yes
	SOX2	—	ND
	SSEA-1	—	ND
	SSEA-3	—	ND
	SSEA-4	—	ND
DNMT3B	ND	Yes	

Figure 28 The mRNA and Protein expression of ADSCs.

There are various types of markers such as neural marker, growth factors and pluripotency markers [90].

**ADSCs have differentiation properties to become adipocytes and osteocytes.**

There was a factor to induce the differentiation of ADSCs into adipocytes and osteocytes. That was differentiated media. These media can activate/non-activate transcription factors.

For adipogenic differentiation, there was a critical regular gene to control the differentiation and dedifferentiation. In this case, ADSC induces into the multilocular cell by C/EBP $\beta$  and C/EBP $\delta$ . Then, the process was continuously into a unilocular cell or lipid tissue by PPAR $\gamma$ . The chemical substances of adipogenic differentiation contained Dexamethasone, IBMX, Indomethacin, and ITS (Insulin Transferrin selenium). They activated in different transcription factors. However, the mature adipocytes were activated by differentiation media within 21 days. [90]. That journal used in different concentration of chemical substances compare with our study. It's depended on the concentration as well to differentiate into adipocytes.



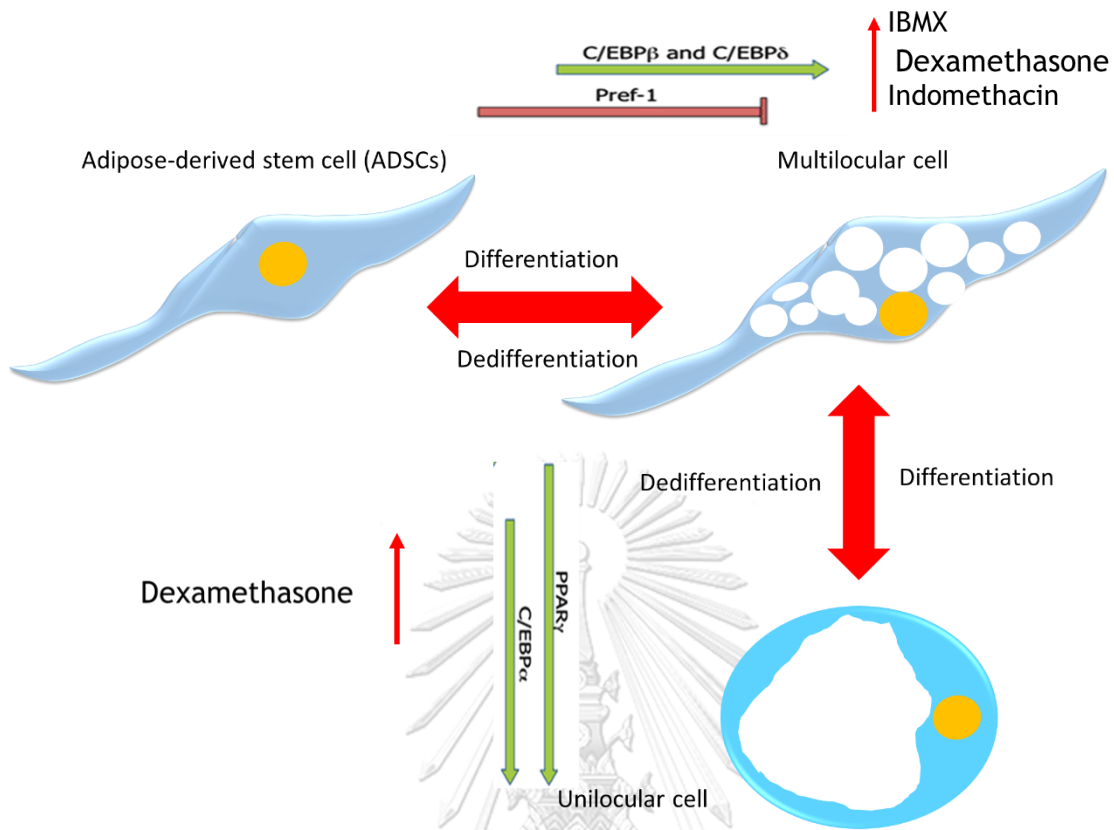
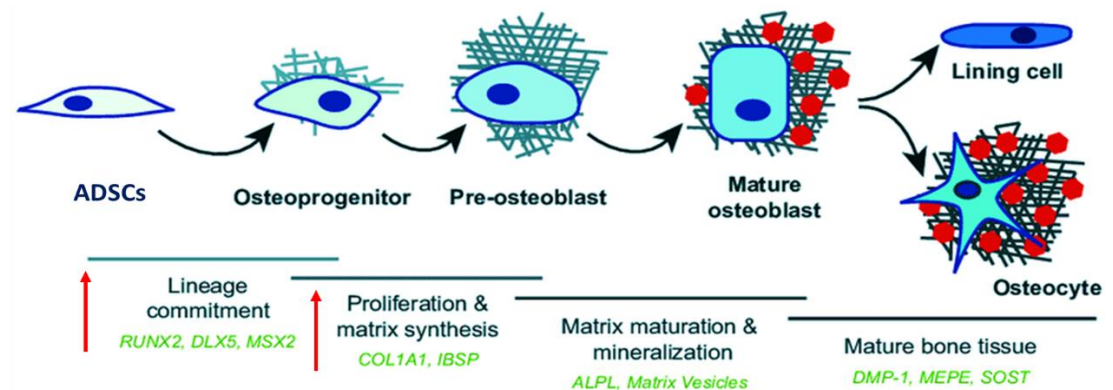


Figure 29 The adipogenic differentiation media on transcription factor regulation. Dexamethasone can induce the PPAR $\gamma$  and C/EBP $\beta$  and C/EBP $\delta$  to activate from ADSC to multilocular cell and unilocular cell. IBMX and indomethacin induced only C/EBP $\beta$  and C/EBP $\delta$ .

For osteogenic differentiation, the critical transcription factor in inducing mature bone is RUNX2 to allow ADSCs to differentiate to osteoprogenitor cells. The  $\beta$ -glycerophosphate and ascorbic acid induce RUNX2 and COL1A1 to differentiate into osteoprogenitor and pre-osteoblast [138]. To evaluate the morphology was used alizarin red s. The result found that the non-mature bone because the density of cell packing was not dense. The red color on the spot might be some mannerization. Osteogenic differentiation was the mature stage on 21 days. [90].

In conclusion in this part, we found the differentiation capacity of ADSCs to be adipocyte and osteocytes. This capacity might benefit for differentiated cell transplantation to replace or repair into the damage site.





### Beta-glycerophosphate and ascorbic acid

Figure 30 The osteogenic differentiation media on transcription factor regulation.

The key transcription factor to induce mature bone is RUNX2 to allow ADSCs differentiate to osteoprogenitor cell. The  $\beta$ -glycerophosphate and ascorbic acid induce RUNX2 and COL1A1 to differentiate into osteoprogenitor and pre-osteoblast.

**ADSCs have antioxidative properties.**

We found that ADSCs have antioxidant properties to protect themselves from ROS, which generated from environment factors.

Antioxidant enzymes showed that four activities in many cell sources, including SOD1, GPx, CAT, and GSH in human and other animal types, were reported. Cu-Zn SOD or SOD1 in human cells showed different activity values. In human serum, there are higher SOD1 than mesenchymal stem cells (MSCs) and ADSCs. MSCs are the same lineage with ADSCs. SOD1 should be the same trend. So, ADSCs can remove superoxide anion and change to hydrogen peroxide to reduce the toxicity level in cells, although the SOD1 unit was of different value.

Finally, the new trend of facial anti-aging is widely used for the many old persons who lose fat from their faces. The adipose tissues on the face were a loss, depending on time [139]. Therefore, the value of ADSCs, in this study, found that they can protect themselves from ROS in normal conditions (normal condition = no treat with H<sub>2</sub>O<sub>2</sub>). We hypothesized that antioxidant enzymes in normal conditions could have the potential to protect the cell from ROS.

However, we did not use ADSCs on facial anti-aging on our experiment. This is a kind of property of ADSCs. We believed that every cell has the antioxidant role themselves. But for our study, we found some potential of antioxidant enzymes similar with HaCaT cells.

**Filter paper cannot be a good representative material for tissue engineering.**

The capacity of filter paper to allow cell attachment and to supply the oxygen and nutrients were deficient. This material is a 2D scaffold (not the thickness). This reason can refer to our result that ADSCs on filter paper moved out from filter paper. They showed the white area on CAM. According to our result from the % porosity of filter paper, the data indicated that filter paper has less pore size. It might not allow mass transfer to the tissue when filter paper applied on tissue damage site. Therefore, we need to change other materials to have a higher % porosity than filter paper. Moreover, the filter paper is not protein material. It is hard to cause protein-protein interaction. Therefore, the filter paper and albumin had not interacted each other.



### The 3D structure of salt-leached SF scaffolds versus SF scaffolds.

We try to find the differences between salt-leached/normal structure of SF scaffolds on the NCBI protein database. We found that the 3D structure of salt-leached scaffolds was not reported yet. The main structure might be  $\beta$ -sheet and alpha-helix, which are formed the tertiary structure. Therefore, the structure of salt-leached SF scaffolds might not different from the original structure.





Figure 31 Biological Unit of Fibroin Heavy Chain (pink color) for 3UA0: tetrameric; determined by author and by software (PISA) [140].

Fibroins serve as the major building blocks of silk fiber. As the major component of fibroin, the fibroin heavy chain is a considerably large protein comprising N-terminal and C-terminal hydrophilic domains and 12 highly repetitive Gly-Ala-rich regions flanked by internal hydrophilic blocks.

### **Solid scaffold can apply on angi irritation test on HET-CAM assay.**

We showed, for the first time, that salt-leached SF scaffolds did not cause angi irritation in chick embryos. By adapting the OECD TG 405 guideline, the recommendation in this guideline mentioned that “a solid sample of less than 100 mg can be apply on rabbit eyes”. Our SF scaffolds for angi irritation assay weighed 10.20 mg on average [51]. The result reaffirms the safety of the SF scaffold for angiogenesis. Therefore, we discovered firstly this testing for solid scaffolds on angi irritation followed by OECD TG 405 guideline.

OECD guideline TG 405 is revised to improve weight-of-evidence analysis in several times. In terms of pharmaceutical research and drug development. There was some limitation for using only eyes to test in short time irritation. Moreover, the Draize eye test naturally fails to add the potential drug on the eyes, as it doesn't cover all forms of possible exposure scenarios. Another critical point is the high variation of control of reproducibility, application, and evaluation during the feeding and development [141-143].

However, OECD guideline TG 405 can use as a guideline model because this test is suitable for rabbit eyes irritation. In our study, we used CAM assay, which is the alternative method of angi irritation is the hen's egg test – chorioallantoic membrane (HET-CAM) assay (or like CAM assay) does not use corneal tissue [48, 141-143]. The supporting evidence from other some organization that involved in irritation test. They mentioned that the important part is the chorioallantoic membrane because the membrane has similar structure on the membrane as on the eyes. Interestingly, the HET-CAM assay is in process validation by the Brazilian Centre for the Validation of Alternative Methods (BraCVAM) and validated but not yet recommended by the Interagency Coordinating Committee on the Validation of Alternative Methods (ICCVAM). Those committees were focused on the eye irritation method. But they suggested that Het-CAM is an alternative model to test on irritation as well [141, 142].

For the criteria of ICCVAM-Recommended Test Method Protocol: Hen's Egg Test – Chorioallantoic Membrane (HET-CAM) Test Method published under originally published as Appendix B3 of “ICCVAM Test Method Evaluation Report: Current Validation Status of In Vitro Test Methods Proposed for Identifying Eye Injury Hazard Potential of Chemicals and Products” by NIH Publication on 2010, they mentioned

solid substance to test on these model [144]; “Apply 0.3 mL of solid, particulate, or granular substances (which have been ground to a fine dust) directly onto the CAM, ensuring that at least 50 % of the CAM surface area is covered. In cases where the total weight of the test substance at this volume is greater than 0.3 g, 0.3 g of the solid, particulate, or granular test substance should be used. In either case, the weight of the test substance should be recorded” [144]. Therefore, the solid sample should dissolve as the solution or can apply 0.3 g solid scaffolds. In our result, we weighted SF scaffolds (7.70 mg on average). This result can accept to use this CAM assay to screen the angi irritation of solid scaffold. Apart from sample testing, the negative control and positive control were mentioned on this guideline as well. They use 0.9% (w/v) sodium chloride (NaCl) in deionized/distilled water and 0.1 N sodium hydroxide (NaOH) in deionized/distilled water [144].

We believed that angi irritative properties of SF scaffolds were not toxic on chick embryo. Even though, the structure was rigidity. This data can confirm that the rigidity of SF scaffolds has the value to apply on wound healing process or regeneration/repairing without any modify structure.

Finally, the tested on % water solubility of SF scaffolds was very low. We cannot dissolve in water to make a solution or suspension applying on Het-CAM assay. We can conclude from ICCVAM test method that we can apply solid scaffold.

### **The rigidity of SF scaffolds can activate angiogenesis.**

The CAM assay is the lack of immune response prevents rejection [45]. So, the scaffolds were not rejected. Moreover, any cells or drugs can apply to CAM easily. Although any cells or drugs can apply to CAM assay, they need to have an angiogenic potential.

Our study, for the first time, employed CAM to investigate the angiogenic potential of SF scaffolds with/without ADSCs. We found that SF scaffolds could activate angiogenesis. Even though CAM assay is not a new model to study angiogenesis, this finding was the first to explore the potential of the rigid SF scaffolds without/with ADSCs in our finding.

In terms of rigidity of SF scaffolds were considered to show the potential for tissue engineering. According to Danyu Yao, et al, their results on ATR-FTIR and XRD proved that the structure of freeze-dried SF scaffold was random coil while that of salt-leached silk fibroin scaffolds was  $\beta$ -sheet [145]. The  $\beta$ -sheet can change to

random coil when it dissolved in water or solution to get more softer than original rigid SF scaffolds [146]. However, in this study, we were not expected to investigate the softer structure. We need to show the rigidity can activate angiogenesis. Therefore, from the result, we can show that SF scaffolds can activate angiogenesis. Even combined with ADSCs, the activation of angiogenesis was better than SF scaffolds.



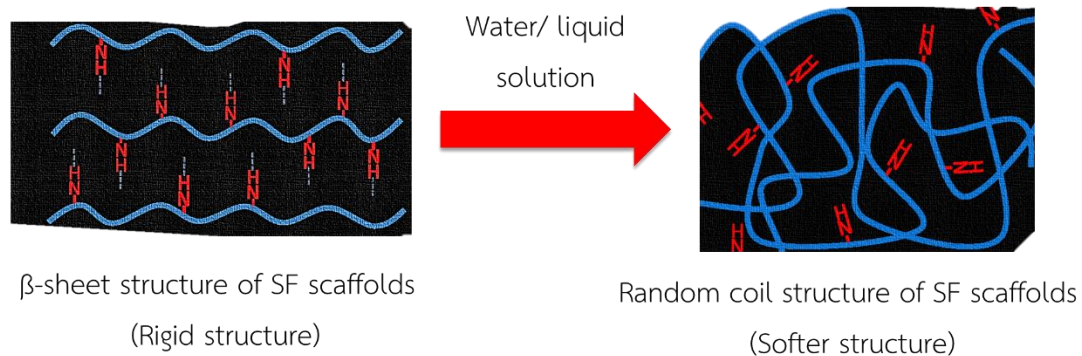


Figure 32 The reaction of SF scaffolds structure after dissolved in water/liquid solution.

The  $\beta$ -sheet conformation was changed to random coil structure after dissolved naturally in water and liquid solution. This structure is softer than rigid conformation.

Apart from structural theory of SF scaffolds, for the physical properties of SF scaffolds that were supported, the SF scaffolds can be applied to tissue engineering. First, % porosity of SF scaffolds was high, allowed oxygens, nutrients and mass transfer. Second, the appropriate % dry weight is in range 7-9% [147]. Therefore, salt-leached silk fibroin scaffolds fabrication process was validated. These SF scaffolds were a good quality for using as the biomaterial for tissue engineering.

The solubility of SF scaffolds by gel fraction assay showed that SF scaffolds were not dissolve in water. This data can support the biodegradable properties of SF scaffolds on CAM assay (see below). It might be gradually decreased in degradation. Therefore, the SF scaffold itself can degrade from the proteolytic enzyme (see the detail for next discussion topic). It was not from the % weight loss of SF scaffolds.

Finally, all supportive physical properties were found that SF scaffold-bound water or liquid solution cannot enhance the interaction from the  $\beta$ -sheet structure to the random coil structure. The SF scaffolds have the porosity capacity to allow cell adhesion instead.

### Effect of NaCl, Na<sup>+</sup> and Cl<sup>-</sup> from salt-leached SF scaffolds on angiogenesis on CAM assay.

In our study, we used salt to generate the pore and rigidity structure of SF scaffolds. Even though, the preparation process was got rid of NaCl by several times of water dilution. The NaCl, Na<sup>+</sup>, and Cl<sup>-</sup> were considered to increase osmosis, hypertonic or hypotonic situation of blood vessels. For the process of preparation, we used 7 g NaCl in 3 ml silk solution. The initiated amount of NaCl was 0.12 mol in 3 ml silk solution (40 mol/L (silk solution)). We believed that the amount of NaCl was decreased by several times of water dilution because the water substitution was 6 days 3 times each. According to Ludwig F. Zeilbeck, et al. 2014, they were incubated with 0.2 mM or 1 mM NaCl for negative control to endothelial Human dermal microvascular endothelial cells (HDMEC). These findings indicated that there was no increase in BrdU uptake and no increase in the Migration of Microvascular Endothelial Cells in vitro [148]. Therefore, we can indicate that a lower concentration of NaCl inside SF scaffolds might not affect cellular osmolarity. We cannot find the data to support that Na<sup>+</sup> and Cl<sup>-</sup> can inhibit the activation of angiogenesis/osmosis situation on CAM assay. Finally, we can conclude that there is no effect of NaCl on the activation of angiogenesis.

### **ADSCs can be cocultured with SF scaffolds.**

The possibility of cell adhesion might arise from the relationship between SF scaffold and ADSC morphology. ADSCs can attach on SF scaffolds surface via their morphology. There were two types of cell adhesion of ADSCs on SF scaffolds. Single cell (circle) was found in the early incubation. Monolayer formation or aggregation appeared on day 21. (But no fibroblastic morphology.) [149]

Moreover, the result of our research was the same as Murphy, Haugh, and O'Brien (2010), they found that the cells which were seeded with the big porous scaffolds allowed the cell proliferation faster than seeding on a scaffold with small pore size [150].

Finally, the chemical structure of SF scaffolds contained alpha-helix,  $\beta$ -sheet, and random coil. This structure also have the roughness of the surface, which is one factors to allow cell attachment [151]. Therefore, we can use SF scaffolds from salt-leaching to combine with ADSCs and to develop the appropriate structure for the tissue engineering field.

### **SF-ADSC scaffolds induced angiogenesis.**

In our study, we used scoring system to validate the capacity of angiogenesis of SF-ADSC scaffolds. We found that the SF-ADSC scaffolds have angiogenic potential to activate blood vessel formation. Moreover, the strongly evidences in our study were histology section of SF-ADSC scaffolds. We can find the blood vessel complex inside SF scaffolds depend on time of incubation. If we can use for long time regeneration (more than 10 day of incubation (at E18), It might induce more blood vessel complex.

Apart from scoring and histology section of SF-ADSC scaffolds, which would be induce angiogenesis was many factors such as the contribution from SF scaffolds and the contribution from ADSCs.

The SF scaffolds provide surface area for cell adhesion, their porosity allows enough mass transfer for cells to maintain their lives. From our finding, we have the % porosity to support the capacity for allow mass transfer and the size form SEM image. Moreover, degradation product of SF scaffolds may be beneficial for angiogenesis. The previous research reported that the cell adhesion is caused by the deposition and remodeling of extracellular matrix which could modulate biochemical signaling [63].



In addition, cell adhesion effects on cellular function, such as migration, proliferation and differentiation. Thus, it is necessary to study the adhesion characteristic [64]. Other report of SF scaffolds for cell adhesion indicated that SF scaffolds alone can allow cell attachment even though the amino acid residue needs to be modified for increasing cell adhesion [65]. We showed by fluorescence microscopy that ADSCs still attached to the SF scaffolds surface after 3 days, and ADSCs maintained the cellular activity for at least 3 days as observed by MTT assay. This data supports our in vivo result. We believe that the cells in the implanted scaffolds were alive and active during 3 days of angiogenesis from E8 to E11. However, we cannot find the proliferation of ADSCs for 3 days because the relative absorbance was slightly decreased.

Secondly, the porosity of SF scaffolds can support cell proliferation, cell differentiation, cell aggregation and vascularization of blood vessel formation [66]. In our study, SF scaffolds had an average pore size of  $513.95 \pm 4.99 \mu\text{m}$ . Interestingly, the experiment of various sizes could be considered. Cell loading efficiencies for 30  $\mu\text{m}$ , 315-500  $\mu\text{m}$ , and 500-1000  $\mu\text{m}$  scaffolds from salt-leaching. They found that the smallest size was the best cell adhesion, although 500-1000  $\mu\text{m}$  scaffolds still showed the cell adhesion from Live/Dead assay [68]. Moreover, the physical chemistry, in our result, % porosity of SF scaffolds, can allow the cell attachment because there was a large pore size. This evidence can supply oxygen and blood vessel to penetrate easily. Therefore, we hypothesized that ADSC and endothelial cells form new blood vessels that could grow and live.

This was a supporting data that ADSCs have angiogenic potential. When ADSCs combined with SF scaffold, they can co-working and activate angiogenesis faster than one individual part. These can conclude that co-working can activate the time of angiogenesis. It can show the value of SF-ADSC scaffolds in terms of tissue engineering so far.

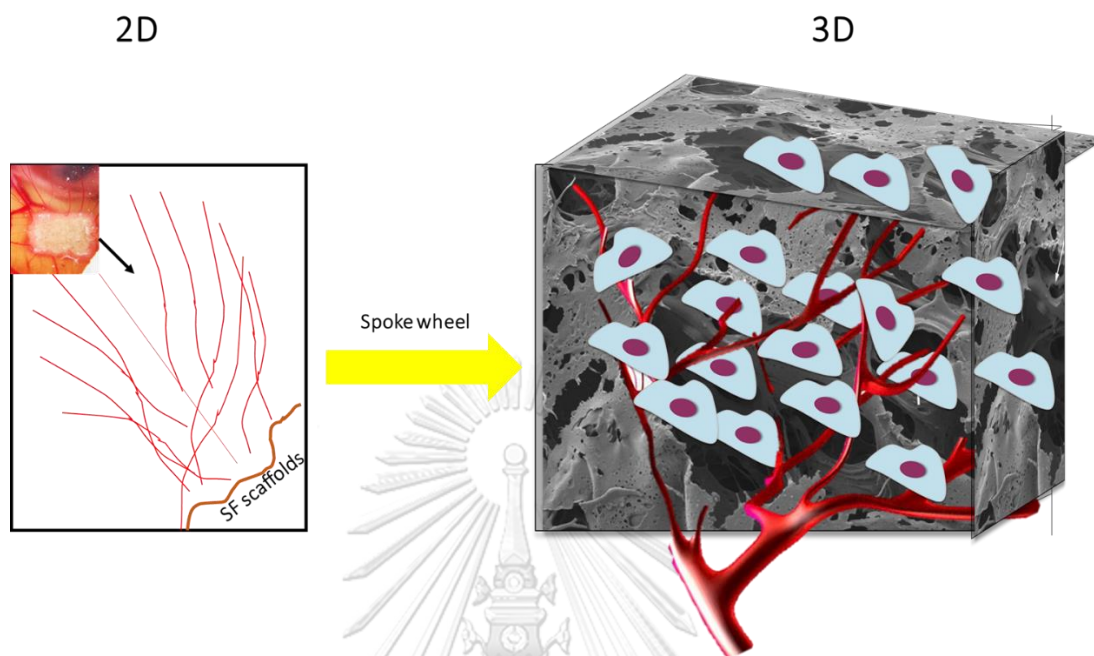


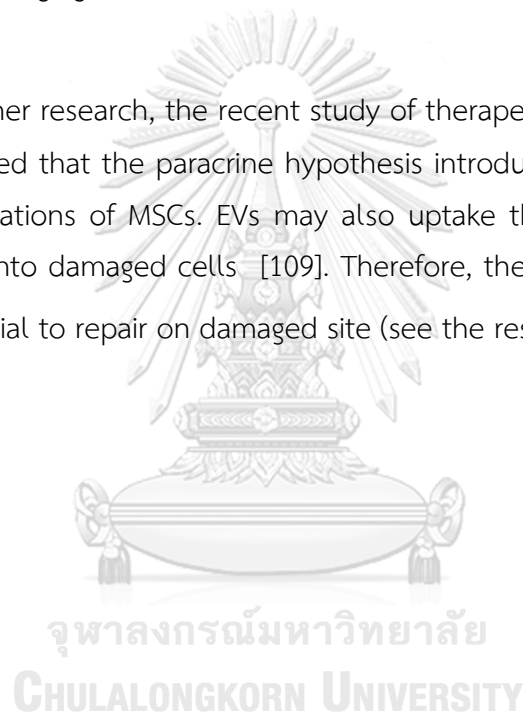
Figure 33 The overview of CAM assay on tissue repair and regeneration.

The main component of 3D biomaterial was ADSCs and SF scaffolds that co-working and enhance efficiency to use as the tissue engineer product because they allow blood vessel to penetrate inside.

### **The possible mechanism to induce angiogenesis of SF-ADSC scaffolds.**

Apart from proteolytic enzymes, which are a possible way to digest the SF scaffolds to activate angiogenesis and ADSCs, which released angiogenic growth factors from previous reports was extracellular vesicles (EVs). The EVs, which released to body fluid and contained many essential molecules. These mechanisms could be a possible way to activate angiogenesis. In our result showed in the appendix, we found that ADSCs release EVs. However, the culture media of ADSCs was not only the EVs but also had another released molecule such as free angiogenic factors in media to activate angiogenesis and EVs as well. This data can support this possible mechanism.

For the other research, the recent study of therapeutic in mesenchymal stem cells (MSCs) showed that the paracrine hypothesis introduces a different way to the therapeutic applications of MSCs. EVs may also uptake the therapeutic proteins or RNAs from MSCs into damaged cells [109]. Therefore, these data indicated that EVs have some potential to repair on damaged site (see the result of EVs at appendix).



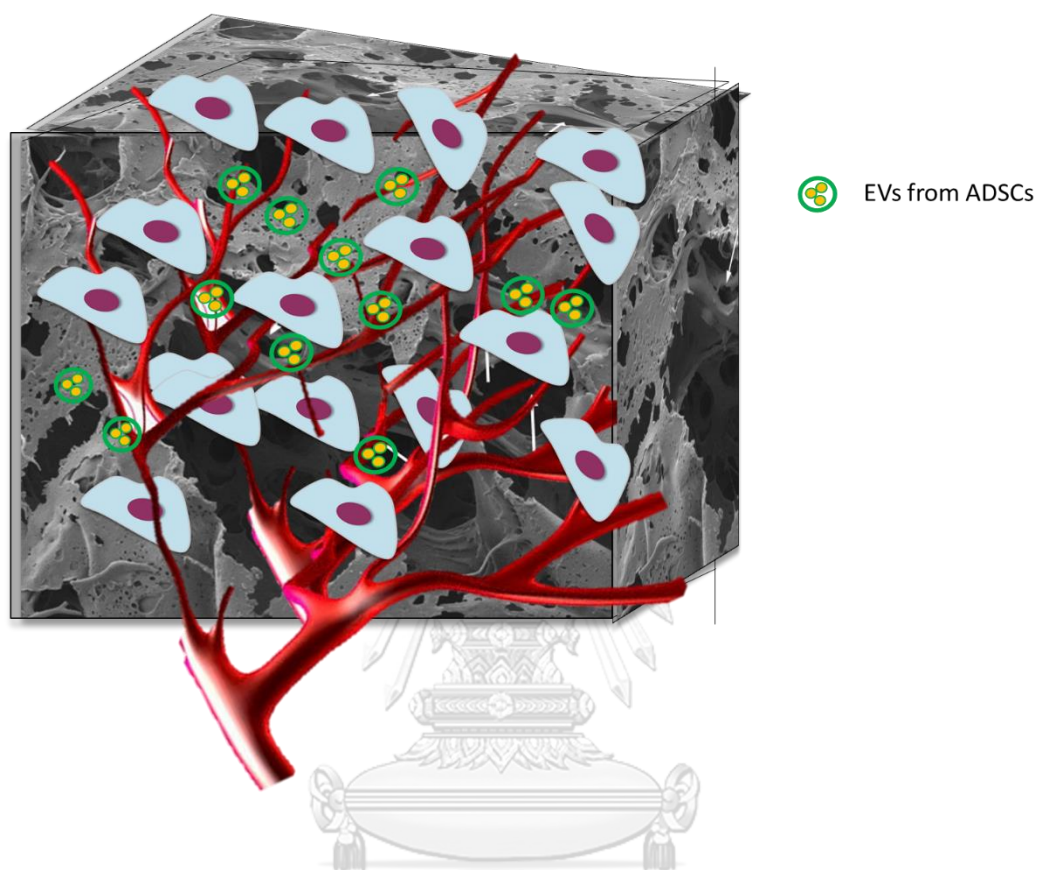


Figure 34 The possible mechanism of angiogenic potential of SF-ADSC scaffolds. The SF-ADSC scaffolds release some EVs from ADSCs and might have the potential to activate angiogenesis.

### **SF-ADSC scaffolds might have protein-protein interaction to induce biodegradable.**

The biodegradable properties of SF-ADSC scaffolds can cause firstly by protein-protein interactions (protein from albumin in chick embryo and protein structure from SF scaffolds) and degrade by proteolytic enzymes [152].

For the degradation of the SF scaffolds, the behind mechanisms are unclear. According to Bai L et al., they found some degradation of silk fibroin film implanted into rat [153]. This degradation of the scaffold might give some potential of angiogenesis.

The degradation products of SF scaffolds activated angiogenesis. The silk fibroin contained a large percentage of glycine, alanine, and serine [69-71]. SF scaffold degradation can be due to enzymatically assisted proteolysis, such as by chymotrypsin and carboxylase. [72-74].

For protein-protein interaction between SF scaffolds and albumin solution, Normally, these interactions could be based on charge-charge interactions, hydrogen bonding, or hydrophobic-hydrophilic interactions between the specific domains of two proteins [154]. For our result, the interaction during CAM assay is hydrophobic-hydrophilic interactions because fibroin is hydrophilic, and albumin is very high solubility; hydrophilic. Therefore, the reason why SF scaffolds can attach to CAM and can degrade over time.

The biodegradable properties were by proteolytic enzymes from CAM during the development. The researchers (M. Da Saliva et al.) proposed the mechanism behind this situation. They found that a total of 12 proteases was detected in the allantois fluid (AIF), compared to 5 in the amniotic fluid (AmF). They indicated that proteolytic enzymes from AIF assumed to participate in digestive system [74].

Moreover, the remaining proteins and proteolytic enzymes redirected to the embryos via the chorioallantoic capillary plexus on CAM. We hypothesized that our SF scaffolds on CAM might be degrade from those enzymes during the development. [74]. However, once degraded, these amino acids are resorbed by the surrounding cells.

The previous data from immunohistochemistry staining indicated that SF scaffold degradation products can induce the endothelial cell proliferation by staining CD34 marker [75].

These data are paralleled by biodegradable properties for 10 days and percentage of weight loss of SF scaffolds. Therefore, SF scaffolds were poor water solubility because they might be degraded by proteolytic enzymes on CAM instead.

Interestingly, the poor water solubility of SF scaffolds has the advantages for preparation SF scaffold with cells in a long time, and these data can benefit for the preparation of 3D bioprinting so far.



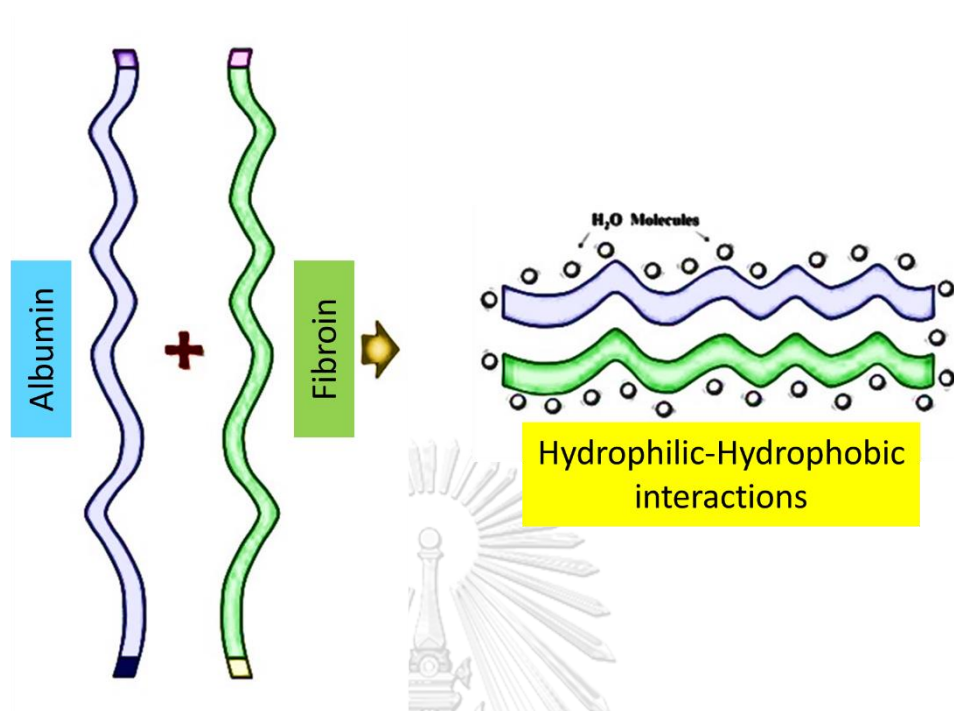


Figure 35 Purpose of protein-protein interactions between albumin and fibrin. The blue line represents the albumin chain that is high hydrophilic and solubility. The green line represents fibrin chain that is hydrophobic. They can bind with hydrophilic-hydrophobic interactions.

## CHAPTER VI CONCLUSION

We believed that the angiogenic properties of SF scaffolds were not toxic to chick embryos. Even the structure was rigid. This data can confirm that the rigidity of SF scaffolds has the value to apply without any modify structure on tissue engineering. Interestingly, the SF scaffolds alone promote angiogenesis by proteolytic enzymes. We hypothesized that the proteolytic enzymes from CAM might degrade SF scaffolds to activate angiogenesis. Cytotoxic and angiogenic effects of the SF scaffolds have not found, reassuring the biocompatibility of the SF scaffolds. We also demonstrated the CAM model that investigated the salt-leached SF-ADSC scaffolds promote angiogenesis. There are many supporting data that ADSCs itself or ADSC's releasing molecules. The angiogenesis effect was achieved earlier, suggesting the combined effect of the ADSCs and SF scaffolds themselves. We also highlighted the use of CAM for in vivo screening of the angiogenic properties of the tissue-engineering scaffold.





## Appendix

This section was showed the raw data and noted the detail; including methods, result, discussion and the other data in thesis.

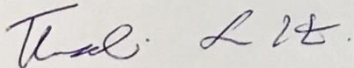
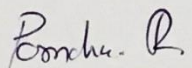
### Animal Ethic statements (No. 16-33-008)

1. The original ethics was approved from May 1, 2017 to April 30, 2019
2. The renew ethics was approved form May 1, 2019 to April 30, 2021



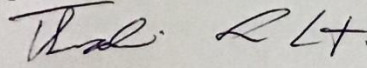
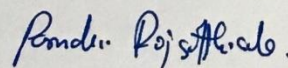


### Chulalongkorn University Animal Care and Use Committee

<b>Certificate of Project Approval</b>	<input checked="" type="checkbox"/> Original <input type="checkbox"/> Renew
<b>Animal Use Protocol No. 16-33-008</b>	<b>Approval No. 16-33-008</b>
<b>Protocol Title</b> Analysis of therapeutic applications from adipose stem cell-derived extracellular vesicles and adipose stem cells on chick embryo.	
<b>Principal Investigator</b> Weerapong PRASONGCHEAN, PhD	
<b>Certification of Institutional Animal Care and Use Committee (IACUC)</b> This project has been reviewed and approved by the IACUC in accordance with university regulations and policies governing the care and use of laboratory animals. The review has followed guidelines documented in Ethical Principles and Guidelines for the Use of Animals for Scientific Purposes edited by the National Research Council of Thailand.	
<b>Date of Approval</b> May 1, 2017	<b>Date of Expiration</b> April 30, 2019
<b>Applicant Faculty/Institution</b> Faculty of Pharmaceutical Sciences, Chulalongkorn University, Phyathai Road., Pathumwan BKK-THAILAND. 10330	
<b>Signature of Chairperson</b>  Name and Title <b>THONGCHAI SOOKSAWATE, Ph.D.</b> <b>Chairman</b>	<b>Signature of Authorized Official</b>  Name and Title <b>PORNCHAI ROJSITTHISAK, Ph.D.</b> <b>Associate Dean (Research and Academic Service)</b>
<p><i>The official signing above certifies that the information provided on this form is correct. The institution assumes that investigators will take responsibility, and follow university regulations and policies for the care and use of animals.</i></p> <p><i>This approval is subjected to assurance given in the animal use protocol and may be required for future investigations and reviews.</i></p>	



### Chulalongkorn University Animal Care and Use Committee

<b>Certificate of Project Approval</b>	<input type="checkbox"/> Original <input checked="" type="checkbox"/> Renew
<b>Animal Use Protocol No. 16-33-008</b>	<b>Approval No. 16-33-008</b>
<b>Protocol Title</b> Analysis of therapeutic applications from adipose stem cell-derived extracellular vesicles and adipose stem cells on chick embryo	
<b>Principal Investigator</b> Weerapong PRASONGCHEAN, PhD	
<b>Certification of Institutional Animal Care and Use Committee (IACUC)</b> This project has been reviewed and approved by the IACUC in accordance with university regulations and policies governing the care and use of laboratory animals. The review has followed guidelines documented in Ethical Principles and Guidelines for the Use of Animals for Scientific Purposes edited by the National Research Council of Thailand.	
<b>Date of Approval</b> May 1, 2019	<b>Date of Expiration</b> April 30, 2021
<b>Applicant Faculty/Institution</b> Faculty of Pharmaceutical Sciences, Chulalongkorn University, Phythai Road., Pathumwan BKK-THAILAND. 10330	
<b>Signature of Chairperson</b>  Name and Title <b>THONGCHAI SOOKSAWATE, Ph.D.</b> Chairman	<b>Signature of Authorized Official</b>  Name and Title <b>PORNCHAI ROJSITHISAK, Ph.D.</b> Associate Dean (Research and Academic Service)
<p><i>The official signing above certifies that the information provided on this form is correct. The institution assumes that investigators will take responsibility, and follow university regulations and policies for the care and use of animals.</i></p> <p><i>This approval is subjected to assurance given in the animal use protocol and may be required for future investigations and reviews.</i></p>	

## Supplement data from ADSC-EVs

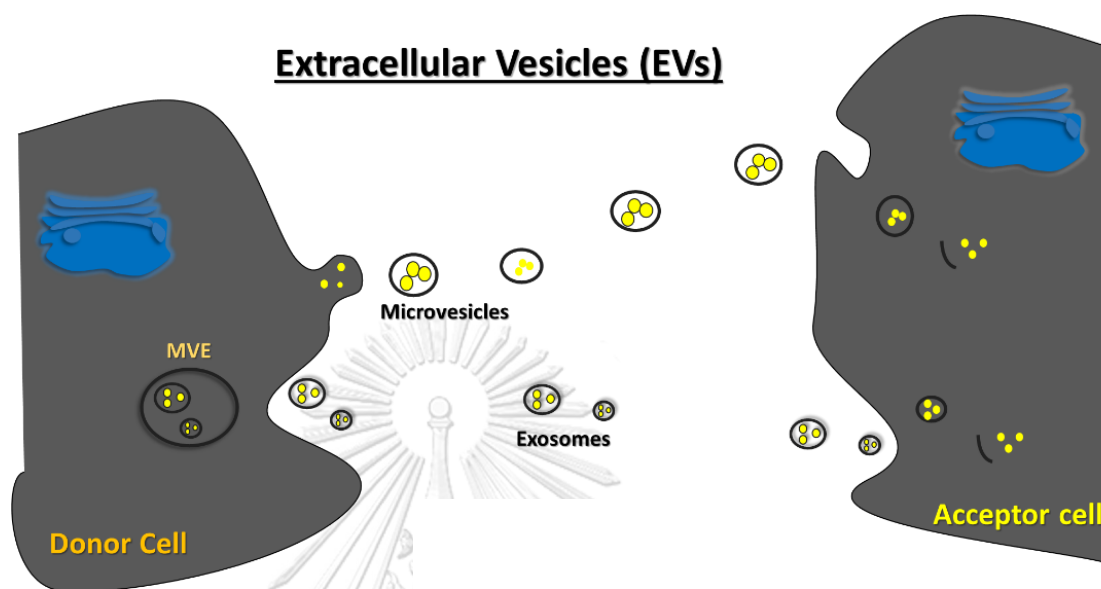


Figure 36 Biogenesis of EVs and their types.

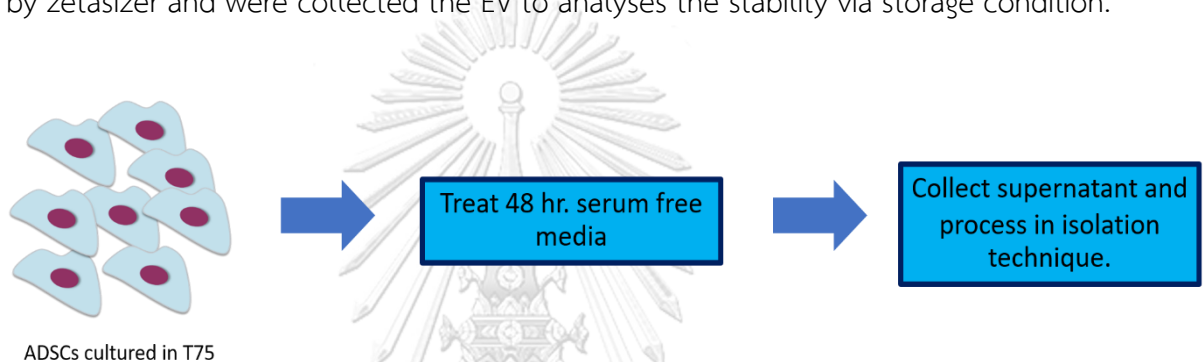
There are two types of extracellular vesicles, namely microvesicles and exosomes, which are the different particle size and cellular origin compartment. They play a role in cell-cell communications (paracrine communications). The donor cell also releases from different ways to affect the acceptor cell.

## ADSC-EVs characterization

### Methods

#### Cell culture for EVs collection

The condition of EVs collection depends on the number of cell cultures, media, and incubation time. ADSCs passage 3-23 ( $1.5 \times 10^6$  cells) were plated in a T75 flask. They were reached 80% confluent and changed the media to serum-free media (Only DMEM) for 48 hours. CM was collected, followed by the chart. The CM of ASCs will be purified by ultracentrifugation. Moreover, the EVs were determined the size by zetasizer and were collected the EV to analyses the stability via storage condition.



#### EVs isolation and purification

This method was purified ADSC-EVs in many steps. We need to get rid of interruption form xenogeneic sources such as EVs form fetal bovine serum (FBS) or others. These can interfere with the experiment. There were two ways to eliminate interfering exosome [155]; Therefore, in our study, we selected serum-free condition at 48 hours. These conditions were not affect on ADSC morphology and gene expression.

The method is followed by Vlassov et al [156]. Briefly, the supernatant was removed from 80% confluent cells. The supernatant was centrifuged at 300 g for 10 mins at 4°C. Next; the supernatant was transferred to a new tube. It was centrifuged at 2,000 g for 10 -20 mins at 4°C (for removing cell death). Then, the supernatant was transferred to a new tube and centrifuged at 10,000 g for 30 mins at 4° C (for removing cell debris). The solution was filtrated with 0.22 µm filter and centrifuged at 100,000 g ( BECKMAN L-80, rotor type 90 Ti) for 70 mins at 4° C. After



ultracentrifugation. The pellets were resuspended PBS. Finally, the EV pellets can keep it at  $-80^{\circ}\text{C}$  [156].

#### Dynamic light scattering and Nano tracking analysis (NTA)

The method was determined the size by spectrophotometric-based assay, called Zetasizer (Malvern, DKSH). This instrument was detected the size of the particle in nanometers. Dynamic Light Scattering was used to measure particle size, molecular size, and dispersity. Measurement range: 0.3 nm – 10.0 microns (diameter).

We isolated ADSC-EVs from  $1.5 \times 10^6$  cells and ultracentrifuge followed by the protocol above. Then, the fresh ADSC-EVs dilute in 1 ml inject into glass tray. The sample was determined size by Zetasizer. Moreover, the result performed the diameter size in nanometers.

Moreover, the concentration of ADSC-EVs was analyzed by nano tracking analysis (NTA). This method aims to determine the number of nanoparticles (EVs) in particles/ml. This instrument needs to dilute the sample in 1 ml. The acceptable range is  $10^7 - 10^9$  particles/ml [157]. This test needed to determine a part of quality control. The ADSC-EVs which was kept 1 year ago at  $-80^{\circ}\text{C}$  and was prepare freshly were compared the number of particles.

#### Transmission electron microscope (TEM)

TEM can observe many characteristics of the specimen, such as the stress of the specimen, its crystallization, morphology, and even its holography. For investigate the ADSC-EVs structure, TEM was very acceptable method for characterization [158]. Moreover, the scanning electron microscope was an additional result to observe the whole structure of ADSC-EVs.

The method was fixed by 1% glutaraldehyde in cold DPBS for 5 mins to stabilize the immunoreaction, washed in sterile distilled water. The sample ( $1 \times 10^7$  particles/ml) was dropped on CU-grid. Then, the sample on grid was stained with 1% uranyl acetate 3 mins. The sample was made dry in desiccator. A JEOL 1010 TEM was used to image exosome samples at a voltage of 80kV.

## Results

### Determination of ADSC-EVs size

Dynamic Light Scattering is a technique that have the same role of spectrophotometry by generating the light beam to scatter the particles. The result from size distribution profile of small particles in solution especially nanometer size EVs.

This experiment was selected in the measurement range: 0.3 nm – 10.0  $\mu\text{m}$  (diameter). The result showed that the sample size was 170.7 nm on average diameter. These finding indicated that our samples were microvesicle particles.

We collected the data from this technique from the early passage to late passage to fulfil a quality control criterion for clinical trials [159].



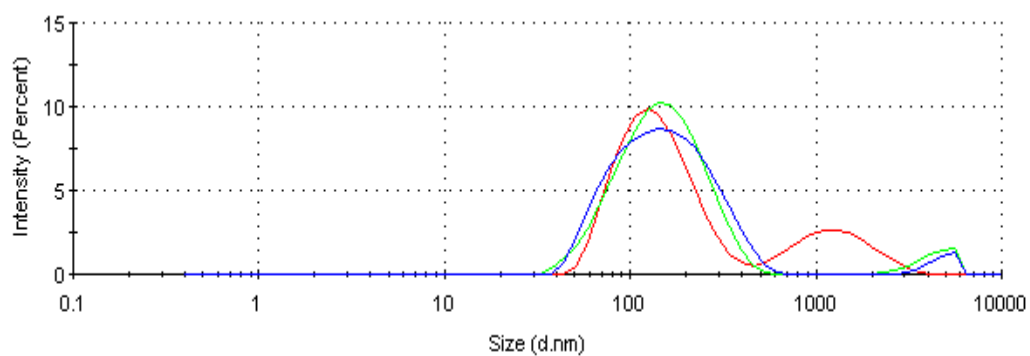


Figure 37 Dynamic light scattering (DLS) of ADSC-EVs.  
The peak was 170.7 nm and 4740 nm were detectable (n=3).





The structure of ADSC-EVs

Transmission electron microscope (TEM) detected the EV structure with osmium tetroxide ( $\text{OsO}_4$ ) and uranyl acetate, respectively. In contrast, TEM was more very popular technique and was more acceptable technique than SEM. Therefore, we decided to observe structure and to accept TEM image in our study.

For TEM images, the size of ADSC-EVs in serum-free conditioned media at 48 hours was approximately 220 nm diameters. It was the similar size from zetasizer on average. They were extracellular-like vesicles. This technique can observe the deep structure inside ADSC-EVs.



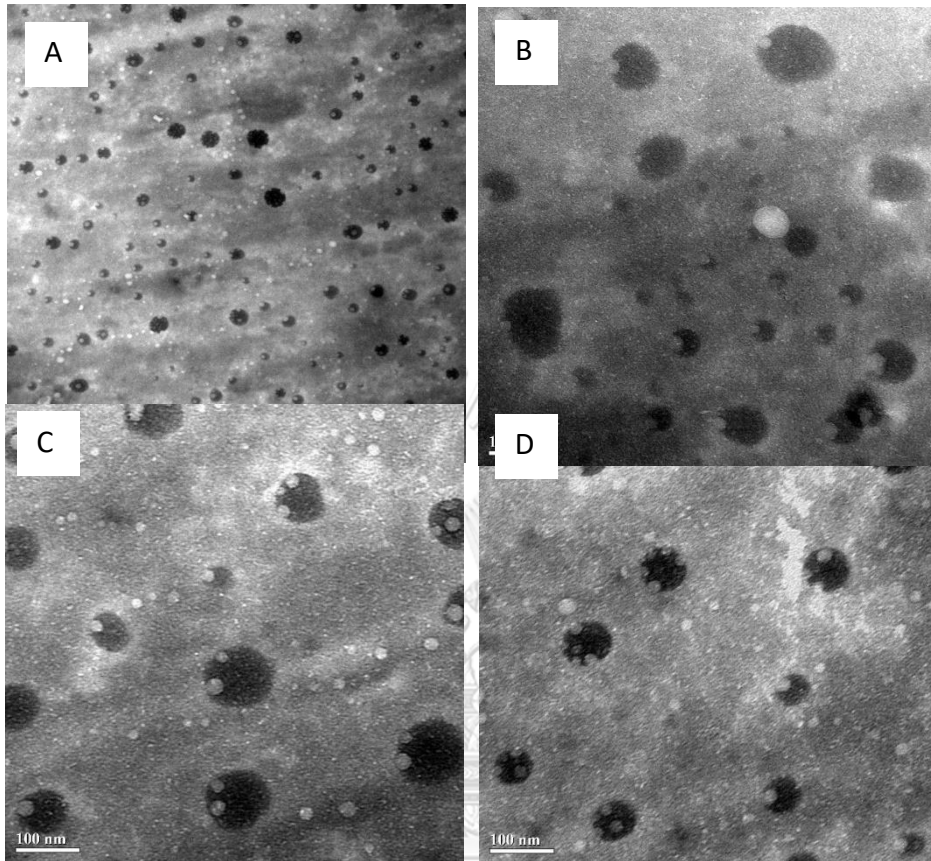


Figure 38 Transmission electron microscope (TEM) of EVs.

The EVs have circle shape. It contained the particles (Black color). The size is approximately 220 nm diameters.

### Characterization of ADSC-EVs

This technique was determined after ultracentrifugation step. The characterization of ADSC-EVs needs to determine by RT-PCR. EV markers such as CD9 and CD81 were selected. GAPDH, which is a housekeeping gene, was also applied, and CD105 was used for checking the EV origin.

The result showed that the gene expression of EVs was CD9 and CD81 as tetraspanin group for identify EVs, Moreover, we found the expression of CD105, which is ADSC marker. The result indicated that EV-containing molecules had been release from ADSCs because there was an expression of ADSCs marker; CD105.



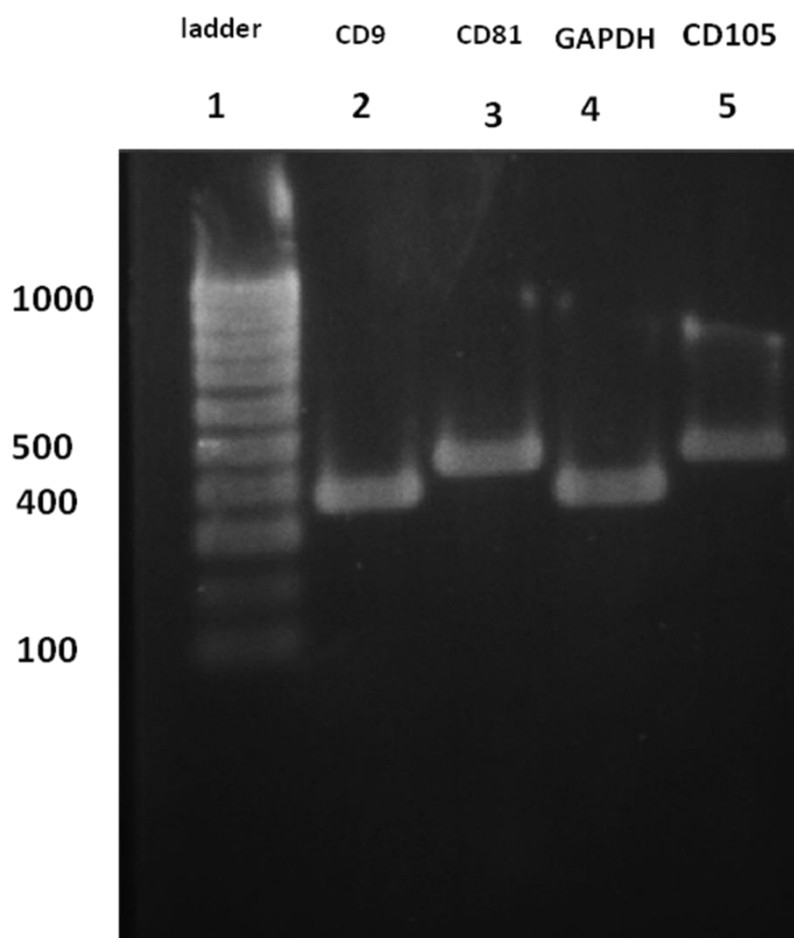


Figure 39 The expression of ADSC-EVs performed by RT-PCR.

Lane 1 indicates DNA ladder, Lane 2 indicates CD 9, Lane 3 indicates CD 81, Lane 4 indicates GAPDH and Lane 5 indicates CD 105.

### Storage condition of ADSC-EVs

EVs were secreted *in vitro* by cultured cells. Their composition should ideally be compared with that of the secreting cells to determine the level of the EVs components [160]. In terms of molecular markers, the presence of different marker proteins or lipids should be analyzed in a semi-quantitative manner in any EVs preparation [159], including EVs isolate from secreting cells *in vitro*. The expected proteins should be characterized in the EVs of interest, especially transmembrane proteins and cytosolic proteins with membrane binding capacity [160].

The effect of passage number of ADSCs on EVs and ADSCs marker expression was investigated. ADSCs were plated at the same density (cell/ml) and added the same volume of serum-free media after 80% confluence. EVs were collected by ultracentrifugation after 48 hours in a different passage.

The other effect of storage of ADSC-EVs was determined by NTA and gene expression. The reason is when you would like to develop the drug from EVs, you should have the stability of EVs for sortation time. In this study, we compared between the old stock for 1 year and freshly prepare.

The criteria and the result for storage of pharmaceutical product was followed;

1. Sanitation = transport and clearness
2. Temperature =  $-80^{\circ}\text{C}$  can store and maintain the stability.
3. Light = should be wrap with foil or use protective container.
4. Moisture = in case of solid/powder.
5. Solution = dissolved ADSCs in sterilized PBS at  $-80^{\circ}\text{C}$
6. Segregation = always used ultracentrifugation and all condition was the same.

Usually, the number of cells that use to study quality control is approximately  $1 \times 10^6 - 1 \times 10^8$  [161]. Media was added the same volume after 80% confluence and incubated 48 hours. EVs were collected by ultracentrifugation.

ADSC-EVs can store over 1 year and make an information for stabilization

The stability of ADSC-EVs was tested on gene expression by RT-PCR. We hypothesized that ADSC-EVs could stable after one year or more years keeping during storage at -80 °C. However, many publications suggested that EVs storage in -80 °C should be stabilized. The result showed that the EV markers, including CD9 and CD81, expressed. But for our samples tested between ADSC-EVs keeping a year later and fresh ADSC-EVs by using nanosight. This data can show that the concentration of the old sample and a fresh sample was in the acceptable range:  $10^7 - 10^9$  particles/ml [157]. The acceptable range of concentration is how to control the concentration of EVs that can detect in appropriate detection by nanosight. Some sample might need to dilute the sample.

Even though, the concentration of ADSC-EVs from the old stock and from freshly prepare was not significantly differenced. But the size distribution was differenced. We found that a year stock was bigger size than fresh preparation. However, the mean size was micovesicles.

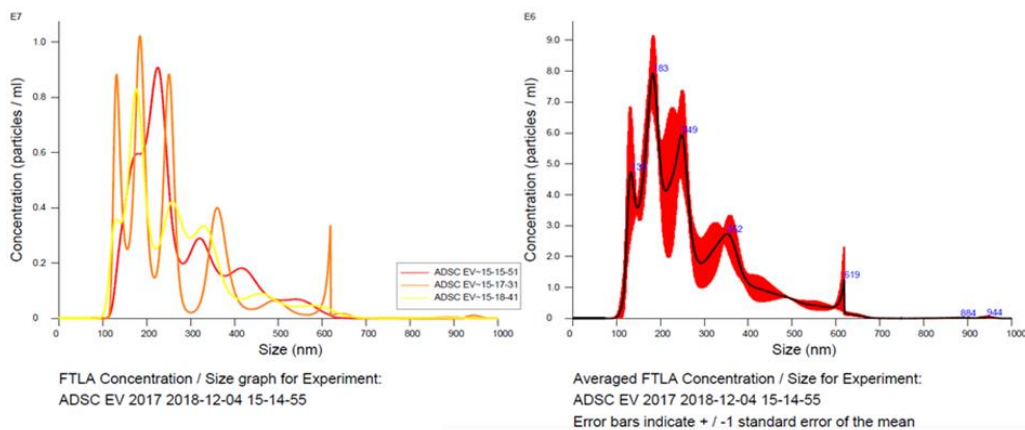
Table 16 The size distribution of ADSC-EVs from the old stock.

Size distribution	Size (nm)
D10	147.4
D50	236.3
D90	433.1
Mean	267.7 ± 3.4

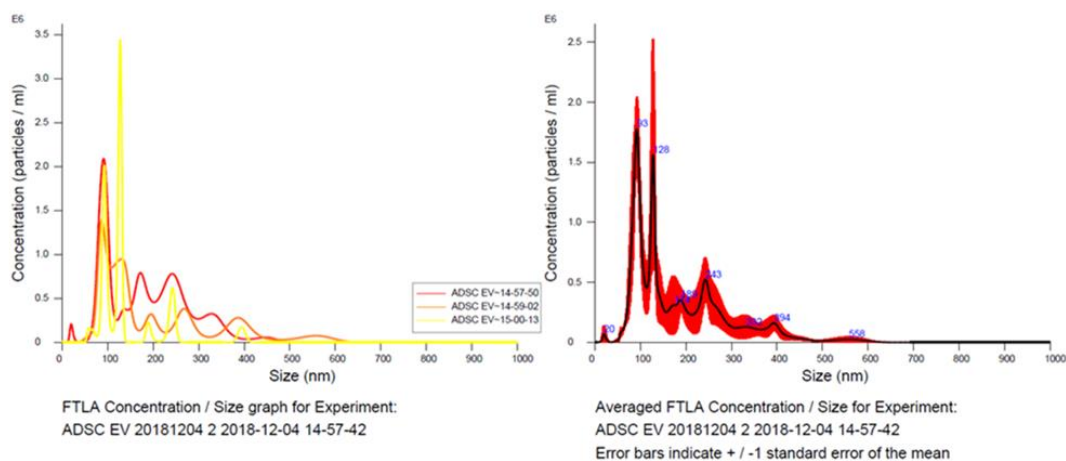
Table 17 The size distribution of ADSC-EVs from fresh preparation.

Size distribution	Size (nm)
D10	84.5
D50	138.6
D90	343.7
Mean	178.4 ± 18.6

### Old stock (1 year keep at -80 °C)



### Fresh preparation



CHULALONGKORN UNIVERSITY

Figure 40 The graph of Nanoparticle tracking analysis (NTA) in different storage conditions.

Top picture indicates the concentration of EVs from the old stock at -80 °C for one year. Below picture indicates the fresh stock prepared after ultracentrifugation.



#### ADSCs gene expression after treated with serum-free condition

Characterization of ADSCs was detected by RT-PCR after we treated with serum-free condition. Even though, Fetal bovine serum (FBS) is an abundant source of the factors required for cell attachment, growth and proliferation. It thus used as an almost universal growth supplement effective for most types of human and animal cells. This section was wondered the effect of cell proliferation and cell morphology changed [162]. Therefore, we need to investigate the effect of gene expression after serum-free condition.

Therefore, the effect of these condition on ADSC morphology was determined. The gene expression of ADSCs was detected by RT-PCR. The band density was analyzed by ImageJ software to compare serum condition and serum-free condition. We found that serum-free condition at 48 hours was not affected on gene expression.

The reason why we selected 48 h for collect ADSC-EVs. The appropriate time for treatment was 24-72 hours [163]. If ADSCs were cultured more than 72 hours. It can lead to occur oxidative stress. These evidences can suggest that our condition to isolate ADSC-EVs was appropriated. Interestingly, the morphology of ADSCs was not changed. Moreover, we found ADSC marker; CD105 in ADSC-EVs. This gene expression was confirmed that EVs were released from ADSCs.

Moreover, the band density of ADSC gene expression was analyzed by ImageJ software. The result showed that the gene expression did not changed significantly after serum-free condition at 48 hours. It showed in % control (Control was serum condition, which was 100% and compared with the serum-free condition). In terms of the physical appearance of ADSCs, most morphology of ADSCs was not changed after treated with the serum-free condition. Therefore, they still fibroblast-like cells.

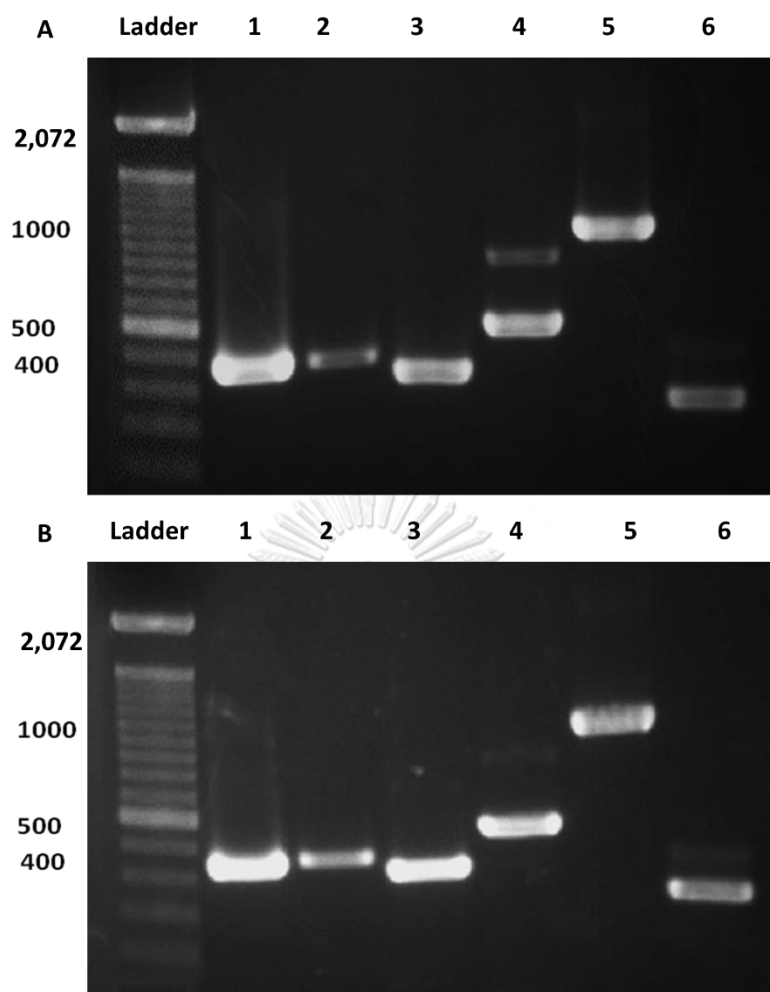


Figure 41 The effect of serum-free condition on ADSCs gene expression after 48 h treatment.

A) indicates the expression of ADSCs in serum condition. B) indicates the gene expression of ADSCs in serum-free condition. Lane 1 indicates  $\beta$ -III tubulin, 2 indicates nestin, 3 indicates CD105, 4 indicates CD90, 5 indicates Stro-1 and 6 indicates GAPDH.

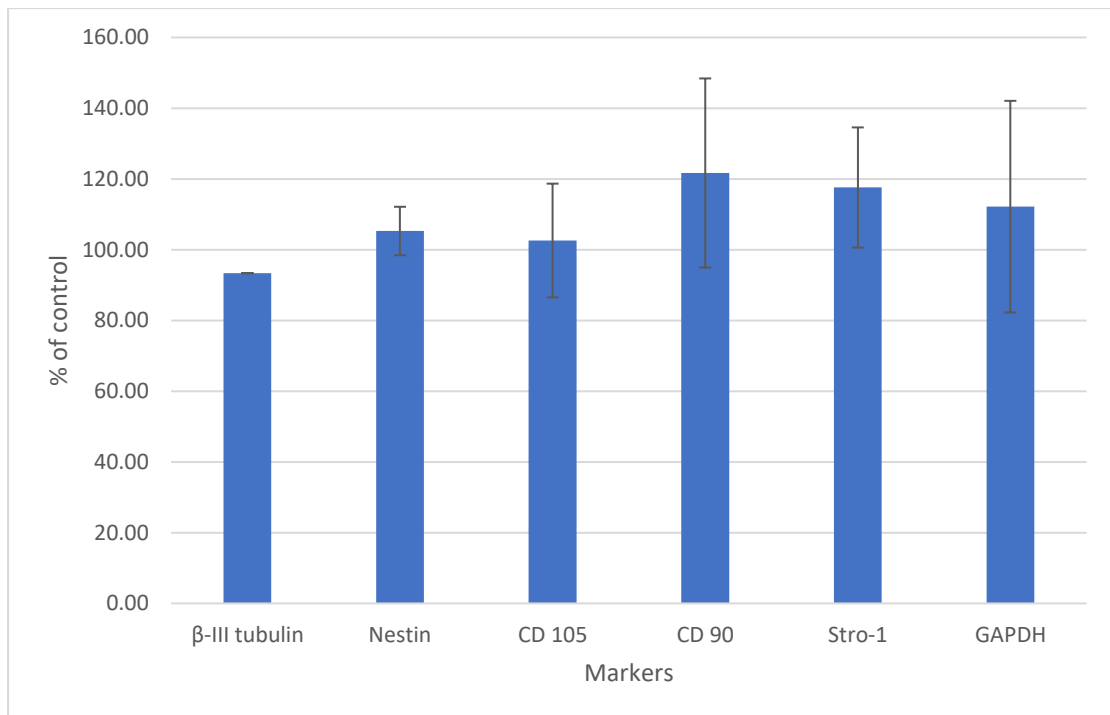


Figure 42 The gene expression of serum-free condition after treated with serum-free media.

This data compared between serum condition (control) and serum-free condition after 48 hours. The markers were compared the same set of gene expression from RT-PCR. They were not significant different ( $p$ -value  $< 0.05$ ) ( $n=3$ ).

## Discussion for ADSC-EVs

ADSCs secrete EVs into culture media

For EV characterization, the stabilization and size of EVs should be concerned. During the experiment or isolation step, we need to follow the quality control from the clinical guideline [14].

Moreover, the EVs characterization of TEM and SEM image should be discussed. The previous result, Exosome-derived ADSCs showed that ADSCs release the EVs, size approximately 1.7 – 3  $\mu\text{m}$  by using SEM. ADSCs can release EVs to cell-cell communication effects on the target cells and protect themselves from life [164].

The result of TEM image was compared with this article [25] . They reported that the TEM image from exosome secreted by MSC was size less than 500 nm and the structure is black and have some white particles inside like our study [25].



ADSC-EVs contains ADSC markers

During the RT-PCR step for characterization of ADSC-EVs. We found GAPDH gene in ADSC-EVs expressed in PCR product because the intercellular communication obtains biomolecules as mRNA and proteins. According to Arshlan 2013, MSC exosomes were found GAPDH in EVs [165]. Other findings showed that GAPDH expression was determined by qRT-PCR from HeLa cell-derived exosome [166].

Interestingly, we also found ADSC marker in ADSC-EVs; CD 105. These evidences could reconfirm where the biogenesis of EV come from ADSCs. This finding can conclude that we can use ADSC-EVs in terms of cell-free therapeutic application [167].

Moreover, we linked our finding to cell-free therapeutic application. According to Hyun Ok Kim, et al. [167], they found the conditioned medium collected from MSC promotes proliferation and migration of endothelial cells and vascular smooth muscle cells in vitro and mediates blood flow recovery of ischemic hindlimb<sup>77</sup> and cardiac infarction [167]. The composition that they found followed.

Table 18 The conclusion of size of ADSC-EVs from different bathes.

No.	EVs from different Batch (form serum-free condition of ADSC)	No. Peak	peak 1 (nm)	peak 2 (nm)
1	ADSC P. 3	1	301.80	
2	ADSC P. 4	1	309.90	
3	ADSC P. 5	1	385.70	
4	ADSC P. 7	2	216.20	5432.00
5	ADSC P. 8	2	474.40	87.45
6	ADSC P. 8	2	170.70	355.40
7	ADSC P.12	1	180.50	
8	ADSC p.16 #1	2	186.60	50.60
9	ADSC p.16 #2	1	161.80	
10	ADSC P.18	1	147.30	
11	ADSC p.19 #1	2	170.40	14.84
12	ADSC p.19 #2	2	119.20	20.41
13	ADSC p.19 #3	1	237.00	
14	ADSC p.20 #1	1	118.80	
15	ADSC P.20 #2	1	118.80	
16	ADSC P.21	1	128.80	
17	ADSC P.22 #1	2	158.80	13.60
18	ADSC P.22 #2	1	365.30	
19	ADSC P.22 #3	2	140.20	3662.00
20	ADSC P.23	1	115.30	
21	ADSC P.24	1	198.20	
Average			209.80	1204.54
	PBS	2	393.60	3.88
	PBS	1	186.80	

Average	199.93	1084.47
---------	--------	---------

Note Table 18: #1 is first time, #2 is second time and #3 is third time. P. indicate the passage no.

Moreover, we tested the concentration of ADSC-EVs in late-stage compared a year stock at -80 °C and freshly prepared stock. We found that the concentration was not significantly different because the data from NTA had an acceptable range of  $2 \times 10^8$  to  $20 \times 10^8$  particles/ml [168, 169]. In our study, the concentration compared between old stock and freshly preparation were  $1.18 \times 10^9 \pm 4.63 \times 10^7$  particles/ml and  $1.33 \times 10^8 \pm 2.82 \times 10^7$  particles/ml respectively. Therefore, the data of the storage condition at -80 °C was stable. This data was indicated that we can get a one part of quality control requirements. However, the data was not covered all the quality control lists.

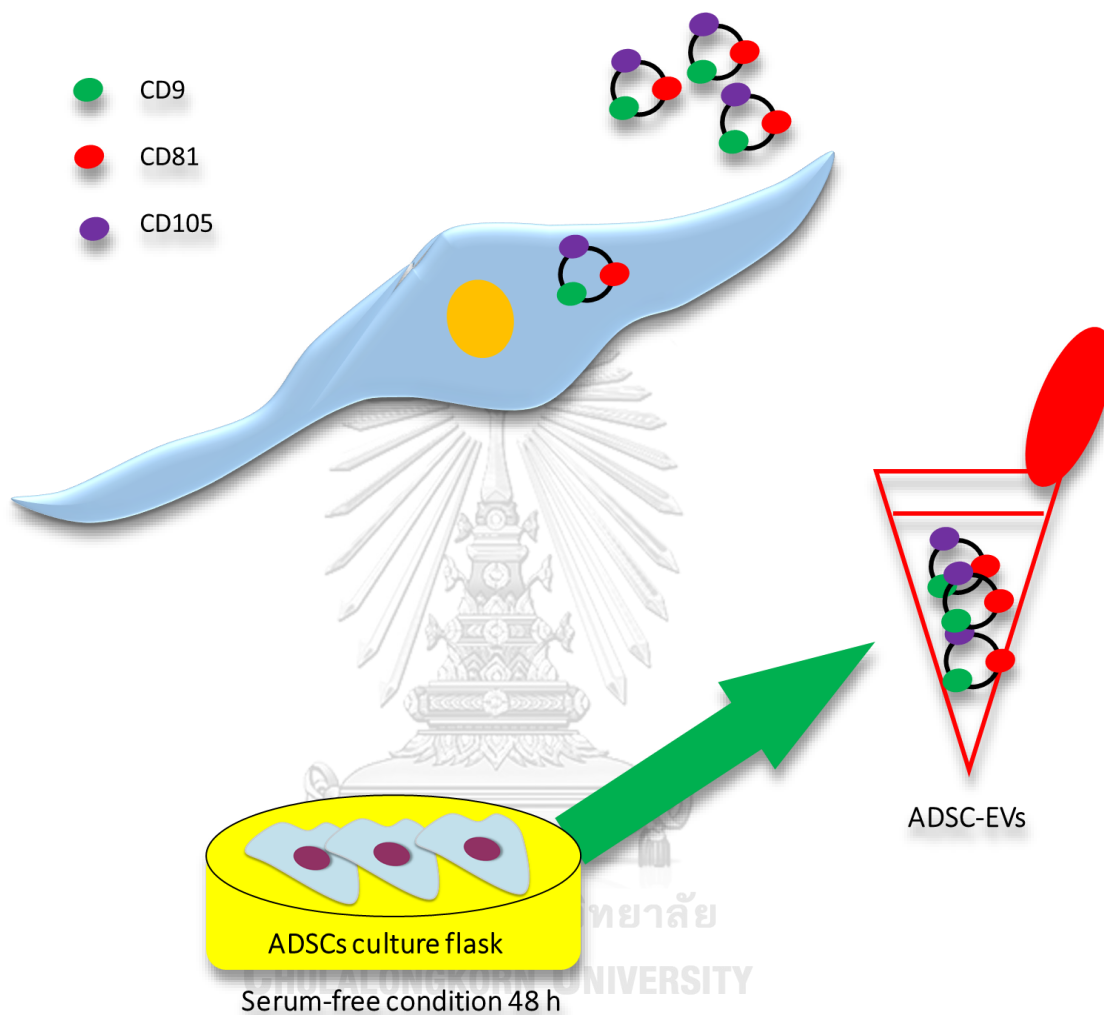


Figure 43 The concept of ADSC-EVs from cell cultured in serum-free media. ADSCs release EVs in serum-free condition after 48 hours. The gene expression of EVs showed EVs markers (CD9 and CD81). We also found ADSC marker; CD105 expressed in EVs.



### Supplement data of SF-MCF-7 on angiogenesis.

The result of cell viability was detected by MTT assay Live/Dead staining

The viability of cells, after combined with scaffolds was also studied. First, the MTT assay was performed to determine the effect of SF scaffolds on cell viability. We found that the SF-MCF-7 scaffolds was significantly different compared to silk fibroin without cell. However, the relative absorbance of SF-MCF-7 scaffolds was slightly decreased.

The data was not significant. Then, Cell staining by acridine orange and Hoechst 33342 validated cell live/viability for all kinds of SF scaffolds, indicating a non-toxic effect of SF scaffolds. This data showed the brighten blue/green spot inside SF scaffolds. The data supported the cell viability of ADCSs on SF scaffolds after three days of incubation and showed the localization of MCF-7 on silk scaffolds. These results indicated that MCF-7 still live and can refer to the activation of angiogenesis on CAM assay.

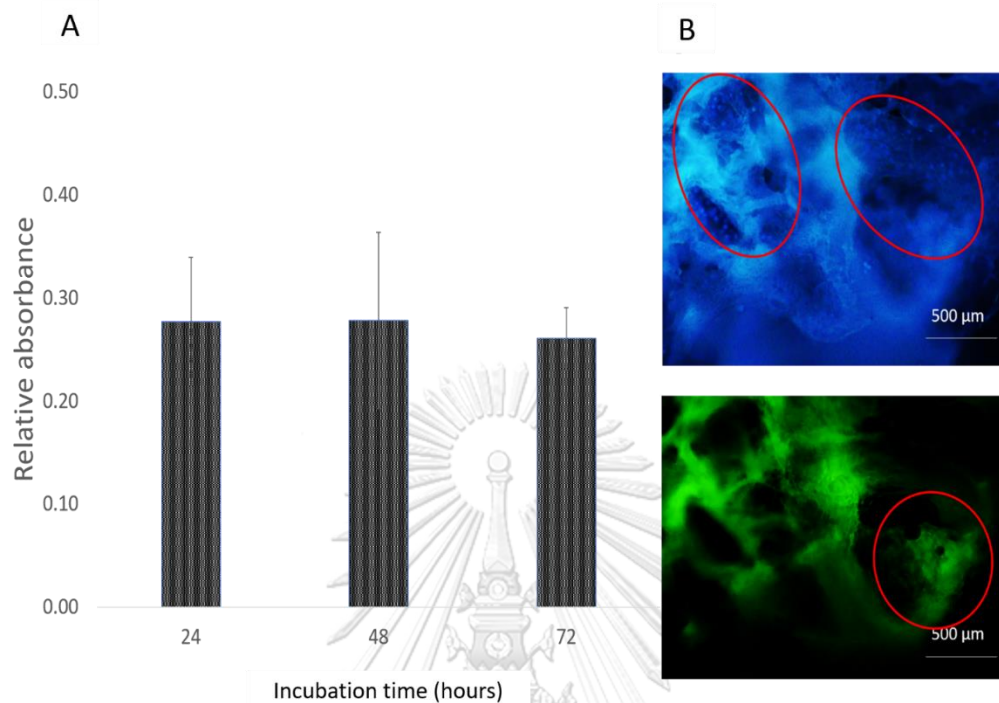


Figure 44 The effect of SF scaffolds on MCF-7 viability by MTT assay and cellular live/dead fluorescence staining of SF-MCF-7 scaffolds by Hoechst and Acridine orange.

A) indicate the relative absorbance of SF-MCF-7 scaffolds. The data calculated from the absorbance of SF-MCF-7 scaffolds minus the absorbance of SF scaffolds. It showed no significant difference and no proliferation of MCF-7. This result was not significantly differenced ( $p < 0.05$ ). B) indicate Live/dead fluorescence staining after 3 days of incubation. The bright green spots are live cells, and the bright blue spots are the nucleus.

SF-MCF-7 scaffolds activates angiogenesis on CAM assay that caused the spoked-wheel pattern.

The indicative angiogenic properties were observed by the spoke-wheel formation of blood vessels around the SF scaffolds in various groups. Then, the data was given a score by the blind method, compared among E12, E14, and E18 of chicken embryo development. This method needs to determine the blood vessel formation or to observe a spoked-wheel pattern. The SF scaffolds induced the angiogenesis at E14. Whereas the SF-MCF-7 scaffolds also induced the angiogenesis at E12. This finding indicated that the scaffolds either with or without MCF-7 could activate angiogenesis. The SF-MCF-7 scaffolds promote angiogenesis at an earlier developmental time point.

Moreover, we compared the angiogenic properties between filter paper as a sham material and SF scaffolds. The result showed that the filter paper showed significantly lower scores than other groups. If we compared filter paper and SF scaffolds can induce the formation of blood vessels, only the SF scaffolds allowed penetration of blood vessels into the scaffolds.

Table 19 Angiogenesis scoring of MCF-7 or no cell implanted with SF scaffolds.

Scaffolds	Angiogenesis score (0-5)			
	Score at E8	Score at E12	Score at E14	Score at E18
SF scaffolds	0.00 ± 0.00	2.40 ± 0.24	3.60 ± 0.24	3.75 ± 0.25
SF-MCF-7 scaffolds	0.00 ± 0.00	3.75 ± 0.47	4.25 ± 0.25	4.5 ± 0.50
Filter paper	0.00 ± 0.00	2.33 ± 0.57	2.55 ± 0.25	Not determined

The cryostat machine cut SF-MCF-7 scaffolds after fixation. The implanted scaffolds were dissected to observe a group of blood vessels penetrated porous structures in the scaffolds. We detected blood vessels in both types of scaffolds at E18. Histological analysis revealed that the blood vessels penetrated throughout the scaffolds. Moreover, there were different sizes of blood vessels inside the scaffolds. The penetration of blood vessels was early in E12 when the implanted scaffolds had been seeded with MCF-7. The scaffolds had the penetration starting from E14. This data will give strong evidence to support the angiogenic capacity on CAM assay. Moreover, to make sure that cancer cells can activate angiogenesis faster than SF scaffolds without cells.

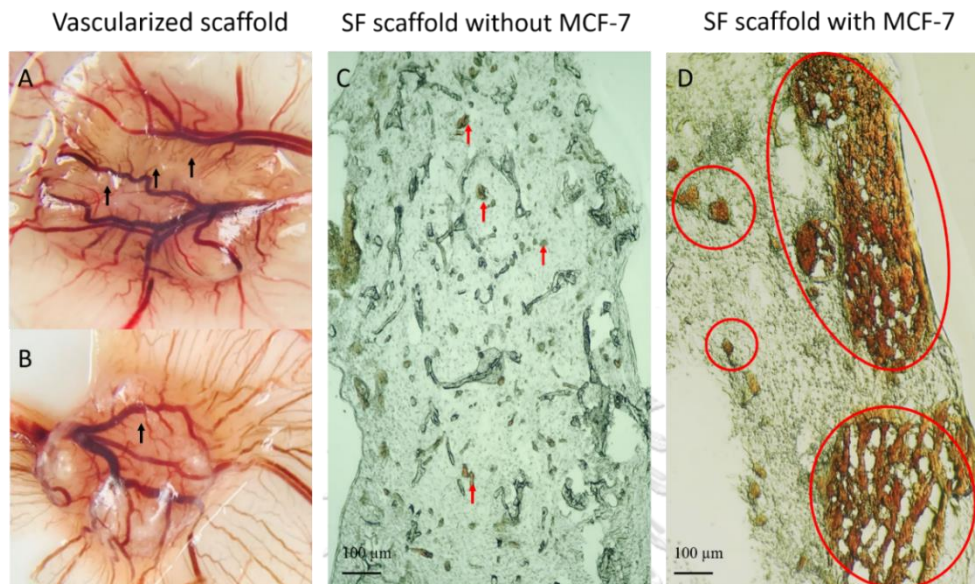


Figure 45 The vascular network formation of blood vessels on SF-MCF-7 scaffolds. A) indicates the vascularized SF-MCF-7 scaffolds of under-CAM., B) indicates the vascularized SF scaffolds of under-CAM; Dark arrows indicate branching of blood vessels, C) indicates the histology of SF-MCF-7 scaffolds, D) indicates the histology of SF scaffolds; Red circles indicate well-organized blood vessels. The Scale bar was 100  $\mu\text{m}$ . The magnification of image indicates 10X.

### Secondary stock calculation for adipogenic differentiation

20 mM dexamethasone >>>> 10 mM dexamethasone

- a. 2<sup>nd</sup> stock of 10 mM dexamethasone 1 ml

$$20 \times V1 = 10 \times 1 \text{ ml}$$

$$V1 = 0.5 \text{ ml}$$

So, add 100% ethanol 0.5 ml to total at 1 ml

- b. 3<sup>rd</sup> stock from 10 mM dexamethasone >>100  $\mu$ M dexamethasone 1 ml

$$10 \times 10^{-3} \times V1 = 100 \times 10^{-6} \times 1 \text{ ml}$$

$$V1 = 0.01 \text{ ml}$$

So, add ethanol 0.99 ml to total 1 ml

- c. Final conc. from 100  $\mu$ M dexamethasone to 1  $\mu$ M dexamethasone in 16

ml media

$$N1 \times V1 = N2 \times V2$$

$$100 \times V1 = 1 \times 16 \text{ ml}$$

$$V1 = 0.16 \text{ ml}$$

So, pipette 0.16 ml from 20 mM dexamethasone into media.

2. 250 mM IBMX >>> 100 mM IBMX

- a. 2<sup>nd</sup> stock of 100 mM IBMX 0.5 ml

$$250 \times V1 = 100 \times 1 \text{ ml}$$

$$V1 = 0.2 \text{ ml in DMSO 0.3 ml}$$

- b. 3<sup>rd</sup> stock of 100 mM to 250  $\mu$ M IBMX

$$100 \times 10^{-3} \times V1 = 250 \times 10^{-6} \times 10 \text{ ml}$$

$$V1 = 0.025 \text{ ml}$$

So, add DMSO 9.75 ml to the total 10 ml

- c. Calculate final conc. from 250  $\mu$ M IBMX to 0.5  $\mu$ M IBMX 16 ml media

$$250 \times V1 = 0.5 \times 16 \text{ ml}$$

$$V1 = 0.032 \text{ ml}$$

So, pipette 0.032 ml from 0.5  $\mu$ M IBMX into media

### Secondary stock for Osteogenic differentiation

First, calculate the final concentration of 10 nM dexamethasone from 100  $\mu$ M dexamethasone from adipogenic differentiation stock. Dilute it into 10 nM dexamethasone before adding to the media at 16 ml total solution, followed by

$$100 \times 10^{-6} \times V1 = 10 \times 10^{-9} \times 1600 \mu\text{l}$$

$$V1 = 1.6 \mu\text{l}$$

So, pipette 1.6  $\mu$ l from 100  $\mu$ M dexamethasone into media

### Calculation of 200nM L (+) ascorbic acid (Primary stock)

Prepare 10 ml of PBS, M.W. = 176.13 g/mol

$$\begin{aligned} (\text{g}) &= \frac{200 \times 10^{-3} \times 10 \times 176.13}{1000} \\ &= 0.35226 \text{ g} \end{aligned}$$

### Preparing incomplete media

Dulbecco's Modified Eagle Medium was diluted with ultrapure water. It mixed with  $\text{NaHCO}_3$  7.41 g/2 liters pH 7.202. Filtered it by using pump.

## Catalase activities law data

$$k/g \text{ prot} = 69/Dt \times \log(A1/A2)/ \text{prot g/ ml}$$

N1

keratinocyte	time (sec.)	Absorbance	Absorbance	Absorbance	mean	k/g prot	SD	SEM
	0	0.519	0.60	0.5287	0.548967	48.74432	0.081599	0.047111
	300	0.369	0.47	0.5708	0.4707			
ADSCs	time (sec.)	Absorbance	Absorbance	Absorbance	mean	k/g prot		
	0	0.573	0.500	0.578	0.550	10.62	0.036451	0.021045
	300	0.561	0.499	0.565	0.542			

N2

keratinocyte	time (sec.)	Absorbance	Absorbance	Absorbance	mean	k/g prot	SD	SEM
	0	0.678	0.678	0.678	0.678	63.92416	2.253953	1.30132
	300	0.385	0.398	0.398	0.394			
ADSCs	time (sec.)	Absorbance	Absorbance	Absorbance	mean	k/g prot		
	0	0.495	0.486	0.484	0.366	4.194576	0.711605	0.410846
	300	0.486	0.474	0.474	0.478			

N3

keratinocyte	time (sec.)	Absorbance	Absorbance	Absorbance	mean	k/g prot	SD	SEM
	0	0.387	0.352	0.359	0.366	63.8737	15.09877	8.717276
	300	0.18	0.217	0.202	0.200			
ADSCs	time (sec.)	Absorbance	Absorbance	Absorbance	mean	k/g prot		
	0	0.377	0.384	0.378	0.285	6.125463	0.281291	0.162403
	300	0.363	0.37	0.363	0.365			

Table 20 The conclusion of CAT activity (U/g prot.).

Sample	catalase activity (k/g prot)			mean	SD	SEM
	1	2	3			
Keratinocyte cells	48.744	63.924	63.874	58.847	8.7496	5.0516
ADSCs	10.619	4.195	6.125	6.980	3.2963	1.9031

## GPx activities law data

Keratinocytes 1 = Passage 98

Keratinocytes 2 = Passage 99



Keratinocytes 3 = Passage 100

ADSC 1 = Passage 9

ADSC 2 = Passage 10

ADSC 3 = Passage 11

### N1

HaCaT	time (sec.)	P98	P99	P100	mean		
	0	0.6650	0.6287	0.6030	0.632233333		
	300	0.6008	0.5845	0.5590	0.581433333		
	A1-A2	0.0642	0.0442	0.0440	0.0508	SD	SEM
	GPx act	5.0362	3.6851	3.2029	3.9747	0.95	0.55
ADSCs	time (sec.)	P3/6	P3/7	P3/8	mean		
	0	0.6514	0.5793	0.5789	0.6032		
	300	0.6160	0.5474	0.5429	0.568766667		
	A1-A2	0.0354	0.0319	0.0360	0.034433333	SD	SEM
	GPx act	3.778	2.754	4.523	3.685	0.888144	0.51277

### N2

HaCaT	time (sec.)	P98	P99	P100	mean		
	0	0.6688	0.6633	0.6834	0.672		
	300	0.6255	0.6185	0.6288	0.624		
	A1-A2	0.0433	0.0448	0.0546	0.048	SD	SEM
	GPx act	2.64403	3.777228	4.629345	3.684	0.995968	0.575023
ADSCs	time (sec.)	P3/6	P3/7	P3/8	mean		
	0	0.6414	0.5893	0.5789	0.603		
	300	0.6147	0.5788	0.5442	0.579		
	A1-A2	0.0267	0.0105	0.0347	0.024	SD	SEM
	GPx act	1.615502	2.471779	4.15112	2.746	1.289881	0.744713

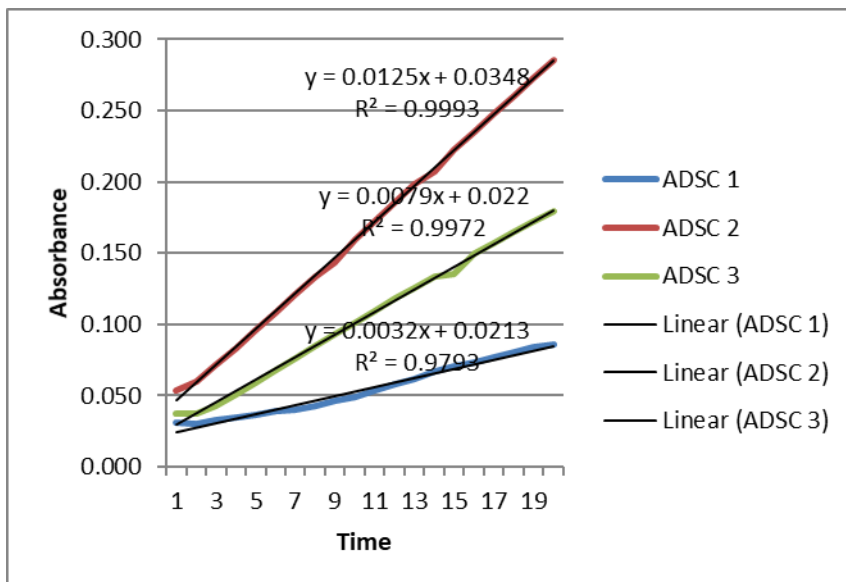
### N3

HaCaT	time (sec.)	P98	P99	P100	mean		
	0	0.6688	0.6633	0.6834	0.671833		
	300	0.62255	0.6185	0.6411	0.627383		
	A1-A2	0.04625	0.0448	0.0423	0.04445	SD	SEM
	GPx act	2.981687	3.777228	2.974085	3.244333	0.461516	0.266456
ADSCs	time (sec.)	P3/6	P3/7	P3/8	mean		
	0	0.6414	0.5893	0.5789	0.6032		
	300	0.6107	0.5496	0.5453	0.568533		
	A1-A2	0.0307	0.0397	0.0336	0.034667	SD	SEM
	GPx act	2.609657	4.590446	3.836207	3.67877	0.999736	0.577198

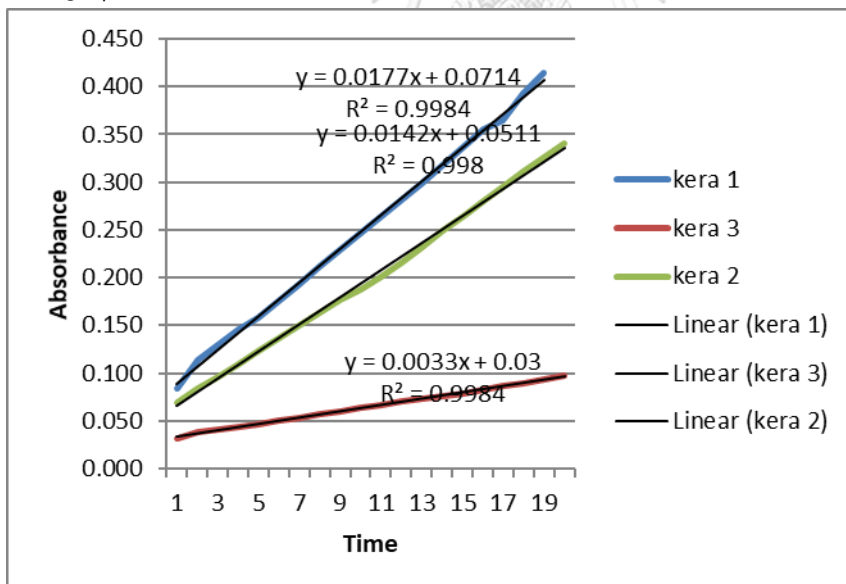


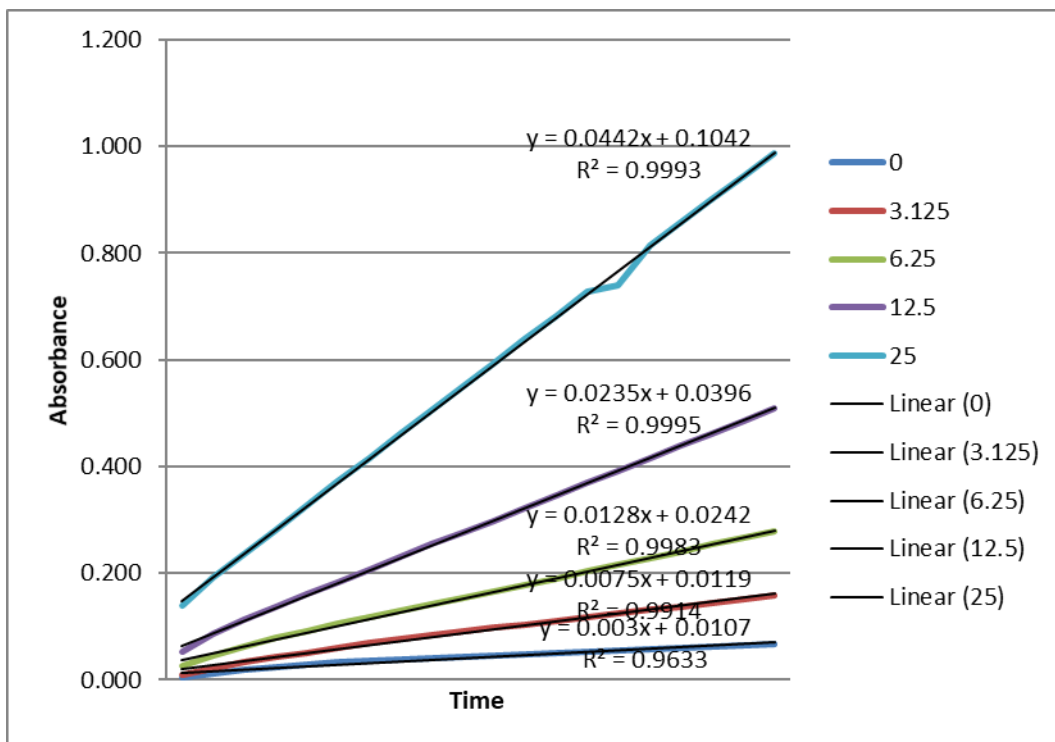
### GSH levels Law data

The graph of ADSCs in various time.

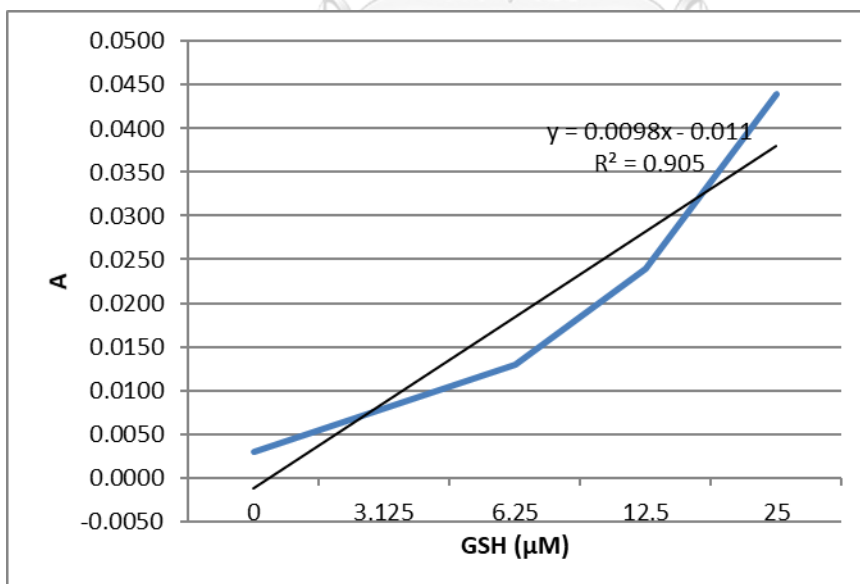


The graph of HaCAT in various time.



Standard Curve of GSH ( $\mu\text{M}$ )

To find "a" from the standard curve



GSH ( $\mu\text{M}$ )	a
0	0.0030
3.125	0.0080
6.25	0.0130
12.5	0.0240
25	0.0440

Find the "a" (absorbance) of Sample

Keratinocytes 1 = Passage 98

Keratinocytes 2 = Passage 99

Keratinocytes 3 = Passage 100

ADSC 1 = Passage 9

ADSC 2 = Passage 10

ADSC 3 = Passage 11

Table 21 The absorbance and calculation data of GSH level ( $\mu\text{M}$ ).

keratinocyte	a	a	a		GSH( $\mu\text{M}$ )	GSH( $\mu\text{M}$ )	GSH( $\mu\text{M}$ )	Mean	SD	SEM	MEAN	Ave SEM
1	0.0155	0.0265	0.0110		2.704	3.827	2.245	2.925	0.728	0.42		
2	0.01195	0.00915	0.0215		2.342	2.056	3.316	2.571	0.591	0.34		
3	0.0072	0.00195	0.0005		1.857	1.321	1.173	1.451	0.322	0.19	2.32	0.32
ADSC	a	a	a		GSH( $\mu\text{M}$ )	GSH( $\mu\text{M}$ )	GSH( $\mu\text{M}$ )	Mean				
1	0.0032	0.003	0.003		1.449	1.429	1.469	1.449	0.018	0.01		
2	0.0125	0.0124	0.013		2.398	2.388	2.398	2.395	0.005	0.00		
3	0.0079	0.0078	0.008000		1.929	1.918	1.939	1.929	0.009	0.01	1.92	0.01



### SOD contents law data

Standard curve of CU-Zn SOD

Table 22 Standard curve of CU-Zn SOD

1.5625	0.1696	7.926167
3.125	0.1602	13.02932
6.25	0.1307	29.04452
12.5	0.1148	37.67644
25	0.0858	53.4202
50	0.0834	54.72313
blank	0.1842	0

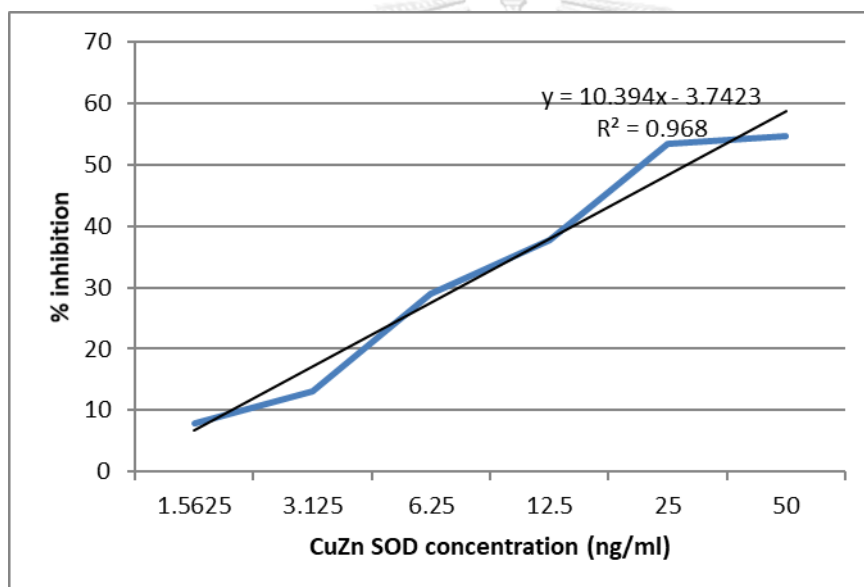


Table 23 The absorbance of SOD activities and the calculation of % inhibition and SOD contents.

cell type	sample	A560	A560	A560	%inhibition	%inhibition	%inhibition	SOD content	SOD content	SOD content	SOD content	SOD content	Mean	SD	SEM
Keratinocyte (HaCat)	P98	0.138	0.135	0.141	25.0814	26.7101	23.4528	2.7731	2.9298	2.6164	2.7731	2.7731	0.140	0.08	
	P99	0.1336	0.1326	0.1329	27.4701	28.0130	27.8502	3.0029	3.0552	3.0395	3.0325	3.0325	0.024	0.01	
	P100	0.1699	0.158	0.1622	7.7633	14.2237	11.9435	1.1069	1.7285	1.5091	1.4482	1.4482	0.282	0.16	
	Mean	0.1472	0.1419	0.1454	20.1050	22.9823	21.0822	2.2943	2.5712	2.3883	2.4179	2.4179	0.126	0.07	
*	P3/6	0.1442	0.1343	0.1243	21.7155	27.0901	32.5190	2.4493	2.9664	3.4887	2.9681	2.9681	0.465	0.27	
	P3/7	0.1863	0.1764	0.1664	-1.1401	4.2345	9.6634	0.2504	0.7674	1.2898	0.7692	0.7692	0.465	0.27	
	P3/8	0.1507	0.1408	0.1306	18.1868	23.5613	29.0988	2.1098	2.6269	3.1596	2.6321	2.6321	0.470	0.27	
ADSCs	Mean	0.1604	0.1505	0.140433	12.92073833	18.295331	23.760405	1.6031	2.1202	2.6460	2.1231	2.1231	0.466	0.27	

\* P3/6 = Passage 9

P3/7 = Passage 10

P3/8 = Passage 11



จุฬาลงกรณ์มหาวิทยาลัย  
**CHULALONGKORN UNIVERSITY**



## REFERENCES

1. Gerecht, J.V.S.a.S., *Vascular tissue engineering: biodegradable scaffold platforms to promote angiogenesis*. Serbo and Gerecht Stem Cell Research & Therapy, 2013. **4**(8): p. 1-8.
2. Pina, S., et al., *Scaffolding Strategies for Tissue Engineering and Regenerative Medicine Applications*. Materials (Basel), 2019. **12**(11).
3. Chaudhari, A.A., et al., *Future Prospects for Scaffolding Methods and Biomaterials in Skin Tissue Engineering: A Review*. Int J Mol Sci, 2016. **17**(12).
4. Noor Izyan Syazana Mohd Yusoff, M.U.W., Juhana Jaafar, Tuck-Whye Wong, *Structural and characterization studies of insoluble Thai Bombyx mori silk fibroin films*. Malaysian Journal of Fundamental and Applied Sciences, 2019. **15**(1): p. 18-22.
5. O'Brien, F.J., *Biomaterials & scaffolds for tissue engineering*. Materials Today, 2011. **14**(3): p. 88-95.
6. Li, Z.-H., et al., *Silk fibroin-based scaffolds for tissue engineering*. Frontiers of Materials Science, 2013. **7**(3): p. 237-247.
7. Vepari, C. and D.L. Kaplan, *Silk as a Biomaterial*. Prog Polym Sci, 2007. **32**(8-9): p. 991-1007.
8. Wu, Y.Y., et al., *Experimental Study on Effects of Adipose-Derived Stem Cell-Seeded Silk Fibroin Chitosan Film on Wound Healing of a Diabetic Rat Model*. Ann Plast Surg, 2018. **80**(5): p. 572-580.
9. Amar J. Majmundar, Waihay J. Wong\*, and M. Celeste Simon, *Hypoxia inducible factors and the response to hypoxic stress*. Mol Cell., 2010. **40**(2): p. 294-309.
10. Jung, S. and J. Kleinheinz, *Angiogenesis — The Key to Regeneration, in Regenerative Medicine and Tissue Engineering*. 2013.
11. Mastrullo, V., et al., *Angiogenesis in Tissue Engineering: As Nature Intended?* Front Bioeng Biotechnol, 2020. **8**: p. 188.
12. Bai, Y., et al., *Localized delivery of growth factors for angiogenesis and bone formation in tissue engineering*. Int Immunopharmacol, 2013. **16**(2): p. 214-23.

13. Bhang, S.H., et al., *Locally delivered growth factor enhances the angiogenic efficacy of adipose-derived stromal cells transplanted to ischemic limbs*. *Stem Cells*, 2009. **27**(8): p. 1976-86.
14. Zhao, L., T. Johnson, and D. Liu, *Therapeutic angiogenesis of adipose-derived stem cells for ischemic diseases*. *Stem Cell Res Ther*, 2017. **8**(1): p. 125.
15. Yuan, Y.J., et al., *Application of the chick embryo chorioallantoic membrane in neurosurgery disease*. *Int J Med Sci*, 2014. **11**(12): p. 1275-81.
16. Hill, D.M. *Animal Development*. *Animal Development* June 2019 [cited November 2019 11].
17. Ehsan Jabbarzadeh, T.S., Yusuf M. Khan, Tao Jiang, Anthony J. Wirtel, Meng Deng, Qing Lv, Lakshmi S. Nair, Steven B. Doty, and Cato T. Laurencin, *Induction of angiogenesis in tissue-engineered scaffolds designed for bone repair: A combined gene therapy– cell transplantation approach*. *PNAS*, 2008. **105**(32): p. 11099-11104.
18. Jabbarzadeh, E., et al., *Induction of angiogenesis in tissue-engineered scaffolds designed for bone repair: a combined gene therapy-cell transplantation approach*. *Proc Natl Acad Sci U S A*, 2008. **105**(32): p. 11099-104.
19. Wang, W., et al., *Silk fibroin scaffolds loaded with angiogenic genes in adenovirus vectors for tissue regeneration*. *J Tissue Eng Regen Med*, 2019. **13**(5): p. 715-728.
20. Adelheid H. Brantner', F.Q., Asima Chakraborty', Iutta Polligger', Silvio Sosa' and a.R.D. Loggia, *HET-CAM Bioassay as In Vitro Alternative to the Croton Oil Test for Investigating Steroidal and Non-steroidal Compounds*. *ALTEX*, 2002. **19**(2): p. 51-56.
21. Laschke, M.W. and M.D. Menger, *Vascularization in tissue engineering: angiogenesis versus inosculation*. *Eur Surg Res*, 2012. **48**(2): p. 85-92.
22. Rouwkema, J., N.C. Rivron, and C.A. van Blitterswijk, *Vascularization in tissue engineering*. *Trends Biotechnol*, 2008. **26**(8): p. 434-41.
23. Greenberg, D.A. and K. Jin, *From angiogenesis to neuropathology*. *Nature*, 2005. **438**(7070): p. 954-9.
24. Carolyn A. Staton, S.M.S., Simon Tazzyman, Russell Hughes, Nicola J. Brown and

- Claire E. Lewis, *Current methods for assaying angiogenesis in vitro and in vivo*. INTERNATIONAL JOURNAL OF EXPERIMENTAL PATHOLOGY, 2004. **85**: p. 233-248.
25. Lai, R.C., et al., *Exosome secreted by MSC reduces myocardial ischemia/reperfusion injury*. Stem Cell Res, 2010. **4**(3): p. 214-22.
  26. Nowak-Sliwinska, P., T. Segura, and M.L. Iruela-Arispe, *The chicken chorioallantoic membrane model in biology, medicine and bioengineering*. Angiogenesis, 2014. **17**(4): p. 779-804.
  27. Norrby, K., *In vivo models of angiogenesis*. J. Cell. Mol. Med, 2006. **10**(3): p. 588-612.
  28. Feder, D., et al., *Standardization of a method to study angiogenesis in a mouse model*. An Acad Bras Cienc, 2013. **85**(4): p. 1483-7.
  29. Birsner, A.E., O. Benny, and R.J. D'Amato, *The corneal micropocket assay: a model of angiogenesis in the mouse eye*. J Vis Exp, 2014(90).
  30. Coleman, C.M., *Chicken embryo as a model for regenerative medicine*. Birth Defects Res C Embryo Today, 2008. **84**(3): p. 245-56.
  31. Linhoss, D.J.E. *Stages in chick embryo development*. Dr. George Thomas Tabler 2018 [cited 2019 27]; Available from: <http://extension.msstate.edu/content/stages-chick-embryo-development>.
  32. Fauzia, E., et al., *Chick Embryo: A Preclinical Model for Understanding Ischemia-Reperfusion Mechanism*. Front Pharmacol, 2018. **9**: p. 1034.
  33. Stern, C.D., *The Chick: A Great Model System Becomes Even Greater*. Developmental Cell, 2005. **8**(1): p. 9-17.
  34. Özpolat, B.D., et al., *Regeneration of the elbow joint in the developing chick embryo recapitulates development*. Developmental Biology, 2012. **372**(2): p. 229-238.
  35. Kelder, T.P., et al., *The avian embryo to study development of the cardiac conduction system*. Differentiation, 2016. **91**(4-5): p. 90-103.
  36. Prasongchean, W., et al., *Amniotic fluid stem cells increase embryo survival following injury*. Stem Cells Dev, 2012. **21**(5): p. 675-88.
  37. Al Naieb, S., C.M. Happel, and T.M. Yelbuz, *A detailed atlas of chick heart*

- development in vivo*. *Ann Anat*, 2013. **195**(4): p. 324-41.
38. Lokman, N.A., et al., *Chick chorioallantoic membrane (CAM) assay as an in vivo model to study the effect of newly identified molecules on ovarian cancer invasion and metastasis*. *Int J Mol Sci*, 2012. **13**(8): p. 9959-70.
  39. Tufan, A.C. and N.L. Satiroglu-Tufan, *The chick embryo chorioallantoic membrane as a model system for the study of tumor angiogenesis, invasion and development of anti-angiogenic agents*. (1568-0096 (Print)).
  40. Zhenguo Chen, Z.W., *In vivo Chick Chorioallantoic Membrane (CAM) Angiogenesis Assays*. *bio-protocol*, 2013. **3**(18): p. 1-5.
  41. Kain, K.H., et al., *The chick embryo as an expanding experimental model for cancer and cardiovascular research*. *Dev Dyn*, 2014. **243**(2): p. 216-28.
  42. Ribatti, D., *The chick embryo chorioallantoic membrane (CAM) assay*. *Reprod Toxicol*, 2017. **70**: p. 97-101.
  43. Schomann, T., et al., *Improved method for ex ovo-cultivation of developing chicken embryos for human stem cell xenografts*. *Stem Cells Int*, 2013. **2013**: p. 960958.
  44. ION MÎNDRILĂ), H.P., DANIEL PIRICI), MIHAELA NICULESCU), SANDRA ALICE BUTEICA), OANA TAISESCU), DĂNUȚ NICOLAE TARNIȚĂ), *The chick chorioallantoic membrane: a model of short-term study of Dupuytren's disease*. *Romanian Journal of Morphology & Embryology*, 2014. **55**(2): p. 377-382.
  45. Martinez-Madrid, B., et al., *Chick embryo chorioallantoic membrane (CAM) model: a useful tool to study short-term transplantation of cryopreserved human ovarian tissue*. *Fertil Steril*, 2009. **91**(1): p. 285-92.
  46. Vargas, A., et al., *The chick embryo and its chorioallantoic membrane (CAM) for the in vivo evaluation of drug delivery systems*. *Adv Drug Deliv Rev*, 2007. **59**(11): p. 1162-76.
  47. Ribatti, D., et al., *Angiogenic response induced by acellular brain scaffolds grafted onto the chick embryo chorioallantoic membrane*. *Brain Research*, 2003. **989**(1): p. 9-15.

48. Palmeira-de-Oliveira, R., et al., *Testing vaginal irritation with the Hen's Egg Test-Chorioallantoic Membrane assay*. ALTEX, 2018. **35**(4): p. 495-503.
49. Wutzler, P., et al., *Comparative Testing of Liposomal and Aqueous Formulations of Povidone-Iodine for Their Angioirritative Potential at the Chorioallantoic Membrane of ex ovo Cultivated Chick Embryos*. *Dermatology*, 2003. **207**(1): p. 43-47.
50. Marquardt, C., et al., *Evaluation of the tissue toxicity of antiseptics by the hen's egg test on the chorioallantoic membrane (HETCAM)*. *European Journal of Medical Research*, 2010. **15**(5).
51. OECD, *Test No. 405: Acute Eye Irritation/Corrosion*. 2017.
52. Fukayama, T., et al., *Effect of fibroin sponge coating on in vivo performance of knitted silk small diameter vascular grafts*. *Organogenesis*, 2015. **11**(3): p. 137-51.
53. MONDAL M., T.K., NIRMAL KUMAR S., *The silk properties, sericin and fibroin in silkworm, Bombyx Mori Linn., - A review* CASPIAN JOURNAL OF ENVIRONMENTAL SCIENCES (CJES) 2007. **5**(2): p. 63-76.
54. Kaewprasit, K., et al., *Physico-chemical properties and in vitro response of silk fibroin from various domestic races*. *J Biomed Mater Res B Appl Biomater*, 2014. **102**(8): p. 1639-47.
55. Wongputtaraksa, T., et al., *Surface modification of Thai silk fibroin scaffolds with gelatin and chitooligosaccharide for enhanced osteogenic differentiation of bone marrow-derived mesenchymal stem cells*. *J Biomed Mater Res B Appl Biomater*, 2012. **100**(8): p. 2307-15.
56. Lerdchai, K., et al., *Thai Silk Fibroin/Gelatin Sponges for the Dual Controlled Release of Curcumin and Docosahexaenoic Acid for Anticancer Treatment*. *J Pharm Sci*, 2016. **105**(1): p. 221-30.
57. Liu, J., et al., *Flexible Water-Absorbing Silk-Fibroin Biomaterial Sponges with Unique Pore Structure for Tissue Engineering*. *ACS Biomaterials Science & Engineering*, 2020. **6**(3): p. 1641-1649.
58. Mulinti, P., et al., *10 - Strategies to improve the hemocompatibility of biodegradable biomaterials*, in *Hemocompatibility of Biomaterials for Clinical*

- Applications*, C.A. Siedlecki, Editor. 2018, Woodhead Publishing. p. 253-278.
59. Ude, A.U., et al., *Bombyx mori silk fibre and its composite: A review of contemporary developments*. *Materials & Design*, 2014. **57**: p. 298-305.
  60. Teimouri, A., et al., *Preparation, characterization, degradation and biocompatibility of different silk fibroin based composite scaffolds prepared by freeze-drying method for tissue engineering application*. *Polymer Degradation and Stability*, 2015. **121**: p. 18-29.
  61. Shimada, K., et al., *The effect of a silk Fibroin/Polyurethane blend patch on rat Vessels*. *Organogenesis*, 2017. **13**(4): p. 115-124.
  62. Miyamoto, S., et al., *Bombyx mori silk fibroin scaffolds for bone regeneration studied by bone differentiation experiment*. *J Biosci Bioeng*, 2013. **115**(5): p. 575-8.
  63. Wang, Y., et al., *A Biomimetic Silk Fibroin/Sodium Alginate Composite Scaffold for Soft Tissue Engineering*. *Sci Rep*, 2016. **6**: p. 39477.
  64. Xiaojie Lia, S.L., Liming Liu, Rui Xu, Miaomiao Du, Song Wang, Hesun Zhu, Qiang Lu, Quanyou Zhang, Yali Wu, Di Huang and Yan Wei, *A study of the initial adhesive force of cells on silk fibroin-based materials using micropipette aspiration*. *Regenerative Biomaterials*, 2018: p. 151-157.
  65. Dhyani, V. and N. Singh, *Controlling the cell adhesion property of silk films by graft polymerization*. *ACS Appl Mater Interfaces*, 2014. **6**(7): p. 5005-11.
  66. Sundelacruz, S. and D.L. Kaplan, *Stem cell- and scaffold-based tissue engineering approaches to osteochondral regenerative medicine*. *Semin Cell Dev Biol*, 2009. **20**(6): p. 646-55.
  67. Rina Nazarov, H.-J.J., and David L. Kaplan, *Porous 3-D Scaffolds from Regenerated Silk Fibroin*. *Biomacromolecules*, 2004. **5**: p. 718-726.
  68. Wang, Y.M., A; Lee, CSD; Pelcastre ; Bella ; Migliaresi; Schwartz; Boyan, *Influence of Pore Size of Silk Fibroin Scaffolds on Chondrocyte Differentiation in Static and Rotation Culture Conditions*. 2016: 55th Annual Meeting of the Orthopaedic Research Society.
  69. Boccafoschi, F., et al., *Biological Grafts: Surgical Use and Vascular Tissue Engineering Options for Peripheral Vascular Implants*, in *Encyclopedia of*

- Biomedical Engineering*. 2019. p. 310-321.
70. Hu, Y., et al., *The Relationship between Secondary Structure and Biodegradation Behavior of Silk Fibroin Scaffolds*. *Advances in Materials Science and Engineering*, 2012. **2012**: p. 1-5.
  71. Janin, C.Z.Z.F.C.M.J.R.P.Z.G.L.J., *Silk fibroin: Structural implications of a remarkable amino acid sequence*. *PROTEINS: Structure, Function, and Genetics*, 2001. **44**: p. 119-122.
  72. Bailey, K., *Potential Applications of Silk Fibroin as a Biomaterial*, in *Chemical Engineering*. 2013, the University of Waterloo: Waterloo, Ontario, Canada,. p. 149.
  73. Shbailat, S.J., S. Qanadilo, and F.A. Al-Soubani, *Protease activity in the egg yolk during the development of Meleagris gallopavo (Galliformes: Phasianidae) embryos*. *Italian Journal of Zoology*, 2016. **83**(3): p. 291-297.
  74. Da Silva, M., et al., *Investigating proteins and proteases composing amniotic and allantoic fluids during chicken embryonic development*. *Poult Sci*, 2017. **96**(8): p. 2931-2941.
  75. Zhang, L., et al., *Tailoring degradation rates of silk fibroin scaffolds for tissue engineering*. *J Biomed Mater Res A*, 2019. **107**(1): p. 104-113.
  76. Fernandez-Colino, A., et al., *Fibrosis in tissue engineering and regenerative medicine: treat or trigger?* *Adv Drug Deliv Rev*, 2019. **146**: p. 17-36.
  77. Dzobo, K., et al., *Advances in Regenerative Medicine and Tissue Engineering: Innovation and Transformation of Medicine*. *Stem Cells Int*, 2018. **2018**: p. 2495848.
  78. Chagastelles, P.C. and N.B. Nardi, *Biology of stem cells: an overview*. *Kidney Int Suppl* (2011), 2011. **1**(3): p. 63-67.
  79. Xu, Y., Y. Shi, and S. Ding, *A chemical approach to stem-cell biology and regenerative medicine*. *Nature*, 2008. **453**(7193): p. 338-44.
  80. Lee, J., et al., *Promotion of stem cell proliferation by vegetable peptone*. *Cell Prolif*, 2009. **42**(5): p. 595-601.
  81. BIOLOGY, S.O.S.C., ed. *Stem cells in the limelight*. 2016/02/26 ed. *Nat Cell Biol*, ed. S.O.S.C. BIOLOGY. Vol. 18. 2016. 235.
  82. Thomson, J.Y.a.J.A., *EMBRYONIC STEM CELLS*. 2006, *Genetics and Biotechnology*

Building: Terese Winslow.

83. Mazo, I.B., S. Massberg, and U.H. von Andrian, *Hematopoietic stem and progenitor cell trafficking*. Trends Immunol, 2011. **32**(10): p. 493-503.
84. Walker, G.E., et al., *The pathophysiology of abdominal adipose tissue depots in health and disease*. Horm Mol Biol Clin Investig, 2014. **19**(1): p. 57-74.
85. Carvalho, K.A.T., *Mesenchymal Stem Cells Seeded on Biofunctionalized Scaffold for Tissue Engineering*. 2017: p. 349-367.
86. Ghorbani, A., S.A. Jalali, and M. Varedi, *Isolation of adipose tissue mesenchymal stem cells without tissue destruction: a non-enzymatic method*. Tissue Cell, 2014. **46**(1): p. 54-8.
87. Alireza Abdanipour, T.T.a.A.D., *Trans-differentiation of the Adipose Tissue-Derived Stem Cells into Neuron-Like Cells Expressing Neurotrophins by Selegiline*. Iranian Biomedical Journal, 2011. **15**(4): p. 113-121.
88. Cowan, *Adipose*. StemBook, 2009.
89. Gimble, J.M., A.J. Katz, and B.A. Bunnell, *Adipose-derived stem cells for regenerative medicine*. Circ Res, 2007. **100**(9): p. 1249-60.
90. Guasti, L., et al., *High plasticity of pediatric adipose tissue-derived stem cells: too much for selective skeletogenic differentiation?* Stem Cells Transl Med, 2012. **1**(5): p. 384-95.
91. Bunnell, B.A., et al., *Adipose-derived stem cells: isolation, expansion and differentiation*. Methods, 2008. **45**(2): p. 115-20.
92. Evan D. Rosen, C.J.W., Pere Puigserver, and Bruce M. Spiegelman, *Transcriptional regulation of adipogenesis*. GENES & DEVELOPMENT, 2000. **14**: p. 1293-1307.
93. E. Birmingham, G.L.N., P.E. McHugh, G. Shaw, F.P. Barry and L.M. McNamara, *OSTEOGENIC DIFFERENTIATION OF MESENCHYMAL STEM CELLS IS REGULATED BY OSTEOCYTE AND OSTEOBLAST CELLS IN A SIMPLIFIED BONE NICHE*. European Cells and Materials, 2012. **23**: p. 13-27.
94. I S Young, J.V.W., *Antioxidants in health and disease*. J Clin Pathol, 2001. **54**: p. 176-186.
95. Chanwitheesuk, A., A. Teerawutgulrag, and N. Rakariyatham, *Screening of antioxidant activity and antioxidant compounds of some edible plants of*



- Thailand. Food Chemistry, 2005. **92**(3): p. 491-497.
96. Verma, A.R., et al., *In vitro and in vivo antioxidant properties of different fractions of Moringa oleifera leaves*. Food Chem Toxicol, 2009. **47**(9): p. 2196-201.
  97. Hall, E.D., *Antioxidant therapies for acute spinal cord injury*. Neurotherapeutics, 2011. **8**(2): p. 152-67.
  98. Ali, S., et al., *The ecotoxicological and interactive effects of chromium and aluminum on growth, oxidative damage and antioxidant enzymes on two barley genotypes differing in Al tolerance*. Environmental and Experimental Botany, 2011. **70**(2-3): p. 185-191.
  99. Kehinde, B.A., et al., *The Effects of an Experimentally Induced Unilateral Varicose Ovarian Vein on the Activities of Anti-Oxidant Enzymes in an Adult Rat Ovary*. International Journal of Morphology, 2016. **34**(4): p. 1436-1441.
  100. Katalinic, V., et al., *Screening of 70 medicinal plant extracts for antioxidant capacity and total phenols*. Food Chemistry, 2006. **94**(4): p. 550-557.
  101. Shiekh, P.A., A. Singh, and A. Kumar, *Engineering Bioinspired Antioxidant Materials Promoting Cardiomyocyte Functionality and Maturation for Tissue Engineering Application*. ACS Applied Materials & Interfaces, 2018. **10**(4): p. 3260-3273.
  102. Kim, W.S., et al., *Evidence supporting antioxidant action of adipose-derived stem cells: protection of human dermal fibroblasts from oxidative stress*. J Dermatol Sci, 2008. **49**(2): p. 133-42.
  103. Owczarczyk-Saczonek, A., et al., *The Use of Adipose-Derived Stem Cells in Selected Skin Diseases (Vitiligo, Alopecia, and Nonhealing Wounds)*. Stem Cells Int, 2017. **2017**: p. 4740709.
  104. Bellei, B., et al., *Adipose tissue-derived extracellular fraction characterization: biological and clinical considerations in regenerative medicine*. Stem Cell Res Ther, 2018. **9**(1): p. 207.
  105. Seoane-Vazquez, E., V. Shukla, and R. Rodriguez-Monguio, *Innovation and competition in advanced therapy medicinal products*. EMBO Mol Med, 2019. **11**(3).

106. Regev-Rudzki, N., et al., *Cell-cell communication between malaria-infected red blood cells via exosome-like vesicles*. Cell, 2013. **153**(5): p. 1120-33.
107. Makridakis, M., M.G. Roubelakis, and A. Vlahou, *Stem cells: Insights into the secretome*. Biochim Biophys Acta, 2013.
108. Lai, C.P. and X.O. Breakefield, *Role of exosomes/microvesicles in the nervous system and use in emerging therapies*. Front Physiol, 2012. **3**: p. 228.
109. Ruenn Chai Lai, T.S.C.S.K.L., *Mesenchymal stem cell exosome: a novel stem cell-based therapy for cardiovascular disease*. Regen. Med 2011. **6**(4): p. 481-492.
110. Manotham, K., S. Chattong, and A. Setpakdee, *Generation of CCR5-defective CD34 cells from ZFN-driven stop codon-integrated mesenchymal stem cell clones*. J Biomed Sci, 2015. **22**: p. 25.
111. Huaxian Chen, J.K., Sean Sissons, Karen Cox, William Matter, Fred Chadwell, and C.J.V. Peng Luan, Amy Schutz-Geschwender, and D. Michael Olive, *A Cell Based Immunocytochemical Assay For Monitoring Kinase Signaling Pathways And Drug Efficacy*. Analytical Biochemistry, 2005. **338**: p. 136-142.
112. Lulevich, V., et al., *Single cell mechanics of keratinocyte cells*. Ultramicroscopy, 2010. **110**(12): p. 1435-42.
113. Cristofol Vives-Ba uza, A.S. and a.E. Garcia-Arumi, *Chapter 19 Measurements of the antioxidant enzyme activities of SOD,catalase,and GPx*. METHODS IN CELL BIOLOGY, 2007. **80**: p. 379-393.
114. VI Sun, L.O., and Ving U', *A Simple Method for Clinical Assay of Superoxide Dismutase*. CLINICAL CHEMISTRY,, 1988. **34**(3): p. 497-500.
115. Cullen, C.J.W.a.J.J., *Measurement of SOD CAT GPx in cultured cells and tissue*. National institutes of health, 2010: p. 1-37.
116. Clara, M., et al., *Superoxide Dismutase and Oxidative Stress in Amyotrophic Lateral Sclerosis*, in *Current Advances in Amyotrophic Lateral Sclerosis*. 2013.
117. Cho, J.A., et al., *Exosomes from ovarian cancer cells induce adipose tissue-derived mesenchymal stem cells to acquire the physical and functional characteristics of tumor-supporting myofibroblasts*. Gynecol Oncol, 2011. **123**(2): p. 379-86.

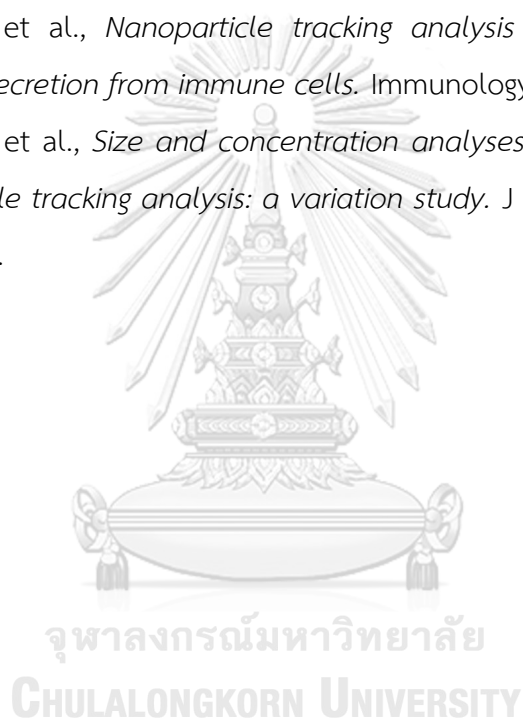
118. Lee, D.H., et al., *Enhanced osteogenesis of beta-tricalcium phosphate reinforced silk fibroin scaffold for bone tissue biofabrication*. *Int J Biol Macromol*, 2017. **95**: p. 14-23.
119. Gu Cheng, Z.D., Xin Xing, Xin Yu, Xin Cheng, Zubing Li, Hongbing Deng and Qun Wang, *Advanced Silk Fibroin Biomaterials for Cartilage Regeneration*. *ACS biomaterials science and engineering*, 2018. **4**: p. 2704-2715.
120. Lu, Y., et al., *Silk/agarose scaffolds with tunable properties via SDS assisted rapid gelation*. *RSC Advances*, 2017. **7**(35): p. 21740-21748.
121. Kim, U.J., et al., *Three-dimensional aqueous-derived biomaterial scaffolds from silk fibroin*. *Biomaterials*, 2005. **26**(15): p. 2775-85.
122. Wong, R.S., M. Ashton, and K. Dodou, *Effect of Crosslinking Agent Concentration on the Properties of Unmedicated Hydrogels*. *Pharmaceutics*, 2015. **7**(3): p. 305-19.
123. Cheng, N.C., et al., *Sustained release of adipose-derived stem cells by thermosensitive chitosan/gelatin hydrogel for therapeutic angiogenesis*. *Acta Biomater*, 2017. **51**: p. 258-267.
124. Xiong, G., et al., *A Novel in Vitro Three-Dimensional Macroporous Scaffolds from Bacterial Cellulose for Culture of Breast Cancer Cells*. *Journal of Biomaterials and Nanobiotechnology*, 2013. **04**(04): p. 316-326.
125. Varkey, A., et al., *Impact of silk fibroin-based scaffold structures on human osteoblast MG63 cell attachment and proliferation*. *Int J Nanomedicine*, 2015. **10 Suppl 1**: p. 43-51.
126. Wutzler, P., et al., *Comparative testing of liposomal and aqueous formulations of povidone-iodine for their angiirritative potential at the chorioallantoic membrane of ex ovo cultivated chick embryos*. *Dermatology*, 2003. **207**(1): p. 43-7.
127. Ribatti, D., et al., *The gelatin sponge-chorioallantoic membrane assay*. *Nat Protoc*, 2006. **1**(1): p. 85-91.
128. Ribatti, D., et al., *The gelatin sponge-chorioallantoic membrane assay*. *Nature Protocols*, 2006. **1**: p. 85.
129. Hofmann, U., et al., *A sensitive sensor cell line for the detection of oxidative*

- stress responses in cultured human keratinocytes. Sensors (Basel)*, 2014. **14**(7): p. 11293-307.
130. Chirdchupunseree, H. and P. Pramyothin, *Protective activity of phyllanthin in ethanol-treated primary culture of rat hepatocytes. J Ethnopharmacol*, 2010. **128**(1): p. 172-6.
131. Ligia L. Fernandes, C.X.R., Débora S. Tavares, Gloria A. Soares, Leticia O. Castro, Jose M. Granjeiro, *Cytocompatibility of Chitosan and Collagen-Chitosan Scaffolds for Tissue Engineering. Polímeros*, 2011. **21**: p. 1-6.
132. Cheng, M., et al., *Study on physical properties and nerve cell affinity of composite films from chitosan and gelatin solutions. Biomaterials*, 2003. **24**(17): p. 2871-2880.
133. Nosrati, H., S. Pourmotabed, and E. Sharifi, *A Review on Some Natural Biopolymers and Their Applications in Angiogenesis and Tissue Engineering. Journal of Applied Biotechnology Reports*, 2018. **5**(3): p. 81-91.
134. Woloszyk, A. and T.A. Mitsiadis, *Angiogenesis within Stem Cell-Seeded Silk Scaffolds Cultured on the Chorioallantoic Membrane and Visualized by 3D Imaging. Curr Protoc Stem Cell Biol*, 2017. **41**: p. 1F 19 1-1F 19 9.
135. Actor, J.K., *A Functional Overview of the Immune System and Immune Components*, in *Introductory Immunology*. 2014. p. 1-15.
136. Kays, S.K., et al., *CD105 is a surface marker for receptor-targeted gene transfer into human long-term repopulating hematopoietic stem cells. Stem Cells Dev*, 2015. **24**(6): p. 714-23.
137. Lv, F.J., et al., *Concise review: the surface markers and identity of human mesenchymal stem cells. Stem Cells*, 2014. **32**(6): p. 1408-19.
138. Asnaghi, M.A., et al., *Bioreactors*, in *Tissue Engineering*. 2014. p. 393-425.
139. Nicolò Bertozzi, F.S., Michele Pio Grieco, Eugenio Grignaffini, Edoardo Raposio, *Adipose-derived stem cells as a novel anti-aging therapy in cosmetic Surgery: a concise review. Euromediterranean biomedical journal*, 2018. **13**(10): p. 46-56.
140. He YX, Z.N., Li WF, Jia N, Chen BY, Zhou K, Zhang J, Chen Y, Zhou CZ, *N-Terminal Domain of Bombyx mori Fibroin Mediates the Assembly of Silk in Response to pH Decrease. J. Mol. Biol.*, 2012. **418**: p. 197-207.

141. Lotz, C., et al., *Alternative methods for the replacement of eye irritation testing*. ALTEX, 2016. **33**(1): p. 55-67.
142. Gilleron, L., et al., *Evaluation of the HET-CAM-TSA method as an alternative to the draize eye irritation test*. Toxicology in Vitro, 1997. **11**(5): p. 641-644.
143. Kishore, A.S., et al., *Hen egg chorioallantoic membrane bioassay: an in vitro alternative to draize eye irritation test for pesticide screening*. Int J Toxicol, 2008. **27**(6): p. 449-53.
144. Liebsch, S.a., *ICCVAM-Recommended Test Method Protocol: Hen's Egg Test – Chorioallantoic Membrane (HET-CAM) Test Method in Appendix B3*. 2010, NIH Publication. p. B30-B38.
145. Yao, D., et al., *Salt-leached silk scaffolds with tunable mechanical properties*. Biomacromolecules, 2012. **13**(11): p. 3723-9.
146. Hyoung-Joon Jin, J.P., Regina Valluzzi, Peggy Cebe, and David L. Kaplan, *Biomaterial Films of Bombyx Mori Silk Fibroin with Poly(ethylene oxide)*. Biomacromolecules, 2004. **5**: p. 711-717.
147. Yang, M., et al., *Preparation of porous scaffolds from silk fibroin extracted from the silk gland of Bombyx mori (B. mori)*. Int J Mol Sci, 2012. **13**(6): p. 7762-75.
148. Zeilbeck, L.F., et al., *Differential Angiogenic Properties of Lithium Chloride In Vitro and In Vivo*. PLOS ONE, 2014. **9**(4): p. e95546.
149. Barlian, A., et al., *Chondrogenic differentiation of adipose-derived mesenchymal stem cells induced by L-ascorbic acid and platelet rich plasma on silk fibroin scaffold*. PeerJ, 2018. **6**: p. e5809.
150. Loh, Q.L. and C. Choong, *Three-dimensional scaffolds for tissue engineering applications: role of porosity and pore size*. Tissue Eng Part B Rev, 2013. **19**(6): p. 485-502.
151. Acharya, C., S.K. Ghosh, and S.C. Kundu, *Silk fibroin film from non-mulberry tropical tasar silkworms: A novel substrate for in vitro fibroblast culture*. Acta Biomater, 2009. **5**(1): p. 429-37.
152. Cao, Y. and B. Wang, *Biodegradation of silk biomaterials*. Int J Mol Sci, 2009. **10**(4): p. 1514-24.
153. Bai L, W.D., Xu J, Liu H, Xie M, Guan G, Sun Z, Tan X., *On model of angiogenesis*

- and the mechanism in porous silk fibroin films. *J Mater Sci Mater Med*, 2011. **22**: p. 927-933.
154. Hu, X., et al., *Designing silk-silk protein alloy materials for biomedical applications*. *J Vis Exp*, 2014(90): p. e50891.
  155. Eldh, M., et al., *Importance of RNA isolation methods for analysis of exosomal RNA: evaluation of different methods*. *Mol Immunol*, 2012. **50**(4): p. 278-86.
  156. Vlassov, A.V., et al., *Exosomes: current knowledge of their composition, biological functions, and diagnostic and therapeutic potentials*. *Biochim Biophys Acta*, 2012. **1820**(7): p. 940-8.
  157. Instruments, M., *Nanosight NTA software guide in NanoSight Software NTA*, M.s. software, Editor. 2014, Malvern Instruments Ltd. : Malvern.
  158. Hessvik, N.P. and A. Llorente, *Current knowledge on exosome biogenesis and release*. *Cell Mol Life Sci*, 2018. **75**(2): p. 193-208.
  159. Lener, T., et al., *Applying extracellular vesicles based therapeutics in clinical trials - an ISEV position paper*. *J Extracell Vesicles*, 2015. **4**: p. 30087.
  160. Lotvall, J., et al., *Minimal experimental requirements for definition of extracellular vesicles and their functions: a position statement from the International Society for Extracellular Vesicles*. *J Extracell Vesicles*, 2014. **3**: p. 26913.
  161. Wall, I.B. and N. Davie, *Quality control in cell and tissue engineering*. 2013: p. 148-165.
  162. Daniel Brunner, J.F., Helmut Appl, Harald Schöffl, Walter Pfaller and Gerhard Gstraunthaler, *Serum-free Cell Culture: The Serum-free Media Interactive Online Database*. *Altex*, 2009. **27**(1): p. 53-62.
  163. Doyle, L.M. and M.Z. Wang, *Overview of Extracellular Vesicles, Their Origin, Composition, Purpose, and Methods for Exosome Isolation and Analysis*. *Cells*, 2019. **8**(7).
  164. Strassburg, S., et al., *Bi-directional exchange of membrane components occurs during co-culture of mesenchymal stem cells and nucleus pulposus cells*. *PLoS One*, 2012. **7**(3): p. e33739.
  165. Arslan, F., et al., *Mesenchymal stem cell-derived exosomes increase ATP levels,*

- decrease oxidative stress and activate PI3K/Akt pathway to enhance myocardial viability and prevent adverse remodeling after myocardial ischemia/reperfusion injury. Stem Cell Res, 2013. 10(3): p. 301-12.*
166. Zeringer, E., et al., *Methods for the extraction and RNA profiling of exosomes. World J Methodol, 2013. 3(1): p. 11-8.*
167. Kim, H.O., S.-M. Choi, and H.-S. Kim, *Mesenchymal stem cell-derived secretome and microvesicles as a cell-free therapeutics for neurodegenerative disorders. Tissue Engineering and Regenerative Medicine, 2013. 10(3): p. 93-101.*
168. Soo, C.Y., et al., *Nanoparticle tracking analysis monitors microvesicle and exosome secretion from immune cells. Immunology, 2012. 136(2): p. 192-7.*
169. Vestad, B., et al., *Size and concentration analyses of extracellular vesicles by nanoparticle tracking analysis: a variation study. J Extracell Vesicles, 2017. 6(1): p. 1344087.*





จุฬาลงกรณ์มหาวิทยาลัย  
**CHULALONGKORN UNIVERSITY**



## VITA

**NAME** Tanapong Watchararot

**DATE OF BIRTH** 06 Jan 1990

**PLACE OF BIRTH** Nakorn Nayok

**INSTITUTIONS ATTENDED** Faculty of pharmaceutical science, Chulalongkorn University, Bangkok, Thailand

**HOME ADDRESS** 198 U-center building, Chula 42, Wangmai, Pathumwan, Bangkok, Thailand, 10330

**PUBLICATION** No

**AWARD RECEIVED**

1. Outstanding graduate student award in the academic year 2017 from Chulalongkorn University. and faculty of pharmaceutical science. Chulalongkorn, University
2. Young Thai Science Ambassador 2010 from National Science Museum.